The Pennsylvania State University
The Graduate School

DESIGN OF A MULTIFUNCTIONAL FORCEPS FOR USE IN ENDOSCOPIC SURGERY

A Thesis in
Mechanical Engineering
by
Andrew Charles Rau

Submitted in Partial Fulfillment
of the Requirements
for the Degree of

Master of Science

May 2010

The thesis of Andrew Charles Rau was reviewed and approved* by the following:

Mary I. Frecker
Professor of Mechanical Engineering
Thesis Advisor

Matthew B. Parkinson
Assistant Professor of Engineering Design and Assistant Professor of Mechanical Engineering

Karen A. Thole
Professor of Mechanical Engineering
Department Head of Mechanical and Nuclear Engineering

*Signatures are on file in the Graduate School.

Abstract

Minimally invasive surgery (MIS) has gained tremendous popularity among medical practitioners in a variety of disciplines. The introduction and development of laparoscopy in the late 20^{th} century proved that MIS could be implemented safely and effectively. Laparoscopy provided both an effective alternative to traditional open surgery as well as benefits including reductions in patient recovery time, pain, probability of infection, and cosmetic scaring. In a similar fashion, a developing endoscopic MIS technique called Natural Orifice Transluminal Endoscopic Surgery (NOTES) has the potential to provide surgical alternatives which completely eliminate the need for external incisions, resulting in obvious patient care benefits.

Performance of the endoscopic tools used during endoscopic and NOTES procedures is extremely limited by strict size constraints, thereby significantly impeding the development of experimental MIS procedures. The focus of this work is the design, analysis, and testing of a multifunctional 3.0 mm diameter endoscopic forceps for use in MIS. Models of the proposed design predict considerable improvements in opening range and force application for both grasping and spreading when compared to currently used endoscopic forceps. Electrocautery ability is also provided to increase tool utility; studies are conducted to evaluate cautery performance relative to commercial products. In addition to possessing multifunctional grasping, spreading, and cautery abilities, the tool's design promotes fail-safe malfunctions, including locking prior to failure and a decreased likelihood of part fracture. In order to increase tool utility, a means of providing articulation ability to the tool is investigated. Increased instrument dexterity is desirable for manipulation of tissue in remote regions, but size constraints prevent practical implementation of dextrous endoscopic tools. A practical means of classifying dextrous manipulators is presented and used to evaluate the potential for scalability to the meso level (1-5 mm diameter). A compliant design which provides articulation ability at

the meso scale is introduced and evaluated based on practical efficacy. Results of this evaluation indicate that the concept possesses potential for articulation ability.

Experimental endoscopic procedures often necessitate unique tool performance requirements which currently available tools do not meet. Scaling current tool concepts to the meso level often results in significant performance losses, thereby hindering the development of novel medical procedures. The work detailed in this thesis aims to provide increased surgical capabilities to surgeons during endoscopic procedures.

Table of Contents

List of Figures viii

List of Tables xiii

Acknowledgments xiv

Chapter 1
Background and Motivation 1
1.1 Introduction 1
1.2 Minimally Invasive Surgery 1
1.2.1 Laparoscopy 2
1.2.2 Natural Orifice Transluminal Endoscopic Surgery 2
1.3 An Experimental Minimally Invasive Technique 5
1.4 Endoscopic Tools: Design, Functionality, and Performance 7
1.4.1 Current Tools 7
1.4.2 Multifunctionality 8
1.5 Motivation and Objectives 10

Chapter 2
Design, Analysis and Fabrication of the Multifunctional Forceps 11
2.1 Proposed Tool Concept and Design Process 11
2.2 Design Objectives and Constraints 13
2.3 Design of the Tool Jaws 15
2.3.1 Mechanical Advantage Analysis 15
2.3.2 Finite Element Modeling of the Tool Jaw 18
2.3.3 Finalized Jaw Design and Comparison to Current Forceps . 22
2.4 Design of the Tool Mount 26

2.4.1 Objectives and Initial Concept 26
2.4.2 Finite Element Modeling of the Tool Mount 27
2.4.3 Finalized Tool Mount Design 29
2.5 Finalized Tool Tip Design 29

Chapter 3
Experimental Validation **31**
3.1 Fabrication and Assembly of Prototypes 31
3.2 Mechanical Advantage Validation and Comparison 32
3.2.1 Testing Setup and Methodology 32
3.2.2 Experimental MA Validation Results 33
3.3 Pull-off Force Testing and Comparison 38
3.3.1 Testing Setup and Methodology 39
3.3.2 Results and Discussion 40

Chapter 4
Incorporation of Cautery Ability **44**
4.1 Introduction 44
4.2 Review of Cautery Techniques 44
4.2.1 Electrocautery and Electrosurgery 44
4.2.2 Monopolar and Bipolar Techniques 45
4.3 Tissue Properties and Damage Mechanisms 47
4.4 Electrosurgical Equipment 49
4.4.1 Electrosurgical Generators 49
4.4.2 Electrocautery Devices 51
4.5 Testing of a Cautery Prototype 53
4.5.1 Cautery Test Setup and Methodology 54
4.5.2 Cautery Test Results and Discussion 58
4.5.2.1 Quantitative Test Results and Discussion 58
4.5.2.2 Qualitative Evaluation and Summary 60

Chapter 5
Incorporation of Articulation Capability **62**
5.1 Introduction 62
5.2 Review and Classification of Current Articulating Technologies . . . 64
5.2.1 Manipulator Classification 64
5.2.2 Mechanical Configuration 66
5.2.2.1 Continuous Backbone Mechanisms 66
5.2.2.2 Segmented/Discrete Mechanisms 67
5.2.2.3 Summary of Mechanical Configurations 70

5.2.3 Actuation Methodology 71
5.2.3.1 Fluid-Actuation 71
5.2.3.2 Mechanical Actuation 72
5.2.3.3 Active Material Actuation 75
5.2.4 Discussion of Meso Scale Feasibility 78
5.2.4.1 Mechanical Configurations 78
5.2.4.2 Actuation Methodologies 79
5.2.5 Summary and Conclusions on Current Technologies 79
5.3 Preliminary Investigation of a Meso Scale Articulating Segment . . 80
5.3.1 Introduction 80
5.3.2 Proposed Articulation Concept and Objectives 81
5.3.3 Simulation of Multiple Designs 82
5.3.4 Results and Discussion 86
5.3.5 Summary and Conclusions 90

Chapter 6
Conclusions, Recommendations, and Future Work **91**
6.1 Summary 91
6.2 Conclusions 92
6.3 Research Contributions 93
6.4 Recommendations and Future Work 95

Bibliography **97**

List of Figures

1.1 Cross-section showing abdominal access during laparoscopic surgery, modified from [8]. 3
1.2 Diagram of upper endoscopy via mouth insertion [9]. 3
1.3 Endoscope with an exploded photograph of the tip containing: (A)working channels, (B) light sources, (C) camera and (D) endoscopic tool tip. 4
1.4 Direct puncture gastrotomy: a single incision is made through the stomach wall to access the abdominal cavity [12]. 5
1.5 Steps for the self-approximating transluminal access technique (STAT). In sequence, the endoscope is initially inside the stomach (A), an incision is made in the mucuosa (B), the mucosa and muscular layers of the stomach are separated by tunneling (C), an incision is made in the muscular layer (D) and (E) the endoscope is retracted and the internal mucosal incision is closed, modified from [11]. . . . 6
1.6 (A) Standard configuration of an endoscopic tool with handle, flexible tip and tool tip (modified from [13]), (B) common biopsy forceps tool tip [14], (C) common bipolar cautery probe tool tip [15]. 7
1.7 Multifunctional tool assemblies consisting of mechanical linkages (A and B) and a compliant members (C); modified from [17]. 9
1.8 A multifunctional, compliant forceps/scissors operated by advancing and rotating the housing sheath [18]. 9

2.1 Two currently used endoscopic forceps with one set of actuating wires: (A) Olympus EndoJaw Disposable Biopsy Forceps and (B) Olympus RadialJaw Hot Biopsy Forceps along with (C) the proposed design incorporating 2 sets of actuating wires (patent pending, Provisional Patent Application Serial No. 61/237,954). 12
2.2 Diagram of an endoscope insertion port geometry (Olympus 160 Series Gastroscope). 13
2.3 In-plane diagram of jaw design parameters and load orientations. Note: θ measured from closed position to inner jaw face. 16

2.4 Top view diagram of generalized jaw design with point of view (POV) shown. 17
2.5 Several upper jaw geometries considered for the initial design. Shown on left: outer curvatures. Shown on right:inner profiles) 18
2.6 3D representation of initial jaw design including upper and lower jaw geometries. 19
2.7 (A) Initial jaw geometry and (B) FEA model geometry. 20
2.8 Boundary conditions for opening (o) and closing (c) load cases. For opening case, pressure applied at eyelet "o" and displacement of line "o" fixed. For opening case, pressure applied at eyelet "c" and displacement of line "c" fixed. Inner pin hole fixed in y, z directions for both cases. 21
2.9 Von Mises stress contour plots of the finalized jaw design for closing (A) and opening (B) load cases. Locations of maximum stress at pin holes indicated by arrows. 22
2.10 (A)Measurements of Olympus EndoJaw geometrical parameters and (B) schematic of load orientations and relevant measurements for opening O and closing C cases. 24
2.11 (A) Variation of mechanical advantage (MA) with opening angle θ for proposed final design (red) and currently used products (cyan-EndoJaw, blue-RadialJaw). (B) Percentage improvements in MA relative to EndoJaw(cyan) and RadialJaw(blue). Note: Commercial designs and proposed deisgn shown in Figure 2.1. 25
2.12 Single-piece concept for tool mount with two supports and a wire clearance hole. 26
2.13 Full tool mount model (left) and quarter models with boundary conditions applied: symmetry conditions u_x or u_z=0 (shown in blue) applied to sectioned areas, pressures (red arrows) applied to appropriate areas, and lower faces held fixed (not shown). (A) Longitudinal-Tension, (B) Longitudinal-Compression, (C) Bending-In, (D) Bending-Out. 28
2.14 Von Mises stress contour plots of finalized tool design subjected to maximum loading in each load case. 28
2.15 Two embodiments of the final tool assembly (patent pending). (A) previously discussed tool mount and jaws for precise tissue manipulation. (B) previously discussed tool mount and widened jaws for manipulation of larger amounts of tissue. 30

3.1 Testing tool mount. CAD model (left) and photograph of manufactured testing mount (right) with external threading for fixation and clearance slot for actuating wires. 32
3.2 Test setup for MA validation with force gauge, pulley, weight, testing prototype and protractor to track opening angle. Note: camera and tripod positioned above. 33
3.3 MA model (Equation 2.2) and experimentally determined MA when actuating at eyelet C. 34
3.4 MA model (Equation 2.1) and experimentally determined MA when actuating at eyelet C. 35
3.5 Input and output forces for opening and closing when loading at eyelet O. Note: forces given as gram masses subjected to gravitational loading. 36
3.6 Design jaw Geometry (A) and manufactured jaw (B) (patent pending). Note: thicker opening eyelet causes out of plane loading, leading to increased frictional losses. 37
3.7 Experimental results and MA model of the RadialJaw in closing. . . 38
3.8 Photographs from RadialJaw testing showing the jaw at (A) a small angle $\theta \approx 2^o$ and (B) a larger angle $\theta \approx 57^o$. Notice the actuating wire connected to the input weight is angled off-axis in (B) due to interference created by the tool mount. 39
3.9 Test setup for pull-off measurements (grasping and spreading). . . . 40
3.10 Outer jaw geometries of (A) the proposed design (patent pending) and (B) the RadialJaw. The RadialJaw possesses by a level outer surface with a hole and an exposed edge. The proposed design has a tapered outer surface. 43

4.1 Diagrams of current paths for (A) monopolar (adapted from [23]) and (B) bipolar cautery techniques. Note the distance traveled through the body is significantly longer for the monopolar technique. 46
4.2 Common voltage waveform outputs for electrosurgical generators [23]. Cutting mode characterized by a low voltage continuous waveform, coagulation mode characterized by a high voltage interrupted waveform 50
4.3 (A) Cook Medical monopolar forceps [38]; (B) Cook Medical Bipolar probe [39]; (C) ConMed bipolar probe[40]; (D) Boston Scientific bipolar probe [41]. 51
4.4 Multifunctional bipolar cautery tool and scissors for laparoscopy. Scissors and translating rod act as bipolar electrodes [19]. 52

4.5 Bipolar cautery device consisting of two arms (left) and conducting electrodes mounted on each arm (right) [37]. 52
4.6 Monopolar device used for esophageal cautery consisting of an overtube (OT) with a mesh electrode and inflatable balloon to induce contact; modified from [30]. 53
4.7 Cautery prototype consisting of an early tool tip prototype (patent pending) retrofitted to the handle of a commercial forceps. 54
4.8 Equipment for cautery tests. 55
4.9 Plot of power rating data for SURGISTAT B-20 surgical generator under 500Ω load. 56
4.10 Photograph of the tool prototype cauterizing a piece of raw pork (top) along with the resulting cautery zone (bottom). 57
4.11 (A) Sample specimen photo (top-original, bottom-traced) from Test A. (B) Exploded view of one cauterized section showing the highly (inner) and moderately (outer) damaged zones indicated by arrows. 58

5.1 Two "wrist like" degrees of freedom shown by articulation to an off-axis angle ϕ [43]. 63
5.2 Classification of dexterous mechanical manipulators. 66
5.3 Continuous SMA backbone/actuating wire configurations with (A) 10 mm [47] and (B) 4.2 mm [43] outer diameters. 67
5.4 Segmented articulating configurations with direct hinge connections at different diameters: (A) 6.0 mm [53],(B) 10 mm [70, 71], and (C) 4.0 mm [52]. 68
5.5 12 mm diameter articulating mechanism consisting of inner and outer "snake-like" segmented tubes. Inner and outer tubes slide past each other to enable articulation [72, 73]. 69
5.6 Segmented manipulator (2.4 mm diameter) using non-traditional joining technique [54]. 70
5.7 Schematic and images of a faceted sphere joint configuration for a 6 mm diameter forceps tool [74]. 70
5.8 (A) Pneumatic robot arm performing complicated dexterous tasks and (B) tube actuators used to articulate the assembly. Diameter varies from 6.4 - 9 cm [69]. 73
5.9 Rigid link mechanism for articulation [58]. 74
5.10 Surgical manipulator component (4.75 mm) of the ViaCath System for teleoperated surgery; increased lateral forces were desired [60]. . 74
5.11 Meso scale mechanisms (A) 4.0 mm outer diameter [48] and (B) 2.0mm outer diameter [49] actuated by SMA coils (springs). 77

5.12 (A) Articulating section concept with repeating segments and actuating wires shown; (B) magnified diagram of repeating segment with four labeled design parameters. Note: link thickness indicated by a 83
5.13 Boundary conditions applied to a single segment meshed model. Note that geometrical symmetry allows analysis of a half model. Bottom area fixed in all directions, symmetry BC's (U_y=0) applied to sectioned areas (red), and lower corner of top link displaced in the negative z direction. 84
5.14 (A) Diagram of an deformed shape shown with the undeformed dashed outline and (B) deformed shape shown in x-z plane with deformed coordinates (X_1, Z_1) and (X_2, Z_2) used to calculate articulation angle ϕ. 85
5.15 Plot of maximum articulation angle ϕ (represented in color) relative to design parameters length L, width w, and radius r. 86
5.16 Plot of maximum articulation angle ϕ (represented in color) relative to design parameters length L, width w, and thickness t. 87
5.17 Plot of maximum lateral force (represented in color) relative to design parameters length L, width w, and radius r. 88
5.18 Plot of maximum lateral force (represented in color) relative to design parameters length L, width w, and thickness t. 89

List of Tables

2.1 Design Objectives and Constraints. 14
2.2 Relevant material properties for 316 stainless steel 20
2.3 Summary of jaw FEA results. Note: The minimum load bearing capacity of a single jaw is 1.84 N (shown in bold) 21
2.4 Design parameters of final design. 23
2.5 Geometrical parameters of two commercially available products. . . 23
2.6 Load bearing analysis results for the finalized tool mount design. . . 29

3.1 Grasping pull-off test results. 100 gram weight hung from each actuating wire. 41
3.2 Spreading pull-off test results. 100 gram weight hung from each actuating wire. 42

4.1 Power ratings for SURGISTAT B-20 surgical generator under 500Ω load. 56
4.2 Summary of area calculations for three cautery tests 59

5.1 Summary of articulating mechanisms (Note: NP - information not provided). 65
5.2 Ranges of parametric variation for the articulation and lateral force studies. 85
5.3 Geometrical parameters corresponding to the best performing designs in the free displacement and lateral force cases. 89

Acknowledgments

I would like to gratefully acknowledge the support provided by both the Grace Woodward Engineering-Medicine Grant and the Department of Mechanical and Nuclear Engineering at The Pennsylvania State University. Additionally, I would like to acknowledge Iron Lion Design Challenge members Andrew Baranak, Greg Hayes, and Jeffrey Kingston for their concept development. I would also like to thank my advisor, Dr. Mary Frecker, for her guidance, support, generosity, and patience. I would like to thank Dr. Matthew Parkinson for serving as a reader for my thesis, and Dr. Abraham Mathew for his invaluable contributions to this project. Lastly, I would like to thank my fellow EDOG lab members for their technical contributions to my work, moral support, and friendship during my time at Penn State.

Chapter 1

Background and Motivation

1.1 Introduction

The benefits of minimally invasive surgical procedures have caused a significant drive to replace traditional techniques with minimally invasive methods. Significant resources have been committed to developing clinical techniques which remove the need for external incisions and decrease procedural invasiveness. Because of decreasing instrument size and other constraints, surgical tools used in these efforts suffer from significant performance losses, greatly hindering the development of such experimental procedures. Tools with sufficient performance capabilities must be developed at decreased sizes to enable the advancement of these procedures. This work presents the design, analysis, and testing of a multifunctional endoscopic forceps for use in developing surgical procedures. As an introduction to this work, the fundamental concepts of minimally invasive surgery and tool multifunctionality are introduced, as well as detailed descriptions of the experimental technique and design goals which guided this design.

1.2 Minimally Invasive Surgery

Traditional "open" surgical procedures are conducted through large, external incisions which provide access to internal surgical sites. While open procedures provide the surgeon with the ability to directly interact with the surgical site, the resulting

time needed for patient recovery and the likelihood of infection during surgery are significant. A surgical procedure which significantly limits or reduces the degree of physical trauma to the patient is referred to as minimally invasive surgery (MIS). Minimally invasive procedures often drastically reduce the size of, or completely remove the need for, external incisions. Comparatively, any procedure which reduces the potential for patient pain or reduces the likelihood of surgical complications is considered to be "less invasive".

The benefits of MIS have been discussed extensively in the literature, most notably including reductions in: patient recovery time, procedure time, patient scarring, iatrogenic injury, probability of infection, and cost [1, 2, 3]. Because of these benefits, there has been a strong drive in modern medicine to implement existing MIS methods when possible and develop even less invasive techniques [1, 4, 5, 6, 7].

1.2.1 Laparoscopy

The introduction and development of laparoscopy in the second half of the 20th century represented the first paradigm shift of modern medicine to MIS. During laparoscopic surgery, slender instruments with long, rigid shafts are passed through small incisions in the abdomen. The outer diameter of these instruments usually ranges from 5-10 mm, thereby necessitating only small external incisions to accommodate the tools. A camera is also inserted to provide guidance to the surgeon, and the abdominal cavity in insufflated with inert gas (CO_2) to provide ample visibility and tool maneuverability. The external incisions are fitted with access ports to provide easy instrument exchanges during surgery. A simple diagram of a laparoscopic procedure is shown in Figure 1.1

1.2.2 Natural Orifice Transluminal Endoscopic Surgery

Initially introduced purely for diagnostic purposes, endoscopic surgery has gained significant success and momentum as a therapeutic technique[1, 4, 6, 7]. An endoscope is a medical tool consisting of a long, flexible portion connected to a manually controlled handle. The surgeon can advance the endoscope along the longitudinal axis of the flexible section and the tip can be articulated by manually turning dials

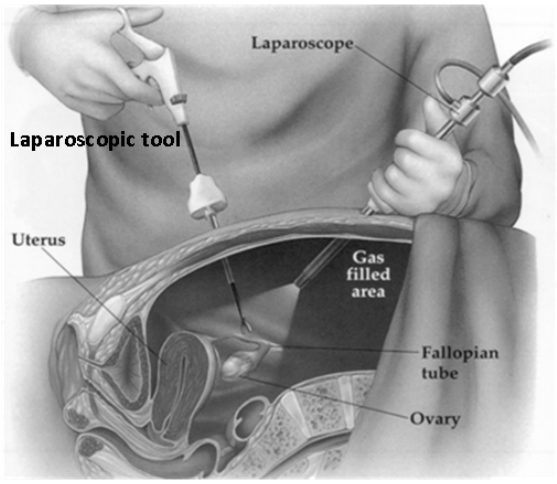

Figure 1.1. Cross-section showing abdominal access during laparoscopic surgery, modified from [8].

on the handle.

During endoscopic procedures, the endoscope is inserted through a natural orifice, *e.g.*, the mouth, anus, or vagina, thereby providing access to an internal site in the digestive or urinary tract as in Figure 1.2. The flexibility of the endoscope enables surgeons to navigate through complicated paths, such as the intestines, and the articulation ability of the tip provides access to the entire workspace around the tip. Traditional endoscopic procedures do not include any external or internal incisions and are usually limited to biopsy sampling, hemostasis or visual diagnosis.

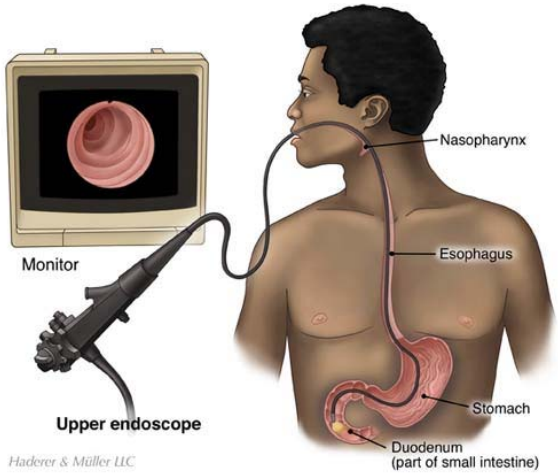

Figure 1.2. Diagram of upper endoscopy via mouth insertion [9].

The flexible portion houses at least one of each of the following: a light source, an image bundle (fiberoptic) and a working channel. The light source and image bundle allow the surgeon to view the field ahead of the flexible tip, and the working channel(s) enable insertion of surgical tools to perform various tasks. In order to further decrease surgical invasiveness, it is desirable to implement smaller diameter endoscopes with smaller working channels, hence many procedures are carried out with endoscopes having working channels in the range of 1-5 mm. A labeled diagram of an endoscope is provided in Figure 1.3.

Figure 1.3. Endoscope with an exploded photograph of the tip containing: (A)working channels, (B) light sources, (C) camera and (D) endoscopic tool tip.

A novel surgical technique known as natural orifice transluminal endoscopic surgery (NOTES) has recently gained popularity and success as a minimally invasive technique. During NOTES, the surgeon passes a flexible endoscope through a natural orifice, *e.g.*, the mouth or anus, and makes an internal incision in order to access an internal surgical site, thereby completely eliminating the need for external incisions. Such a technique provides surgeons with the ability to perform internal surgeries in the abdominal cavity without making any external incisions, providing numerous patient and caregiver benefits as discussed previously. NOTES has been identified as the next step in the advancement of MIS [4, 7, 10], and a tremendous amount of clinical research is being done to expand the capabilities of NOTES procedures.

1.3 An Experimental Minimally Invasive Technique

To date, access to the abdominal cavity during NOTES has been accomplished by direct puncture gastrotomy, *i.e.*, an incision is made directly through both the mucosal and muscular layers of the stomach wall [11] (see Figure 1.4). A novel method for transgastric access during NOTES, referred to as a self-approximating transluminal access technique (STAT), is currently under development at The Pennsylvania State University Hershey Medical Center [5, 11]. During this experimental procedure, the endoscope is inserted through the mouth and a small internal incision is made in the inner lining (mucosa) of the stomach, usually via electrocautery device, *e.g.*, needle knife. The surgeon then tunnels between the mucosa and muscular layer of the stomach wall, creating a submucosal tunnel. Once the tunnel has reached a sufficient length, the surgeon makes an incision in the muscular tissue of the stomach, thereby achieving access to the abdominal cavity. A diagram of the tunneling procedure is shown in Figure 1.5.

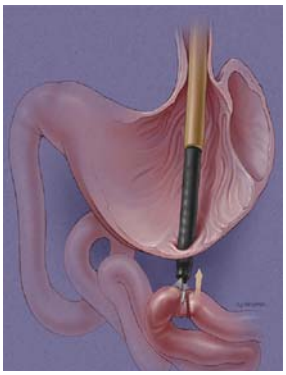

Figure 1.4. Direct puncture gastrotomy: a single incision is made through the stomach wall to access the abdominal cavity [12].

Submucosal tunneling creates an effective seal between the acidic interior of the stomach and the abdominal cavity, preventing unwanted leakage. Self-closure of the outer seromuscular incision is accomplished without the use of sutures or clips, therefore only the mucosal incision must be mechanically sealed. This procedure provides an effective seal between the stomach and abdominal cavity, completely eliminating the need for external incisions and requiring only one internal suturing

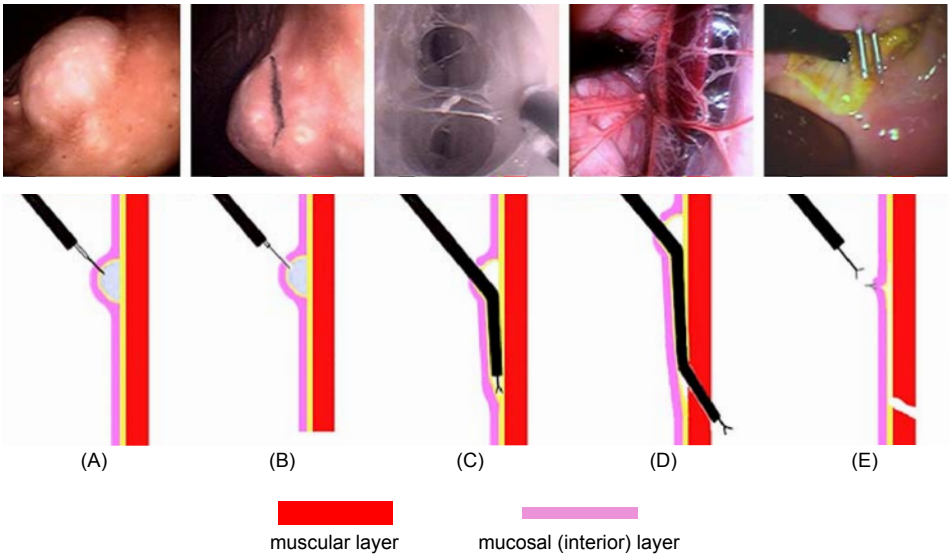

Figure 1.5. Steps for the self-approximating transluminal access technique (STAT). In sequence, the endoscope is initially inside the stomach (A), an incision is made in the mucuosa (B), the mucosa and muscular layers of the stomach are separated by tunneling (C), an incision is made in the muscular layer (D) and (E) the endoscope is retracted and the internal mucosal incision is closed, modified from [11].

site [11].

The previously described tunneling technique is currently carried out via blunt dissection with the endoscope tip or with a commercially available endoscopic forceps. Initial in vivo testing of porcine models revealed that an average of 27.2±8.7 minutes is required to tunnel the distance necessary (10-12 cm) for effective gastric closure [11]; depending on the surgical procedure to be completed, the tunneling step could constitute a significant portion of the operative time. Tissue dissection, in general, has proven to be an extremely tedious and time-consuming task using modern endoscopic tools. Endoscopic tools in the diameter range of 1-5 mm are not capable of applying large spreading forces, which greatly limits the utility of the tools. An effective dissection tool would be useful during any procedure which requires tissue dissection or a spreading action, including esophageal muscle dissection, retroperitoneal dissection, etc. In order to improve both existing and developing endoscopic procedures, tools must be developed with superior tissue dissection capabilities.

1.4 Endoscopic Tools: Design, Functionality, and Performance

1.4.1 Current Tools

Endoscopic tools consist of three main sections: handle, flexible shaft and tool tip (see Figure 1.6). Tool tips range in function and design from forceps for grasping to probes for electrocauterization. The tool tips are mounted on a long, flexible shaft which bends with the endoscope's flexible section inside the working channel , and the surgeon or an assistant operates the tool with the handle at the other end. The tools can be freely advanced along the longitudinal axis of the endoscope, and are often operated by pull wires which attach the tool tip to the handle.

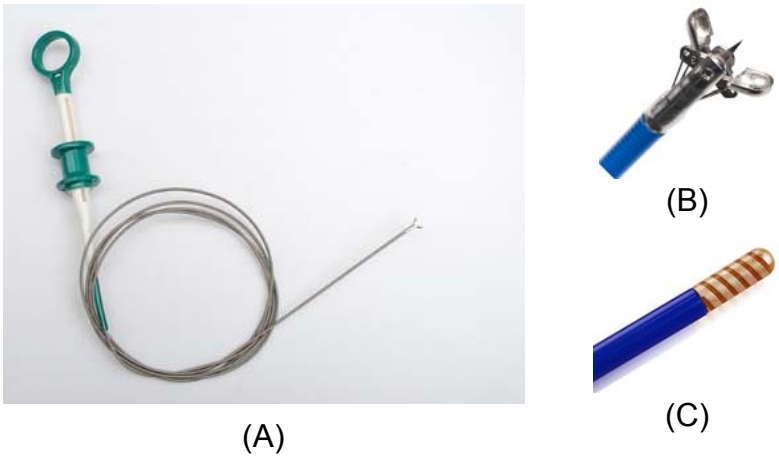

Figure 1.6. (A) Standard configuration of an endoscopic tool with handle, flexible tip and tool tip (modified from [13]), (B) common biopsy forceps tool tip [14], (C) common bipolar cautery probe tool tip [15].

The challenges of endoscopic tool design lie in the size constraints. The tool tip and flexible shaft must fit within the working channel of the endoscope, and demands for decreased invasiveness call for the use of smaller endoscopes during surgery. These smaller endoscopes possess smaller working channels, hence imposing smaller size constraints on endoscopic tools. Emerging endoscopic and NOTES techniques, such as the tunneling discussed previously, seek to minimize surgical invasiveness and increase surgical efficiency by using smaller endoscopes with multiple working channels. Modern "smaller" endoscopes and multichannel

endoscopes often have working channels ranging from 1-5 mm, which dictate the size of the tools.

1.4.2 Multifunctionality

The concept of a single tool being used to perform multiple surgical tasks is referred to as tool multifunctionality. The need for multifunctional tools has been demonstrated, and it is expected that utilizing tools which can perform multiple tasks will improve surgical efficiency and limit the likelihood of iatrogenic injury by reducing the frequency of instrument exchanges [16]. Shortened procedure times and reductions in potential injuries decrease the invasiveness of these procedures. Consequently, medical practitioners from diverse disciplines have sought to implement multifunctional tools to decrease surgical invasiveness and increase operational efficiency.

To date, multifunctional instruments have primarily been developed and implemented for laparoscopic procedures in the 5-10 mm diameter range. Frecker et al. developed and tested several instruments with grasping and cutting multifunctionality in this size range, including 5.0 mm forceps/scissor designs utilizing traditional mechanical joints [17] or compliant sections [18], and some examples are pictured in Figure 1.7. In order to attain multifunctionality, a tool is often required to attain several different kinds of motion. As can be seen from Figure 1.7, complex mechanical assemblies are implemented in the 5-10 mm diameter range to provide complicated motion capability.

Cautery ability has also been implemented as a multifunctional adaptation for laparoscopic tools in several cases. In a summary of clinical trials, it was reported that 166 surgeries were conducted using a multifunctional scissors/manipulator/bipolar electrocautery device, and the significant reduction of instrument exchanges resulted in notable time savings [19]. Another multifunctional laparoscopic cautery device was capable of monopolar cautery, bipolar cautery, suction and irrigation tasks [20]. A novel, finger-like hydraulic gripper with force feedback was designed to limit injury during tissue manipulation [21], and while providing multifunctionality was not the design goal in this case, such a tool could complete many surgical tasks if sufficient dexterity is achieved.

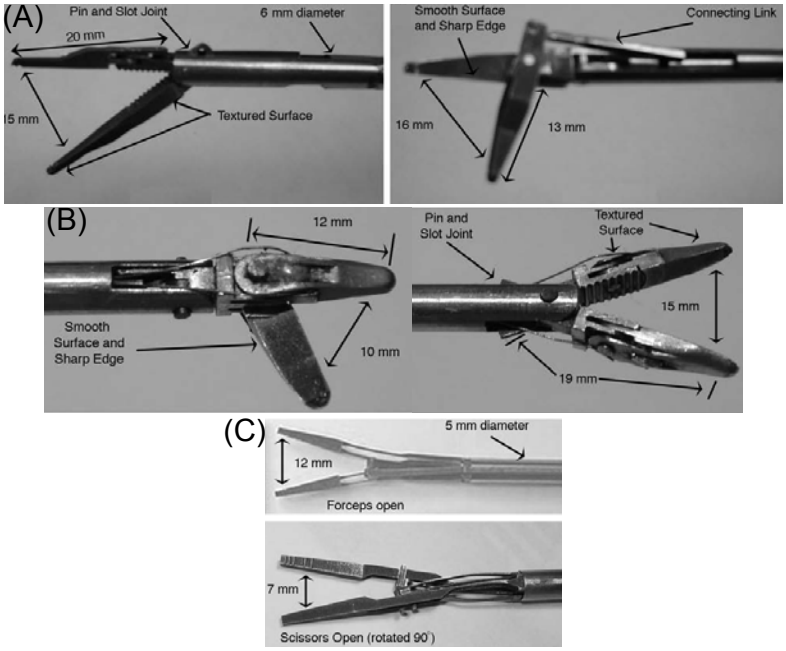

Figure 1.7. Multifunctional tool assemblies consisting of mechanical linkages (A and B) and a compliant members (C); modified from [17].

In the 1-5 mm size range of endoscopic tools, millimeter-sized components with micrometer-sized features become difficult to fabricate and assemble by traditional machining methods. In order to construct functioning (and "multifunctioning") tools in this size range, assemblies must simplified; this is often done by reducing the number of components or implementing compliant mechanisms, *e.g.*, the 5.0 mm compliant forceps/scissors in Figure 1.8 which is operated by advancing or rotating the housing sheath [18].

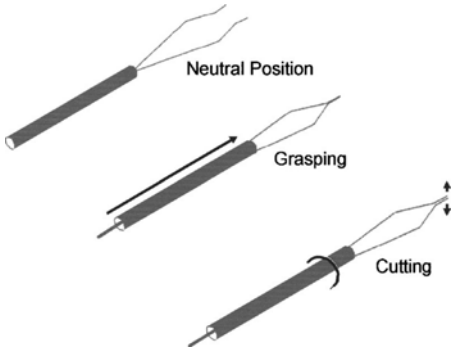

Figure 1.8. A multifunctional, compliant forceps/scissors operated by advancing and rotating the housing sheath [18].

In the specific case of endoscopy, achieving multifunctionality becomes difficult due to size constraints and limited surgical control, *i.e.*, the tool must fit through the small working channel and the tool's available the degrees of freedom are limited to those which can be provided by pull wires. Due to the design challenges, multifunctionality has been extended to endoscopic tools in very few instances. One of the few research efforts on this subject was the design of a 1.0 mm forceps/scissors with potential applications in both endoscopy and laparoscopy [22]. Providing endoscopic tools with multifunctional capabilities is necessary to improve surgical efficiency, and support developing minimally invasive procedures.

1.5 Motivation and Objectives

Recent advances in endoscopy and MIS have created a demand for meso scale tools (1-5 mm) with improved performance characteristics. As the capabilities of endoscopic tools advance, the transformation of endoscopy from a primarily diagnostic to a therapeutic technique continues to gain momentum. Endoscopic procedures do not require external incisions, and smaller scopes are becoming preferential in order to decrease the invasiveness of such procedures. Consequently, it is necessary to develop meso scale tools to be used through these scopes for therapeutic procedures. Furthermore, it is necessary for these tools to be: easily controlled by the operator, of robust design and surgically practical and efficient, including the capability for multifunctionality.

Specifically, the inability to effectively spread and dissect tissue during endoscopic procedures has increased procedure times, decreased surgical efficiency and inhibited the rapid advancement of experimental techniques such as the STAT described previously in Chapter 1. The goal of this research is to design an endoscopic tool with multiple functional capabilities including grasping and spreading with significant force, as well as cautery ability to arrest bleeding and/or cut tissue. The performance of the multifunctional tool design is evaluated using predictive models and experiments. Additionally, another objective is to conceptualize and introduce designs which could potentially provide increased articulation ability and dexterity to the tool.

Chapter 2

Design, Analysis and Fabrication of the Multifunctional Forceps

2.1 Proposed Tool Concept and Design Process

Since tool exchanges have been found to reduce surgical efficiency and increase procedure time, it is desirable to develop tools which serve multiple functions. The focus of this work is on the design of a multifunctional grasper/spreader tool tip which could be used through a 3.3 mm diameter or larger working channel of an endoscope. If a multifunctional forceps could both grasp and spread tissue effectively, it would provide additional versatility to the surgeon and reduce the need for multiple tools and exchanges during surgery.

Two main tool configurations were considered for the design of the multifunctional forceps: compliant mechanisms and traditional pinned linkages. An actuation methodology similar to those used for current endoscopic tools was preferred to promote surgeon familiarity, therefore a manually controlled, wire-actuated operation was selected. Due to the need for high output forces, a pinned assembly consisting of a base mount, two mating jaws, and a connecting pin was utilized. Forceps designs usually include a single set of two wires which control both the opening and closing of the tool (see Figure 2.1(A) and (B)), resulting in poor mechanical advantage (MA) in one loading direction. Tool tips of two commercially available forceps designs are shown in Figure 2.1 (A) and (B). These tools are de-

signed to grasp when the wires are pulled and spread when the wires are advanced, resulting in poor MA in opening. The proposed design concept incorporates a second set of wires (see Figure 2.1(C)) so that both opening and closing actions can be actuated by pulling.

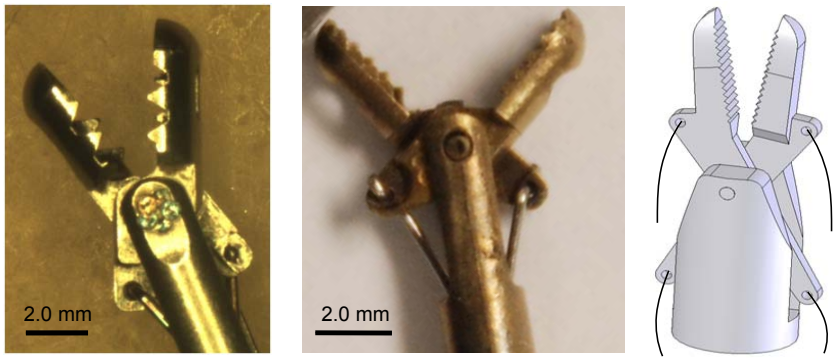

Figure 2.1. Two currently used endoscopic forceps with one set of actuating wires: (A) Olympus EndoJaw Disposable Biopsy Forceps and (B) Olympus RadialJaw Hot Biopsy Forceps along with (C) the proposed design incorporating 2 sets of actuating wires (patent pending, Provisional Patent Application Serial No. 61/237,954).

Given the proposed concept, the jaw and tool mount geometries were designed in order to: (A) efficiently transmit forces from the actuation wires to the tool tip, (B) maximize the load bearing capacity of the jaws and tool mount, and (C) minimize the frictional losses between the actuating wires and tool mount. An iterative process was employed to design both the jaws and tool mount. For the jaw design, an ideal design was first determined by maximizing the MA. This design was then evaluated via FEA, and design modifications were introduced to improve load bearing capacity. The modification and FEA processes were repeated until all performance requirements were met. In a similar manner, an initial design was proposed for the tool mount, and subsequent modifications were introduced to maximize load bearing capacity and minimize the likelihood of frictional losses between the actuating wires and tool mount.

2.2 Design Objectives and Constraints

The design constraints were derived from considerations of fabrication feasibility, surgical practicality, and the load-bearing capacity of the tool. The size of the endoscope working channel imposes stringent size limitations on the forceps tool tip design. Since the tool must be inserted through this working channel, the maximum diameter of the tool must be less than that of the channel. The multi channel scope (Olympus 160 Series Gastroscope) which is currently being used for the STAT procedure has a 3.3 mm working channel, dictating a maximum outer tool diamter of 3.0 mm. Additionally, the tool tip must be able to pass through the rigid, angled insertion port which leads into the working channel (see Figure 2.2); the insertion port is a rigid section which is angled at approximately 120^o from horizontal. The geometry of the insertion port limits the overall rigid length of the tool tip to about 10.0 mm. If the longest rigid section of the tool tip exceeds 10.0 mm, significant deformation will be required to pass the tip through the port. In order to avoid these potentially high stresses, the maximum rigid length of the tool tip was constrained to be below 10.0 mm.

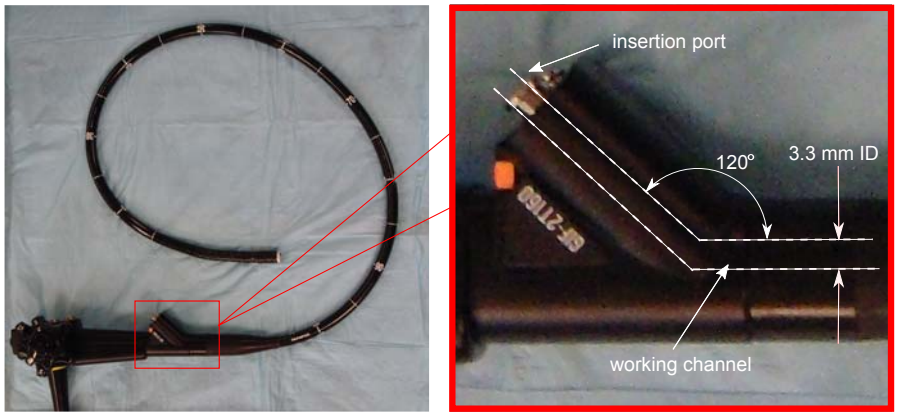

Figure 2.2. Diagram of an endoscope insertion port geometry (Olympus 160 Series Gastroscope).

Certain constraints and objectives were defined to ensure that the forceps design would be practical and feasible for surgical use. The tool must be able to apply sufficiently high forces in order to manipulate tissue during surgery. Tools are used to operate on a variety of tissues, and the forces necessary to manipulate all types of tissue are not well documented. Based on surgical experience, it was estimated

that a minimum of 1-2 N of force would be necessary to effectively grasp/spread loosely connected soft tissue; meaning that each jaw must be capable of exerting 1-2 N at the tip while opening or closing. Additionally, minimum constraints were imposed upon on the inner and outer jaw lengths, as well as the opening range. These requirements were developed to ensure that an adequate amount of tissue could be grasped/spread by the tool. Specifically, in order to maintain surgical feasibility, the forceps must satisfy the following: (1) be able to apply 1-2 N of grasping/spreading force without yielding, (2) be able to open to a minimum jaw-to-jaw angle of 90^o, (3) posses at least 5.0 mm of internal jaw length from pivot point to tip and (4) possess at least 3.25 mm of unobstructed external jaw length.

Wire electrical discharge machining (wire EDM) was selected as the manufacturing method for the tool due to its relatively low cost and its ability to generate some 3D features. This method is quite precise, though certain limitations of the process did constrain the design. The most notable limitations were a minimum thickness requirement of 0.15 mm and a minimum diameter of 0.25 mm for machined holes. A summary of design objectives along with constraints and constraint sources is given in Table 2.1.

Table 2.1. Design Objectives and Constraints.

Objectives: Design a multifunctional tool tip which:
· Opens at least 90^o jaw-to-jaw
· Can apply 1-2 N in grasping and spreading
· Satisfies the constraints below

Constraint:	**Source:**
Max tool tip diameter $D_{max} \leq 3.0$ mm	3.3 mm channel ID
Max rigid length ≤ 10 mm	Rigid insertion port
Internal jaw length $r_{PA} \geq 5.0$ mm	Surgical effectiveness
External jaw length $r_{PA} - r_{PO,y} \geq 3.25$ mm	Surgical effectiveness
Min. material thickness $t_{min} \geq 0.25$ mm	Machining limitations
Min. hole diameter $d_{min} \geq 0.15$ mm	Machining limitations

Note: Corresponding design parameters are shown in Figures 2.3 and 2.4.

The tool tip will operate inside a patient during surgery, therefore, a design which minimizes the risk of fracture is desirable. Since the tool mount acts as the main structural base of the tool tip and connects the assembly to the flexible

tool shaft, failure of the tool mount would increase the likelihood of jaw or pin detachment. Furthermore, it is desirable for some perceptible tool malfunction to precede catastrophic failure so that the operating surgeon could stop the procedure and replace the tool, if necessary.

To provide a "fail-safe" design which noticeably malfunctions before catastrophic failure, the jaws were designed to be the limiting load bearing component of the system. Because the jaws will be connected to two actuating wires, it is less likely that pieces of the jaw would be completely disconnected after failure. Furthermore, the jaw geometry was designed so that the highest stresses would be generated near the pin connection. For such a design, plastic deformation near the pin connection would result from overloading the tool. This would increase the likelihood that the low-tolerance clearance between the pin and jaw would be violated, thus arresting the motion of the jaws and indicating tool failure.

2.3 Design of the Tool Jaws

The jaws were designed to efficiently transmit force from the actuation wires to the tip and to bear loads without failing during surgery. The MA, defined as the ratio of output force at the tool tip to the input force applied by the actuating wires, was maximized by optimizing the placement of the two wire connection points on each jaw. The orientation of the proposed cross-sectional jaw geometry and the design parameters are shown in Figures 2.3 and 2.4. An initial design with an optimal MA was first proposed based on the MA analysis. The load bearing capacity of this design was subsequently evaluated via FEA, and design modifications were introduced to increase load bearing capacity and meet the minimum load bearing objective given in Table 2.1. This iterative process consisting of FEA and design modifications was repeated until performance constraints were met.

2.3.1 Mechanical Advantage Analysis

In order to evaluate tool performance, a means of estimating the force transmitted from the tool to the tissue was developed. Force transmission was quantified by the mechanical advantage (MA), defined as the ratio between the output force (F_O or

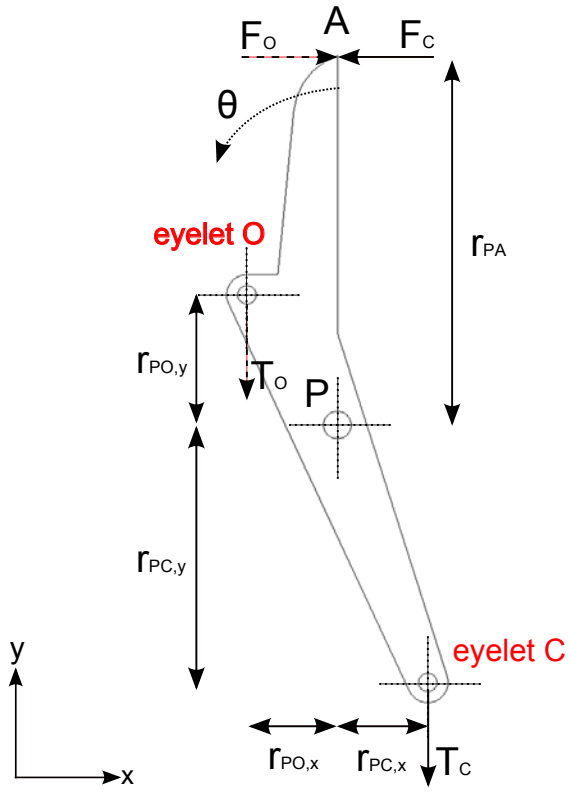

Figure 2.3. In-plane diagram of jaw design parameters and load orientations. Note: θ measured from closed position to inner jaw face.

F_C for opening or closing, respectively) exerted on the tissue and the input tension from the actuating wires (T_O or T_C for opening or closing, respectively). Assuming static equilibrium, an expression for the MA was derived in terms of the design parameters $r_{PO,x}$, $r_{PO,y}$, $r_{PC,x}$, $r_{PC,y}$, r_{PA} and the opening angle θ. The actuation tension (T_O or T_C) was assumed to remain vertical, and the tissue contact force at the tool tip was assumed to be horizontal (x-direction) over the entire angular range (see Figure 2.3). The corresponding expressions for the mechanical advantages in opening (MA_o) and closing (MA_c) are shown in Equations 2.1 and 2.2 respectively:

$$MA_o = \frac{F_o}{T_o} = \frac{r_{PO} \cdot \cos[\arctan[\frac{r_{PO,y}}{r_{PO,x}}] - \theta]}{r_{PA} \cdot \cos[\theta]} \tag{2.1}$$

$$MA_c = \frac{F_c}{T_c} = \frac{r_{PC} \cdot \cos[\arctan[\frac{r_{PC,y}}{r_{PC,x}}] - \theta]}{r_{PA} \cdot \cos[\theta]} \tag{2.2}$$

$$Where\ r_{PO} = \sqrt{r_{PO,x}^2 + r_{PO,y}^2}\ and\ r_{PC} = \sqrt{r_{PC,x}^2 + r_{PC,y}^2}$$

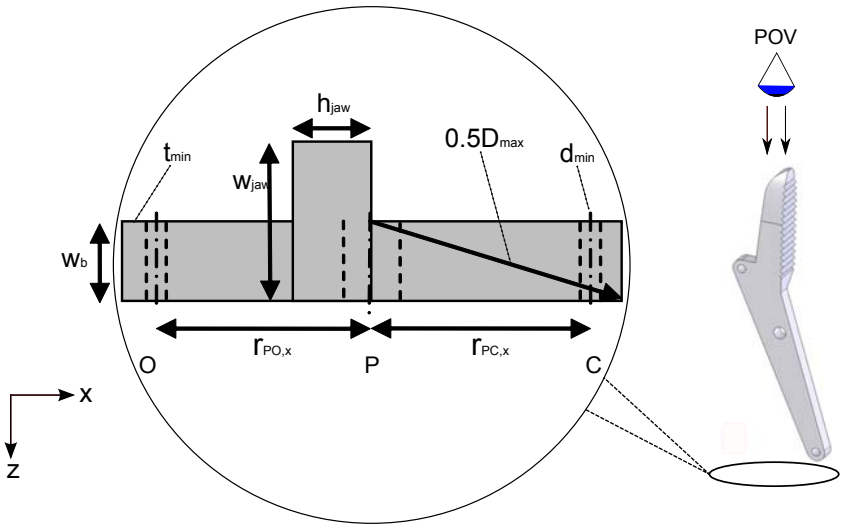

Figure 2.4. Top view diagram of generalized jaw design with point of view (POV) shown.

The MA models presented in Equations 2.1 and 2.2 represent the efficiency of force transmission between the input wires and the tool tip, neglecting frictional losses; these expressions can be used to predict the performance of a given jaw design. Large tool tip forces are necessary at the fully closed position to tightly secure tissue for grasping or to initiate separation of well-connected tissue for spreading. Consequently, the MA in both opening and closing at θ=0 ($MA_o|_{\theta=0}, MA_c|_{\theta=0}$) were the objective functions to be maximized. It should be noted that while the tool performance at the fully closed position was defined as the objective function, the MA over the entire angular range should ideally be high.

From Figures 2.3 and 2.4 and Equations 2.1 and 2.2, it is apparent that the mechanical advantages will be maximized when r_{PA} equals its minimum constraint, and the four quantities $r_{PO,x}, r_{PC,x}, r_{PO,y}, r_{PC,y}$ are equal to their maximum constraints. This reasoning was used to develop an initial design which was later modified to meet load bearing and wire clearance requirements. Considering geometric constraints on the tool diameter, and constraints from machining limitations, the following parameters were set to their limiting values to provide maximized performance: D_{max}=3.0 mm t_{min}=0.15 mm, d_{min}=0.25 mm.

The initial design for the lower sections of the jaws incorporate an offset to facilitate mating of the two jaws. Since the geometry of the upper jaw section was not dictated by any of the design parameters, it was necessary to develop

an upper geometry which was surgically practical and prevented unwanted injury to tissue during surgery. Several curved geometries were proposed and evaluated in collaboration with practicing surgeons in order to determine an appropriate geometry; several examples of the proposed geometries are shown in Figure 2.5.

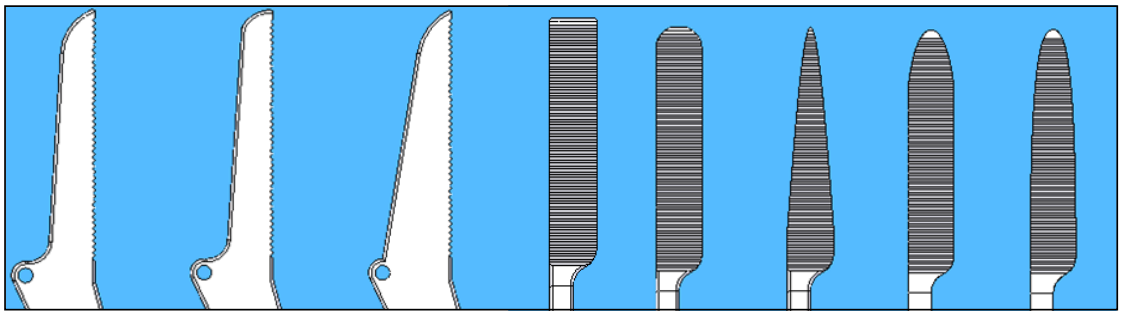

Figure 2.5. Several upper jaw geometries considered for the initial design. Shown on left: outer curvatures. Shown on right:inner profiles)

The ideal outer curvature and inner profile were both chosen to promote dissection capability and prevent iatrogenic injury from accidental puncture. The tool assembly must be thin enough to allow insertion between tightly connected tissue, but blunt enough to prevent accidental tissue puncture. An outer curvature similar to that shown on the far left of Figure 2.5 was implemented; based on surgical experience, this design would allow insertion while preventing puncture in many cases. Similarly, it was determined that a profile similar to that shown on the far right of Figure 2.5 would provide adequate grasping/spreading area while still allowing insertion between tissue and minimizing the likelihood of puncture. To provide additional gripping ability, small teeth were also included on the inner grasping surface. A 3D representation of the initially proposed jaw geometry is shown in Figure 2.6.

2.3.2 Finite Element Modeling of the Tool Jaw

In order to evaluate the surgical practicality of the proposed jaw designs, the maximum load which the jaws could apply without yielding was determined via finite element analysis (FEA). From the FEA results, it was determined whether or not the proposed design met the minimum load bearing requirements (1-2 N) and guided the introduction of design modifications made to improve the load bearing

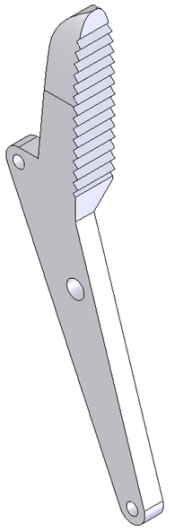

Figure 2.6. 3D representation of initial jaw design including upper and lower jaw geometries.

capacity of the jaws. This iterative procedure was repeated to produce a finalized jaw design.

The jaw model was imported and analyzed with Abaqus (SIMULIA, Providence, RI) finite element software. In order to simplify importation and meshing of the jaw model, two geometrical simplifications were made: (1) the curves on the top outer surface were simplified and (2) the fine teeth on the inside of the jaw were removed (see Figure 3.3.2). As will be shown in the following analysis, stress levels in the upper portion of the jaw remained relatively low compared to the yield stress, therefore these simplifications would not significantly affect the stress distribution or load bearing capacity of the jaws.

Surgical tools are used to manipulate a multitude of tissues with a variety of mechanical properties, therefore it is desirable to model more extreme loading conditions. In order to determine a conservative estimate for the jaw's load bearing capacity, worst-case scenario loading conditions were constructed by simulating jaw tip contact with completely rigid tissue at the maximum desired opening angle θ=45^o for both the opening and closing load cases. It is likely that loading conditions would be much less severe during most endoscopic surgical procedures which primarily involve the manipulation of soft tissue.

Two load cases were constructed to model the opening and closing of a sin-

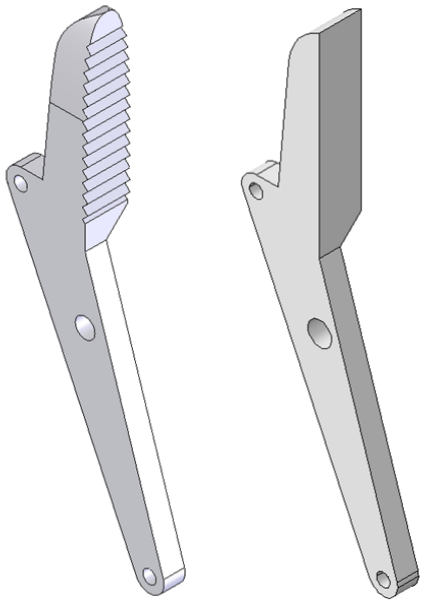

Figure 2.7. (A) Initial jaw geometry and (B) FEA model geometry.

gle jaw. Wire tensions were modeled as pressures applied to one quarter of the inner eyelet area, and contact with rigid tissue was modeled by constraining the displacement of one upper edge in the horizontal (x) direction. Support at the pin hole was modeled by restricting the y, z displacement of the inner area for each case (see Figure 2.8).

Due to its high strength, biocompatibility, and machinability, 316 stainless steel was selected as the fabrication material; relevant material properties are listed in Table 2.2. The model was meshed with 8-node C3D8R hexahedral elements with linear displacement functions.

Table 2.2. Relevant material properties for 316 stainless steel

Property:	**Value for 316 Stainless Steel**
Young's Modulus, E	193 GPa
Poisson's ratio, ν	0.3
Yield Strength, σ_Y	240 MPa

For each load case, the pressure applied to the eyelet was iteratively increased until the von Mises stress reached the yield strength of the material (240 MPa). Between the two load cases, the minimum resultant force necessary to generate

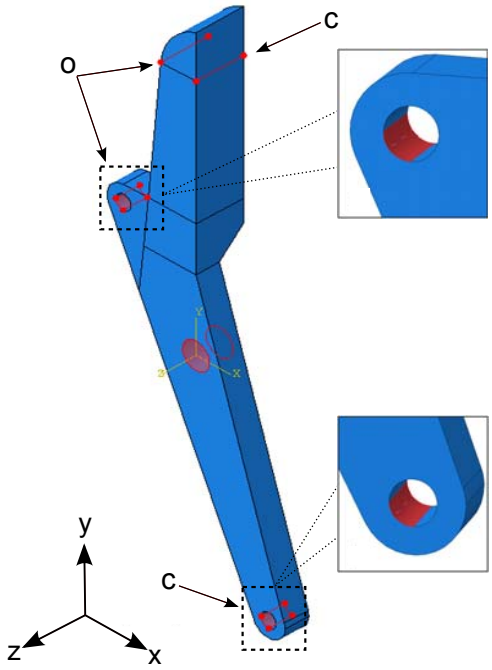

Figure 2.8. Boundary conditions for opening (o) and closing (c) load cases. For opening case, pressure applied at eyelet "o" and displacement of line "o" fixed. For opening case, pressure applied at eyelet "c" and displacement of line "c" fixed. Inner pin hole fixed in y, z directions for both cases.

yield stresses was defined as the load bearing capacity of the jaw. This FEA process was repeated after modifying the main design parameters and other geometrical features, *e.g.*, fillets, eyelet size, jaw thickness, etc. Modifications were made until the load bearing capacity reached the high end of the target range (1-2 N) and the MA remained relatively high; yielding the final design. FEA results for both load cases of the finalized design are summarized in Table 2.3; stress contour plots for the finalized design are shown in Figure 2.9.

Table 2.3. Summary of jaw FEA results. Note: The minimum load bearing capacity of a single jaw is 1.84 N (shown in bold)

	Closing	Opening
Total tension force applied (N)	**1.84**	9.09
Maximum von Mises stress (MPa)	242	240
Location of maximum stress	Pin hole	Pin hole

As Figure 2.9 shows, the maximum von Mises stress occurs at the pin hole in the bottom portion of the jaw for both loading cases. Stresses in the top portion of

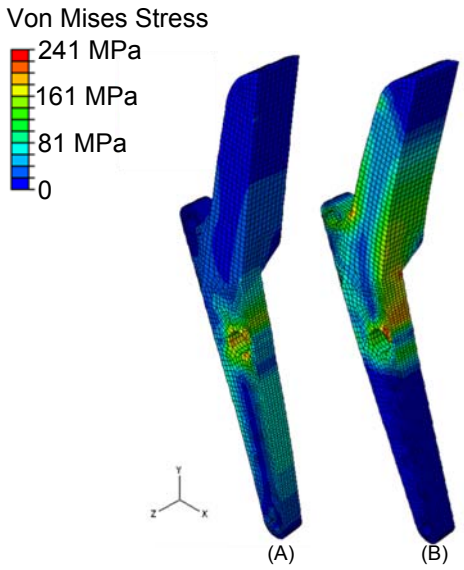

Figure 2.9. Von Mises stress contour plots of the finalized jaw design for closing (A) and opening (B) load cases. Locations of maximum stress at pin holes indicated by arrows.

the jaw remained relatively low compared to the material yield strength, indicating that modifications to the jaw's upper portion would not significantly alter the stress distribution or load capacity of the jaw. As can be seen from Table 2.3, the maximum predicted load bearing capacity of the final jaw design is about 1.84 N. This value meets the previously defined requirement range of 1-2 N.

2.3.3 Finalized Jaw Design and Comparison to Current Forceps

After iterating between design modifications, FEA, and MA analysis, a finalized jaw geometry (shown in Figure 3.3.2 (A)) was reached. The design parameters for the finalized design are listed in Table 2.4. These parameters can be used in the MA models (Equations 2.1 and 2.2) to predict the performance of the tool tip.

In order to evaluate the potential utility of the proposed design, the MA model for the design was compared to the MA for a forceps which is currently used to perform the previously discussed dissection procedure (see Chapter 1, Section 1.3). Currently, the Olympus EndoJaw (Figure 2.1 (A)) and the Olympus RadialJaw (Figure 2.1 (B)) are two of a few endoscopic forceps used to perform these dissection

Table 2.4. Design parameters of final design.

Parameter	Final Value (mm)
r_{PA}	1.22
$r_{PO,x}$	1.75
$r_{PO,y}$	1.22
$r_{PC,x}$	1.22
$r_{PC,x}$	3.5

Note: Corresponding design parameters shown in Figures 2.3 and 2.4.

procedures, therefore these tools were chosen for comparison.

Assumptions used for the MA analysis of both commercial products were identical to those used for the previously discussed analysis, including vertical input tensions and horizontal contact forces. A generalized configuration, which is valid for both tools, including force orientations is shown in Figure 2.10 (B). Because the opening and closing actions of the EndoJaw and RadialJaw are actuated by only one set of wires, expressions for MA_O and MA_C coincide. Furthermore, since both tools have similar assembly configurations, the resulting expressions for the MA of the EndoJaw and RadialJaw are:

$$MA_{C,O} = \frac{F_{O,C}}{T_{O,C}} = \frac{\cos(\theta) \cdot r_{PO,x} + \sin(\theta) \cdot r_{PO,y}}{r_{PA}} \tag{2.3}$$

Digital photography was used to measure the geometries of the EndoJaw and RadialJaw. Geometrical measurements of the EndoJaw were conducted via an optical microscope and were accurate within 1 μm (see Figure 2.10 (A)); measurements of the RadialJaw were conducted via a digital camera (Nikon D80, 10.2 megapixels) and were accurate to within 50 μm. A summary of the geometrical properties of the EndoJaw and RadialJaw is presented in Table 2.5.

Table 2.5. Geometrical parameters of two commercially available products.

Parameter	EndoJaw (mm)	RadialJaw (mm)
r_{PA}	3.680	4.08
$r_{PO,x}$	0.480	0.53
$r_{PO,y}$	1.535	1.88

Note: Corresponding design parameters shown in Figure 2.10 (B).

Figure 2.11 contains plots of the MA model (A) and the improvement in MA (B)

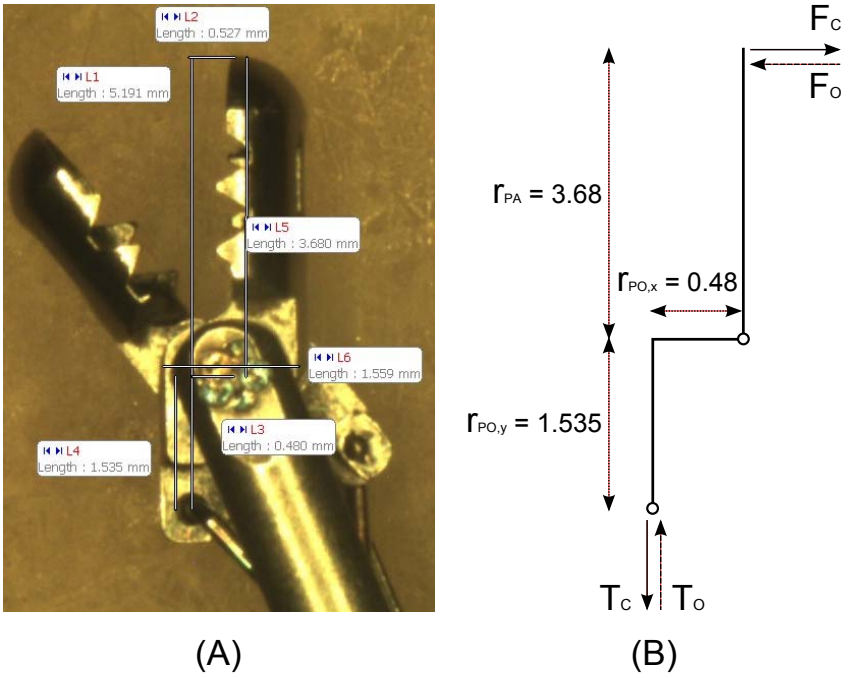

Figure 2.10. (A)Measurements of Olympus EndoJaw geometrical parameters and (B) schematic of load orientations and relevant measurements for opening O and closing C cases.

for the proposed tool design relative to the commercially available products. Due to interference with the tool mount, the EndoJaw and RadialJaw were only able to operate within the limited approximate angular range $0 \leq \theta \leq 60^o$, while the proposed design is predicted to function throughout a larger range of $0 \leq \theta \leq 145^o$.

It is apparent from Figure 2.11that over the entire working range $0 \leq \theta \leq 60^o$, the predicted closing MA of the proposed jaw design is significantly higher than that of both the EndoJaw and RadialJaw. The model also predicts that the opening MA of the proposed concept will be higher than the opening MA of the EndoJaw in the range $0 \leq \theta \leq 60^o$, and higher than that of the RadialJaw in the range $0 \leq \theta \leq 45^o$. The models predict that the RadialJaw will outperform the proposed design in the range $45 \leq \theta \leq 60^o$, but the limited operation range of of the RadialJaw is detrimental to the tool's utility; the ability of a tool to open wider will enable the proposed design to spread tissue farther apart and grasp larger amounts of tissue during surgery.

At the fully closed position ($\theta = 0^o$), the estimated performance of the newly proposed design is approximately 87% higher than the currently used designs.

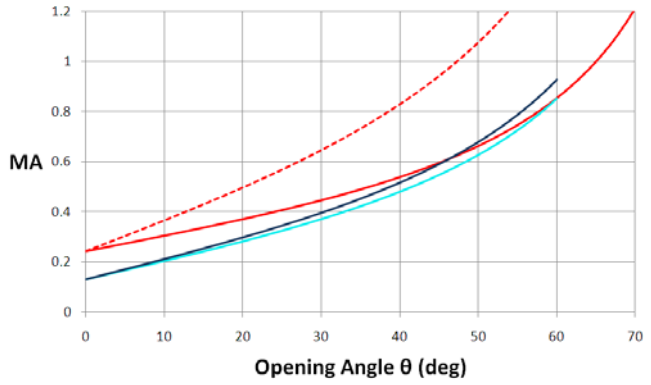

(B)

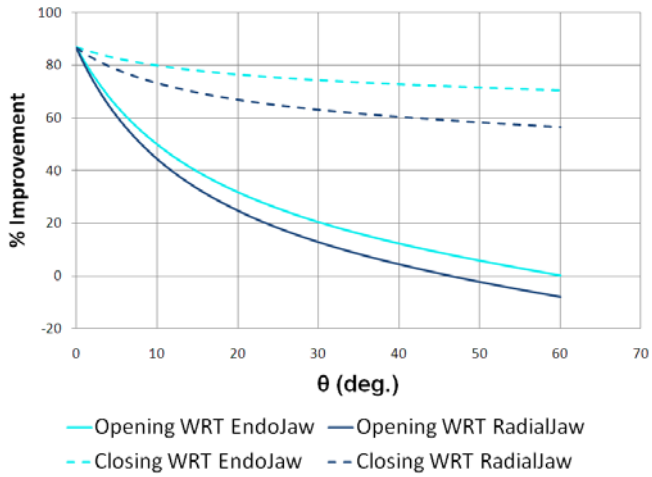

(A)

Figure 2.11. (A) Variation of mechanical advantage (MA) with opening angle θ for proposed final design (red) and currently used products (cyan-EndoJaw, blue-RadialJaw). (B) Percentage improvements in MA relative to EndoJaw(cyan) and RadialJaw(blue). Note: Commercial designs and proposed deisgn shown in Figure 2.1.

This model indicates that if frictional losses from the pinned connection and wire interference with the tool mount are not considered, the proposed design has the potential to transmit higher forces from a given input tension.

2.4 Design of the Tool Mount

2.4.1 Objectives and Initial Concept

A tool mount was designed to secure the jaws and provide ample clearance for rotation. The objective was to design a mount which exhibited maximum load bearing capacity and caused minimal frictional interference between itself and the actuating wires. The initial design concept was a single piece mount consisting of two supports and a clearance hole for the actuating wires (see Figure 2.12). To minimize frictional losses between the actuating wires and the tool mount, the area of the clearance hole was maximized.

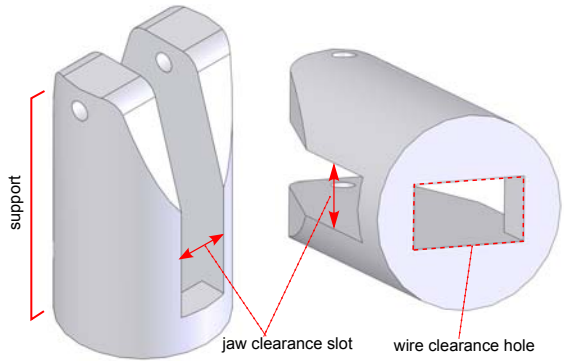

Figure 2.12. Single-piece concept for tool mount with two supports and a wire clearance hole.

The final tool mount design was reached by implementing an iterative design process similar to the process used for the jaw design described in Chapter 2 Section 2.3. The load bearing capacity of the initial design was evaluated via FEA and the results were used to guide design modifications to the support, clearance hole, and base geometries. The process was repeated until a design was reached which possessed a sufficiently higher load bearing capacity than the jaws and large opening area for wire clearance. Similarl to the jaw design, 316 stainless steel was selected as the fabrication material; relevant material properties are listed in Table 2.2.

2.4.2 Finite Element Modeling of the Tool Mount

In order to accurately represent loadings experienced by the forceps, common surgical loads encountered during surgery must be identified. With endoscopic forceps, tissue is most commonly manipulated by grasping tissue and then advancing or retracting the forceps longitudinally. Lateral bending loads are often encountered if the forceps contacts tissue on one side or the flexible section of the tool buckles. These longitudinal and bending loads would commonly be experienced by the tool mount during surgery, so different load cases were set up to simulate these conditions.

Inherent symmetry of the geometry enabled a simplified analysis of a quarter model to be conducted for each design iteration using ANSYS finite element software. Specifically, two load cases were constructed for each longitudinal and bending condition (see Figure 2.13). Longitudinal tension and compression cases were modeled by applying a pressure to the top or bottom portion of the pin hole, respectively. These longitudinal load cases were designed to simulate load transferred from the jaws to the tool mount via the connecting pin. Lateral inward and outward-bending cases were modeled by applying a negative or positive pressure, respectively, on the upper inside face of the mount. The following conditions were applied to all loading cases:

1. Bottom area of mount fixed in all directions

2. Symmetry boundary conditions (x,z displacement u_x=0 or u_z=0) on faces generated by model cut

The pressure applied to the appropriate area in each case was iteratively increased until the von Mises stress reached or exceeded the yield strength of the material (240 MPa). The minimum resultant force of all load cases necessary to generate yield stress in the mount was defined as the load bearing capacity of the tool mount. After several design iterations, a final design was reached which satisfied the clearance and load bearing requirements. Figure 2.14 shows contour plots of the von Mises stress in the finalized design when maximum allowable loads are applied. A summary of the load bearing results for the finalized design is presented in Table 2.6.

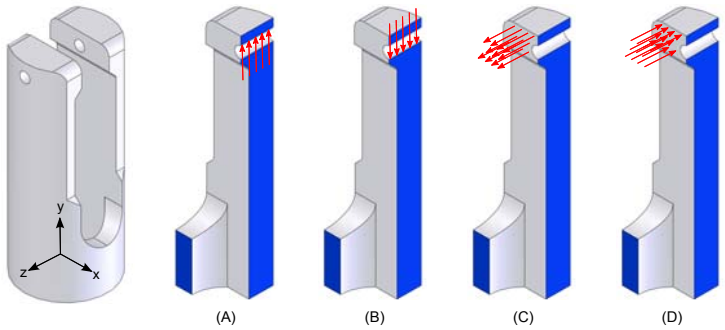

Figure 2.13. Full tool mount model (left) and quarter models with boundary conditions applied: symmetry conditions u_x or u_z=0 (shown in blue) applied to sectioned areas, pressures (red arrows) applied to appropriate areas, and lower faces held fixed (not shown). (A) Longitudinal-Tension, (B) Longitudinal-Compression, (C) Bending-In, (D) Bending-Out.

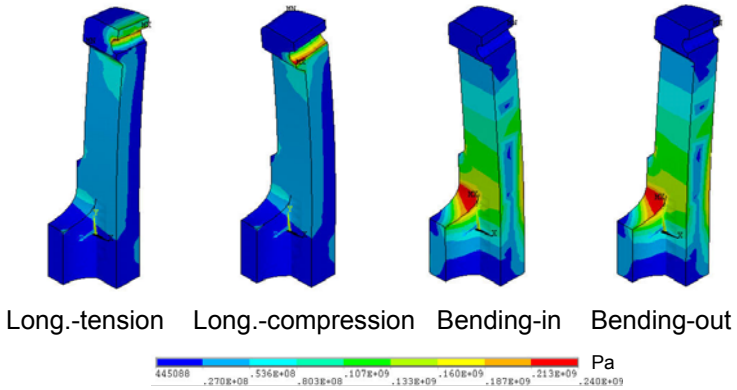

Figure 2.14. Von Mises stress contour plots of finalized tool design subjected to maximum loading in each load case.

As can be seen from Table 2.6, the load bearing capacity (5.5 N) of the tool mount is limited by bending. This indicates that significant lateral loads on the tool mount could cause yielding during surgery. However, the load bearing capacity of the jaws (1.84 N, Table 2.3) is significantly lower than that of the tool mount. This difference in component load bearing capacities indicates that the jaws are likely to be be the limiting structural components of the assembly, providing additional safety in the event of overloading as discussed in Chapter 2, Section 2.2.

Table 2.6. Load bearing analysis results for the finalized tool mount design.

	Max. von Mises stress (MPa)	**Location of max. stress**	**Load bearing capacity (N)**
Longitudinal-Tension	241	Pin hole	82.4
Longitudinal-Compression	240	Pin hole	85.0
Bending-In	240	Base fillet	5.5
Bending-Out	240	Base fillet	5.5

2.4.3 Finalized Tool Mount Design

As shown in Figure 2.13, the finalized jaw design includes several features to limit potential frictional losses between itself and the wires as well as provide sufficient rotation capability to the tool tip. Additional clearance between the jaws and tool mount (jaw clearance slot in Figure 2.12) provided a large maximum opening angle for the assembly 145^o as compared to the maximum 60^o for the Olympus EndoJaw. The final tool mount includes features which help to avoid interference with the jaw and actuating wires. The final design also has a sufficiently high load bearing capacity to prevent yielding during surgery.

2.5 Finalized Tool Tip Design

Two embodiments of the finalized forceps tool tip assembly are shown in Figure 2.15. On the left (A) is shown an assembly consisting of the jaws and mount described previously. On the right (B) is a tool which consists of the previously described tool mount attached to a set of jaws with widened upper sections. Since the location of maximum stress is located in the lower section of the jaw, widening of the upper portion will not appreciably affect stress distributions, and therefore the FEA performed on the jaws with the thinner upper portion is still indicative of actual load bearing capacity.

Introducing an additional jaw geometry to the one previously described could provide a basis for creating a NOTES "toolset". Such a toolset would consist of several tools for performing a multitude of tasks, thereby extending the surgical

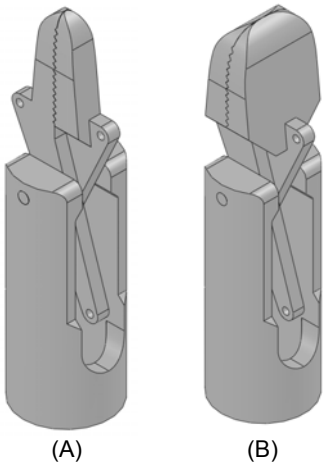

Figure 2.15. Two embodiments of the final tool assembly (patent pending). (A) previously discussed tool mount and jaws for precise tissue manipulation. (B) previously discussed tool mount and widened jaws for manipulation of larger amounts of tissue.

capabilities of NOTES. For these tools, the thinner jaw geometry would be ideal for spreading/grasping tissue in confined areas where the disturbance of other tissues around the site should be avoided. The wider tool embodiment would be used when manipulating larger amounts of tissue.

Chapter 3

Experimental Validation

3.1 Fabrication and Assembly of Prototypes

Three different tool tip prototypes were assembled to independently evaluate several different aspects of the tool tip's performance: a testing prototype to validate the MA model, a cautery prototype to quantify cautery ability , and a finalized prototype for assembly of a working prototype.

The testing prototype was designed and assembled to validate the MA model derived in Chapter 2, Section 2.3. For the testing prototype, the previously described forceps jaws shown in Figure 2.15 (A) were attached to a specially designed testing mount. The testing tool mount has a threaded, extended base with a large clearance slot to minimize contact between the mount and actuating wires, thereby avoiding significant frictional losses and providing consistent input tension (see Figure 3.1).

Due to time constraints and high manufacturing costs, an earlier version of the tool mount was used for the assembly of the cautery tool tip prototype. The finalized tool tip pictured in Figure 2.15 (B) was manufactured for testing and fabrication into a full-scale prototype.

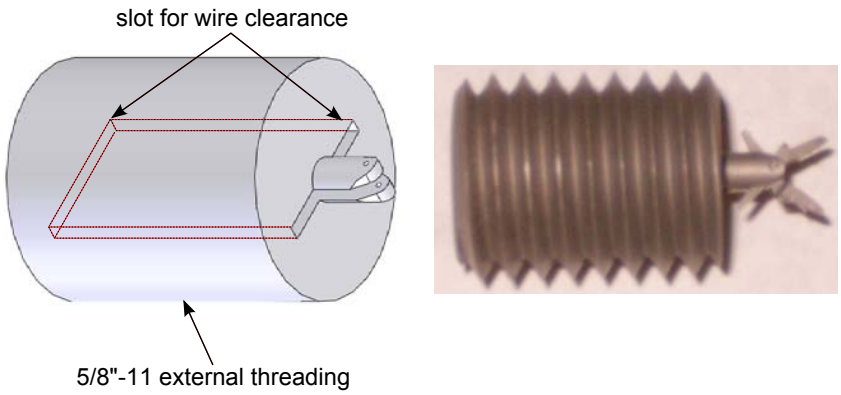

Figure 3.1. Testing tool mount. CAD model (left) and photograph of manufactured testing mount (right) with external threading for fixation and clearance slot for actuating wires.

3.2 Mechanical Advantage Validation and Comparison

3.2.1 Testing Setup and Methodology

A testing setup was designed to simultaneously measure the output tip force and opening angle of the jaws while applying a constant input tension (see Figure 3.2). The testing tool mount was screwed into a nut which was secured to one end of a platform. A pulley was secured at the other end of the platform so that weights could be hung to apply constant input tension to the actuating wires. Nylon cord was glued to the tip of one jaw and connected to a force gauge (Imada DPS-1, 0-4.9 N range, 0.001 N resolution) to measure output force at the tip. A single piece of graphite (0.5 mm OD, 60 mm long) was manually aligned with the clamping surface and glued onto the outer edge of one jaw; a protractor was secured below the assembly to track the opening angle. The jaw opening angle θ was measured by capturing the location of the graphite strip with a camera (Nikkon D80) positioned above the assembly.

For the testing of the opening and closing MA, a pulley and nylon cord was used to connect a known weight to the appropriate jaw eyelet (either "eyelet O" or "eyelet C" in Figure 2.3). Given this known input weight (T_O or T_C, depending on which eyelet was used), the output force at the tip (F) was measured with the force gauge, enabling calculation of the mechanical advantage ($MA_{O,C} = F_{O,C}/T_{O,C}$).

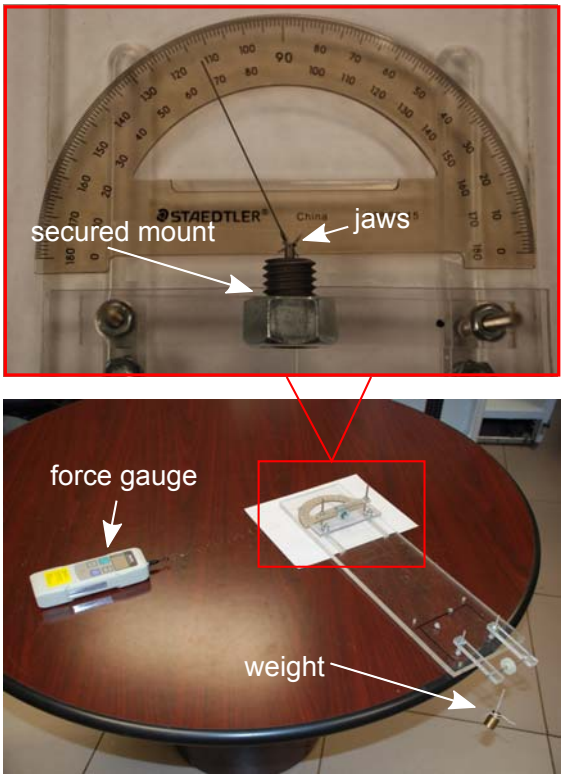

Figure 3.2. Test setup for MA validation with force gauge, pulley, weight, testing prototype and protractor to track opening angle. Note: camera and tripod positioned above.

The jaw was rotated through a range of opening angles by manually translating the force gauge connected to the jaw tip. Due to the stability and geometry of the testing setup, data collection was limited to $0^o < \theta < 80^o$ while closing, and $0^o < \theta < 65^o$ while opening. By using this test methodology, the MA resulting from input at either eyelet O or eyelet C could be determined.

3.2.2 Experimental MA Validation Results

The results of several tests conducted by actuating the forceps through eyelet C are are plotted in Figure 3.3; each set of data points represents one test performed over the working range of the jaws. The experimental results shown in 3.3 agree both quantitatively and qualitatively with the MA model from Equation 2.2, verifying that the MA model is valid for predicting the output force at the tip during closing.

The results of several tests conducted by actuating the forceps through eyelet

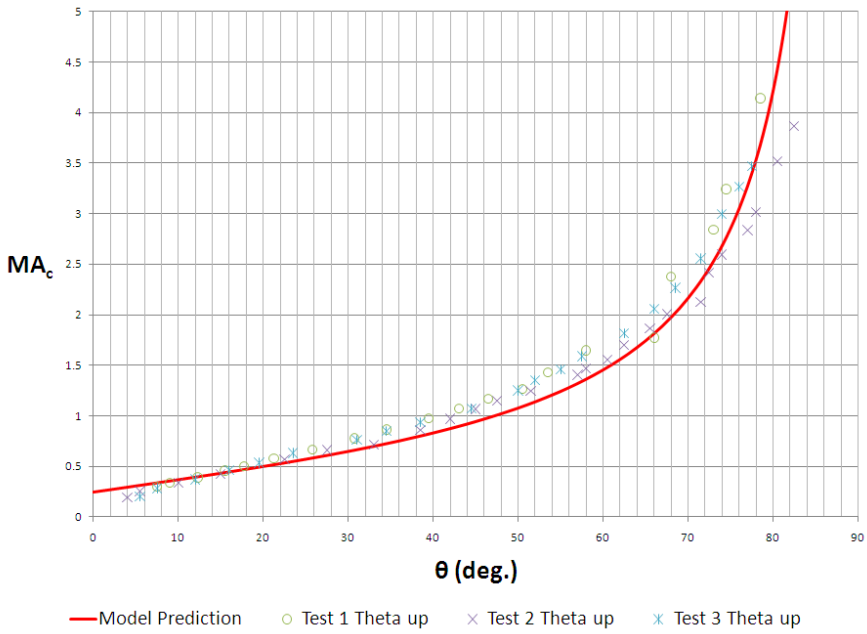

Figure 3.3. MA model (Equation 2.2) and experimentally determined MA when actuating at eyelet C.

O are are plotted in Figure 3.4. The upward trend of all four data sets presented in Figure 3.4 agrees with the opening MA model (Equation 2.1), however, there is an appreciable deviation from expected results for each case. The test was set up such that, regardless of which eyelet was connected, the jaws could be both opened and closed depending on which direction the force gauge was translated. It can be seen from Figure 3.4 that the resulting output force is lower than the model predicts when the jaw is opening (data indicated by blue diamonds) and higher than what the model predicts when closing (multicolored crosses, x's, and asterisks).

The variability in measured output force occurred only when actuating the jaws through eyelet O. To further investigate this discrepancy, one cord was passed through eyelet O and attached to both the input weight and the force gauge. In this way, the force gauge could be oriented so that the forces acting to open and close the jaws posses equal moment arms. For such a setup, the input (weight) and output (gauge) forces must be theoretically equivalent to maintain equilibrium. The test results for this setup are presented in Figure 3.5.

Since the jaw rotation was controlled by translating the force gauge, the fol-

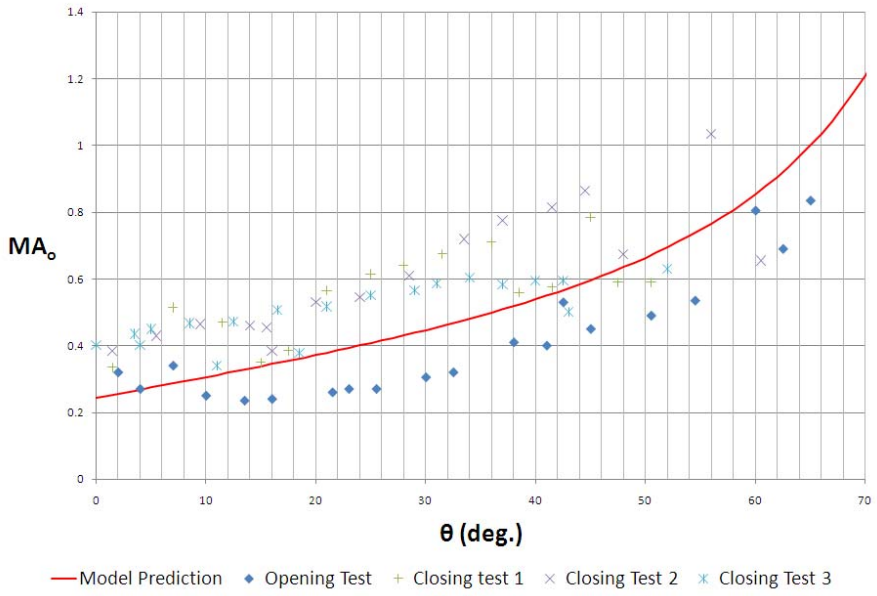

Figure 3.4. MA model (Equation 2.1) and experimentally determined MA when actuating at eyelet C.

lowing is apparent from the results presented in Figure 3.5: 1) during closing, the output force required to close the jaws is higher than expected, and 2) during opening, less output force than expected is required to prevent the jaws from opening. Physically, these results quantify the effects of friction during tool operation. If the jaw is closing, frictional forces will act against that motion, thereby requiring a larger"gauge" force than expected to close the jaw. Similarly, if the jaw is opening, frictional forces will in the same direction as the gauge force, resulting in measured forces which are smaller than expected.

Due to a manufacturing inconsistency, eyelet O is located on a slightly thicker section of the jaws than eyelet C (see Figure 3.6). This caused an out-of-plane moment on the jaw which increased normal forces and friction between the pin and jaws. Consequently, the frictional losses are much more significant when the jaw was loaded at eyelet O. If the additional friction caused by the out-of-plane loading were eliminated, the experimental MA data for opening would shift up and the experimental MA data for closing would shift down. If friction in the pinned assembly were eliminated, all data sets in Figures 3.4 and 3.5 would converge towards the expected values.

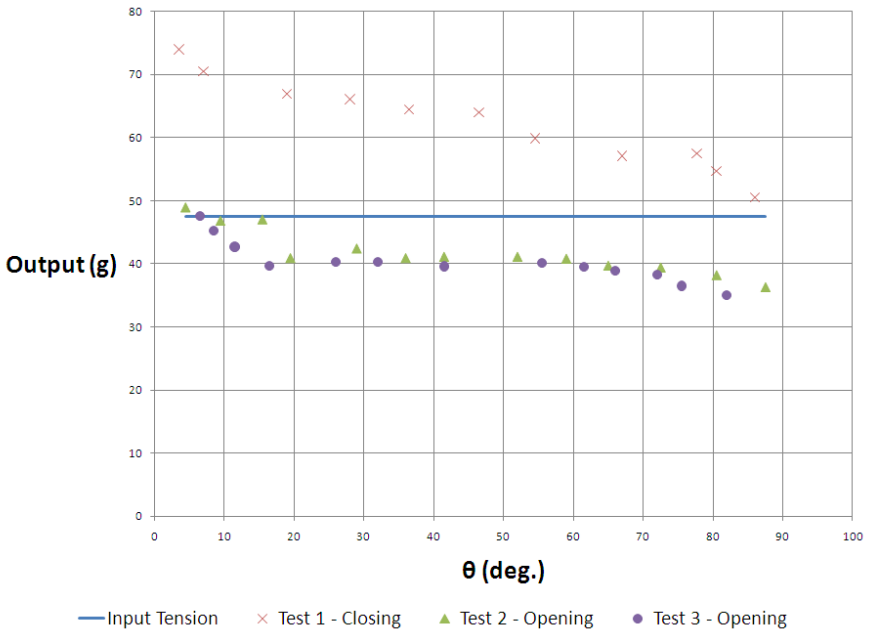

Figure 3.5. Input and output forces for opening and closing when loading at eyelet O. Note: forces given as gram masses subjected to gravitational loading.

Because of the high fabrication and assembly costs, another testing prototype was not made for additional MA model validation. When loaded from eyelet O, experimental results did not coincide exactly with the MA model. However, data generated from testing the jaws in both loading directions from this input eyelet resulted in equally offset data sets, indicating that 1) an accurately machined assembly would perform quite closely to that of the MA model, therefore the MA model is a sufficient approximation to the tool performance and 2) loading orientation of the actuating wires has a significant effect on the performance of the tool tip.

A similar testing setup and methodology were used to evaluate the accuracy of the MA model for the commercial forceps; only the RadialJaw forceps tool was tested. Because a tool mount which eliminated wire interference could not be manufactured for the RadialJaw, the tests were conducted by using tool's own mount. Use of the actual tool mount could potentially contribute to losses between the wires and tool mount. The results of four different tests are shown and compared to the MA model in Figure 3.7. These results follow a similar trend as the model throughout the majority of the RadialJaw's working range, with the

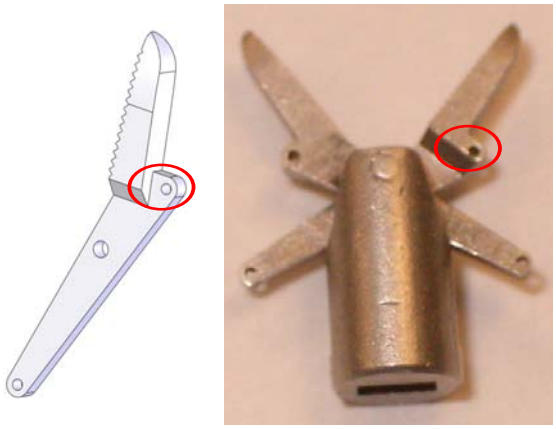

Figure 3.6. Design jaw Geometry (A) and manufactured jaw (B) (patent pending). Note: thicker opening eyelet causes out of plane loading, leading to increased frictional losses.

most significant differences occurring in the range $45^o < \theta < 60^o$.

The discrepancy in the range $45^o < \theta < 60^o$ can be attributed to the interference between the actuating wires and the tool mount. Figure 3.8 contains two of the photographs used to track θ during the RadialJaw tests at both a small angle (A) and a larger angle (B). When comparing the two pictures, it can be seen that the actuating wire has been skewed off the vertical axis for the larger θ in (B) due to interference with the tool mount.

Such increased interference at higher angles results in decreased force transmission to the actuating eyelet, therefore reducing the expected force output at the tip. Because the experimental MA was calculated based on the larger, theoretical input tension, the resulting experimental calculation would actually be larger than that which was calculated and plotted in Figure 3.7. For example, if interference caused an 80% loss in input force between the hanging weight T_{weight} and the actuating eyelet, the experimental and actual MA would be:

$$MA = \frac{F_{out}}{T_{weight}} \tag{3.1}$$

$$MA_{experimental} = \frac{F_{out}}{T_{weight}} \tag{3.2}$$

$$MA_{actual} = \frac{F_{out}}{T_{weight} \cdot (0.8)} \tag{3.3}$$

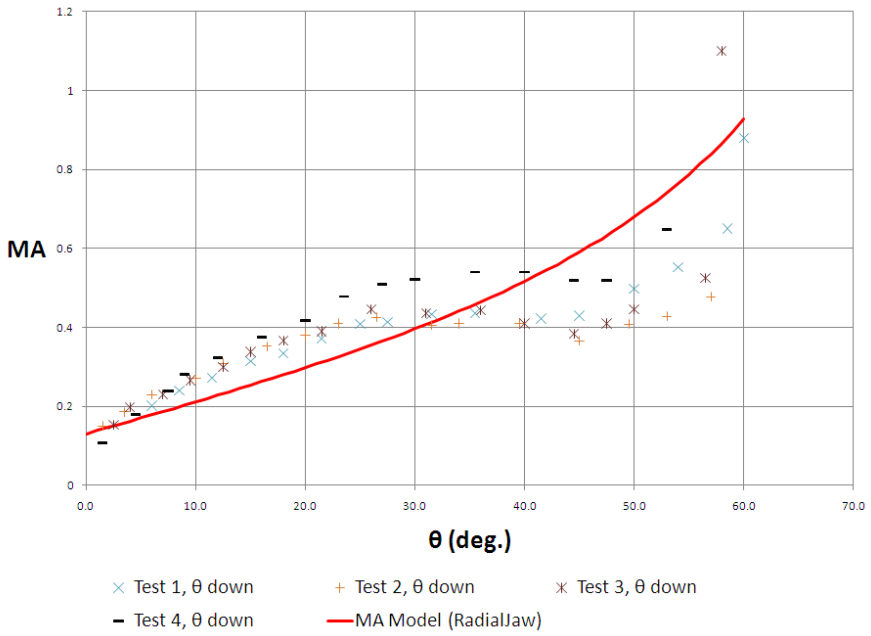

Figure 3.7. Experimental results and MA model of the RadialJaw in closing.

Because the actual input to the eyelet is smaller than it is being assumed to be, the actual MA would be larger than what is calculated. The increased interference at larger angles causes more significant losses in input force, thereby resulting in the calculation of an experimental MA which is lower than it would actually be. Despite this discrepancy, the overall trend of the experimental results agrees well with the model, validating that the MA model is indicative of the output/input relationship for the RadialJaw.

3.3 Pull-off Force Testing and Comparison

By using a specially designed testing tool mount, it has been verified that the MA analysis presented previously is relatively accurate for predicting jaw output/input force relationships when interference between the actuating wires and tool mount is minimized. In order to better compare force application during surgery between tools, tests must be conducted which include the entire tool tip. Pull-off tests were conducted to compare the actual grasping and spreading ability of the proposed design to that of the commercially available RadialJaw. Pull-off tests aim to

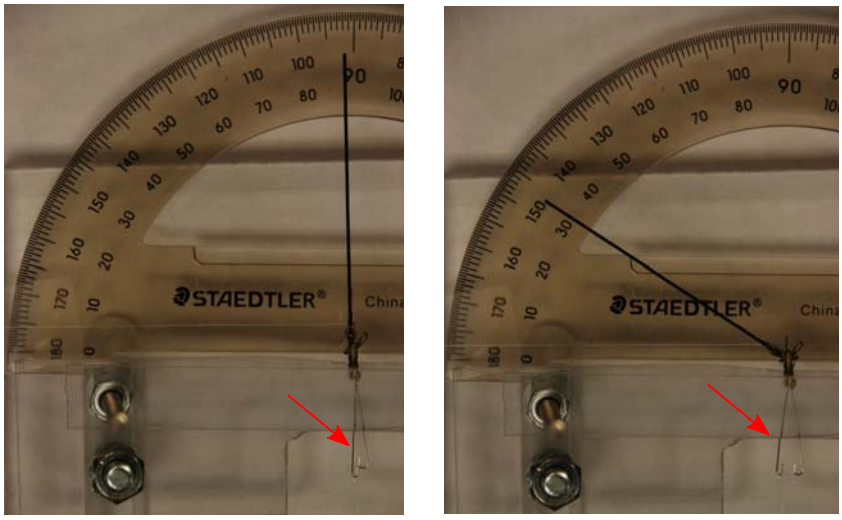

Figure 3.8. Photographs from RadialJaw testing showing the jaw at (A) a small angle $\theta \approx 2^o$ and (B) a larger angle $\theta \approx 57^o$. Notice the actuating wire connected to the input weight is angled off-axis in (B) due to interference created by the tool mount.

quantify the grasping force of mechanism by measuring the force necessary to pull a given material out of the mechanism's grasp.

3.3.1 Testing Setup and Methodology

To perform the pull-off tests, the tool tips were both secured on the platform previously described in Chapter 3, Section 3.2. Weights (100g per wire) were hung to apply constant input tension and the peak force necessary to pull a section of latex tubing (1/8" ID, 1/32" wall thickness) away was measured by a digital force gauge (Imada DPS-1, 0-4.9 N range, 0.001 N resolution). The setup used for the pull-off tests is shown in Figure 3.3.1.

In order to open the RadialJaw the actuating wires must be advanced towards the tool tip. Since the RadialJaw could not be actuated by weights while opening, a second digital force gauge (Imada DS2-110R, 0-500 N range, 0.1 N resolution) was used to apply a compressive force (200g, collectively) to the input wires 0.75" from the tool mount. This method for actuating the RadialJaw could create unequal loading between the actuating wires, but since the input wires were equal lengths, significant differences in loading are unlikely.

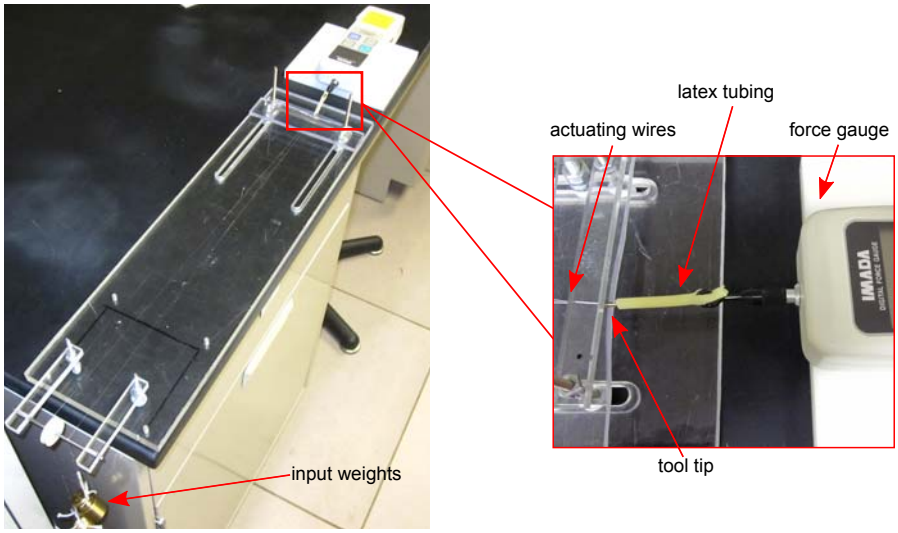

Figure 3.9. Test setup for pull-off measurements (grasping and spreading).

Two tests were conducted for the prototype and the RadialJaw. To test grasping pull-off force, each tool was set up to grasp one layer of the latex tubing while measuring the peak pull-off force. To test spreading pull-off force, each tool tip was inserted into the latex tubing and spread while measuring peak pull-off force. Ten trials were conducted for each trial, additional (5) trials were conducted for the RadialJaw opening test because of the potential variability in input. The results for the pull-off tests are provided in Tables 3.1 and 3.2.

3.3.2 Results and Discussion

It should be noted that the pull-off force is affected by several factors in addition to the grasping/spreading force applied by the forceps. For such a pull-off test, the magnitude of the pull-off force is dictated by:

1. The magnitude of the normal force applied by the forceps
2. The coefficient of friction between the forceps and target material
3. Geometrical features of the forceps and target material

Therefore, while the pull-off test is indicative of grasping force, differences in jaw geometry and materials could affect these results.

Table 3.1. Grasping pull-off test results. 100 gram weight hung from each actuating wire.

Trial	**New Concept (N)**	**RadialJaw (N)**
1	1.531	0.329
2	1.017	0.383
3	1.103	0.305
4	0.998	0.258
5	1.439	0.300
6	1.422	0.290
7	1.020	0.249
8	1.268	0.312
9	1.344	0.279
10	1.179	0.224
Average Pull-off Force ($\bar{p}$)	**1.232**	**0.293**
Standard Deviation (σ)	0.197	0.045
St. Dev. % of Average ($\sigma/\bar{p}$)	15.95%	15.30%

The grasping pull-off results presented in Table 3.1 show that the average force required to pull the latex tubing from the grasp of the proposed design (1.232 N) is much higher than that of the RadialJaw (0.293 N). Additionally, the standard deviations for both sets of data are comparable in terms of percentages of the average pull-off force, indicating that the test methodology between the two tools was consistent. The higher average pull-off force for the proposed concept indicates that this tool could provide higher grasping force than the currently used RadialJaw during surgery.

The spreading pull-off results presented in Table 3.2 show that the average pull-off force for the proposed design (0.676 N) is lower than the average pull-off force for the RadialJaw (1.045 N). The relative standard deviation ($\sigma/\bar{p}$) for each set of tests indicates that the tests conducted for the RadialJaw were even more consistent than those conducted for the prototype design. The low standard deviation for the RadialJaw tests indicates that the method of applying compression to the input wires was consistent. The larger relative standard deviation for the prototype tests is consistent with the tests conduced for the closing tests, which indicates comparable reproducibility for these tests.

The difference in spreading pull-off forces can be largely attributed to the two geometrical features highlighted in Figure 3.3.2. The proposed design incorporates

Table 3.2. Spreading pull-off test results. 100 gram weight hung from each actuating wire.

Trial	**New Concept (N)**	**RadialJaw (N)**
1	0.667	1.064
2	0.695	1.009
3	0.631	0.978
4	0.638	0.980
5	0.662	1.065
6	0.696	1.033
7	0.506	1.053
8	0.790	1.077
9	0.638	1.066
10	0.839	0.962
11	-	1.049
12	-	1.161
13	-	1.085
14	-	1.005
15	-	1.094
Average Pull-off Force ($\bar{p}$)	**0.676**	**1.045**
Standard Deviation (σ)	0.091	0.052
St. Dev. % of Average ($\sigma/\bar{p}$)	13.45%	5.01%

a tapered outer jaw surface to enable insertion between tissue (Chapter 2, Section 2.3), whereas the Radialjaw possesses a straight outer surface with a hole through it. The tapered characteristic of the proposed design reduces the normal force exerted on the latex, thereby reducing the frictional forces which act against the pull-off force. Additionally, the hole through the outer face of the RadialJaw causes the latex tubing to deform around the edges of the opening, thereby increasing the frictional forces. Quantification of these two factors is difficult, but slightly increased pull-off forces for the RadialJaw are expected to result.

By conducting pull-off tests with both the proposed design and the commercially available RadialJaw, the grasping and spreading forces could be quantitatively compared between tools. The new concept outperformed the commercially available tool in the grasping pull-off tests, but required less pull-off force in the spreading tests. Lower spreading pull-off forces can be partially attributed to differences in outer tool jaw geometry which contributed to increased frictional forces for the RadialJaw. Pull-off forces in spreading for the two tools were of similar or-

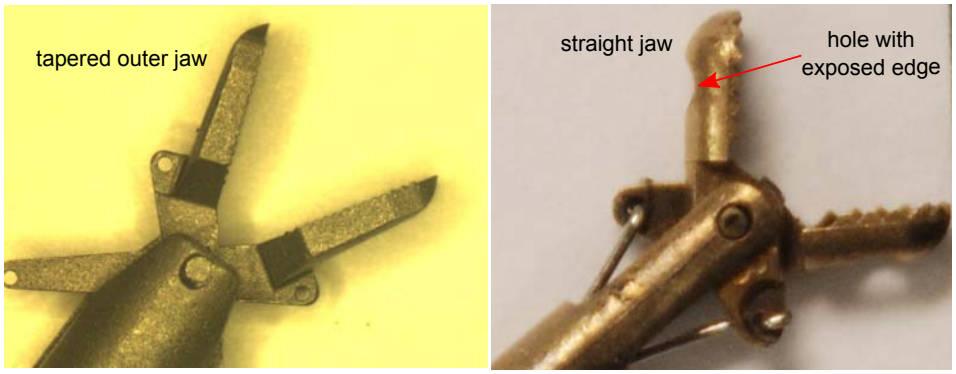

Figure 3.10. Outer jaw geometries of (A) the proposed design (patent pending) and (B) the RadialJaw. The RadialJaw possesses by a level outer surface with a hole and an exposed edge. The proposed design has a tapered outer surface.

ders of magnitude, indicating that actual grasping forces generated by the concept during surgery will be comparable to currently used tools.

Chapter 4

Incorporation of Cautery Ability

4.1 Introduction

During surgical procedures, thermal energy is often applied to cut or stop the bleeding in soft tissues; in general, this process is referred to as cauterization. Cauterization can be implemented to produce several different effects: to cut tissue, remove or ablate tissue or induce hemostasis by causing blood coagulation or vessel sealing [23, 24, 25, 19]. Cauterization is an effect of *intentionally* induced thermal damage; the degree and extent of that damage dictates the resulting physiologic effect. In order to extend the utility of the proposed design concept, it was desirable to provide cautery ability to the tool. If sufficient cautery ability could be implemented, the resulting multifunctionality would provide additional surgical utility and improve surgical effectiveness. A review of modern cautery techniques and tools is presented, followed by an experimental investigation into the extent of tissue damage during cauterization using both the new and commercial tools.

4.2 Review of Cautery Techniques

4.2.1 Electrocautery and Electrosurgery

In the majority of modern cautery techniques, thermal energy is delivered to the tissue via electrical current. These electrically-based techniques can be grouped into two main categories according to the path taken by the applied current: elec-

trocautery and electrosurgery. During electrocautery, a surgical tool is heated by resistive or Joule heating, and the tissue is cauterized through direct contact with the tool. Electrosurgical techniques cause Joule heating of the tissue directly, *i.e.*, the applied current actually passes through the tissue, thereby including the tissue in the electrical current and heating the tissue [23, 26].

Electrosurgery is a more widely used surgical technique and will subsequently be referred to as *cautery* for the remainder of this document. In order to pass electrical current through tissue, all electrosurgical devices consist of a supply and a return electrode. The placement of each electrode and the difference in size between the supply and return electrodes dictate the type of electrosurgical instrument: monopolor or bipolar [27, 23]. Monopolar techniques use a small supply electrode and a grounding pad placed on the patient to complete the circuit, thereby including the patient in the electrical circuit. Bipolar devices consist of small supply and return electrodes located locally at the surgical site, thereby resulting in only a small amount of tissue being included in the circuit. Diagrams of the current paths for monopolar and bipolar cautery devices are shown in Figure 4.1.

4.2.2 Monopolar and Bipolar Techniques

There are benefits and drawbacks to both monopolar and bipolar techniques; the surgical needs and patient condition dictate the appropriate method to implement. Electrical current traveling between bipolar electrodes only passes though the tissue separating those electrodes, thereby yielding a very concentrated and accurate current path as shown in Figure 4.1. The limited current path produces a very high current density and accurate delivery, resulting in highly localized thermal damage with significantly less temperature rise in the surrounding tissue [28]. Monopolar cautery requires more current than bipolar cautery, but deeper penetration of thermal damage can be obtained due to the long trajectory through the body taken by the current [27]. Deep tissue cauterization is desirable during several procedures where tissue damage under the surface of application is required, including the hemostatsis of gastric ulcers [27].

The penetration depth of current density into tissue is also a source of compli-

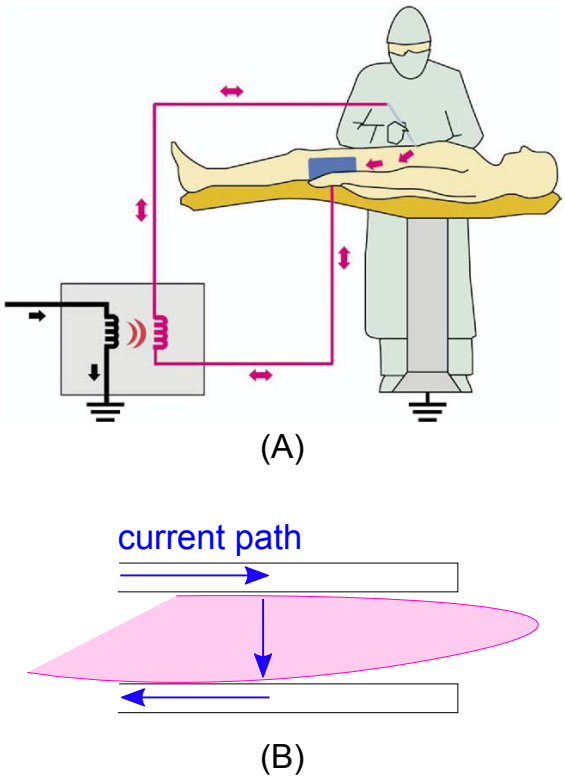

Figure 4.1. Diagrams of current paths for (A) monopolar (adapted from [23]) and (B) bipolar cautery techniques. Note the distance traveled through the body is significantly longer for the monopolar technique.

cations for monopolar cautery, including collateral damage to surrounding tissue, *i.e.*, thermal spread [20, 24]. Passing current through the body can also interfere with the signals of implanted electrical devices, or cause burns when traveling through conductive medical implants [25, 23]. Consequently, the placement of the grounding pad becomes critical to dictate a safe current path, and monopolar techniques are often avoided when a patient has an implanted electrical device, *e.g.*, pacemaker, etc. [23, 25].

The main advantages of monopolar cautery over bipolar cautery are ease of use and a larger penetration depth for treatments. Bipolar devices provide very focused energy delivery with little residual tissue damage and require less current to operate. Depending on the desired clinical outcome, one or both of these methods can be implemented to achieve ideal results.

4.3 Tissue Properties and Damage Mechanisms

The passing of current through tissue causes temperature change by Joule heating. The period of application and the rate of heat generation in the tissue dictates the temperature distribution, and therefore the depth and degree of thermal damage [23]. The time of application depends upon the surgeon and the surgical generator setting; the rate of heat generation in the tissue depends upon the following factors [23, 27, 29]:

1. The density of the current passing through the tissue
2. The resistance (impedance) of the tissue
3. The characteristics of the applied voltage waveform (amplitude, continuous vs. interrupted)

The current density is defined as the current per unit area flowing through a given cross section. The power P, or in this case the heat generation, delivered to the tissue increases with the current density I/a according to the power density law:

$$P = (I/a)^2 \cdot R \tag{4.1}$$

where I is the current in [Amperes], a is the cross sectional area of the tissue, and R is the resistance of the tissue in [Ohms] [30, 23]. Furthermore, the total energy E delivered to the tissue over a given time period t can be defined by

$$E = (I/a)^2 \cdot R \cdot t \tag{4.2}$$

It is obvious from Equations (4.1) and (4.2) that large current densities, long application times, and high tissue resistances increase the energy delivered to the tissue, thereby affecting the temperature distribution and increasing the degree and size of the thermally damaged zone. Cauterization initiates around 60 degrees C with the denaturing of proteins and coagulation of blood in the tissue [31, 32, 27], and at 100 °C the water in the cell evaporates [33, 34]. When heated in excess of 100 C, tissue will either desiccate or vaporize from slow or fast heating, respectively [23].

The rate of heat generation and the resulting temperature distribution in the tissue depend on the electrical and thermal properties of the tissue, which vary significantly with tissue type [26]. Since the mechanism for heat generation is Joule heating, the rate of heat generation is directly proportional to the the electrical resistance of the tissue as shown in Equations (4.1) and (4.2). Additionally, given a rate of heat generation, differing levels of tissue thermal conductivity will affect the temperature distribution and extent of the thermally damaged zone. Less apparent damage mechanisms do occur during electrocautery, including cavitation (rapid expansion and contraction of vapor bubbles), and electroporation (polarization and subsequent depolarization of a cell by an electrical field), but these effects are usually only significant is cellular precision is desired [34].

Modeling and analysis techniques are used to predict electrosurgical outcomes, but accurate prediction remains difficult due to tissue complexities such as temperature dependent electrical and thermal properties [32, 24, 35]. The bioheat equation has served as the fundamental basis for most modern theoretical electrocautery models:

$$\rho \cdot c \cdot \frac{\partial T}{\partial t} = \nabla k \nabla T + q - Q_p + Q_m \text{ [36]} \tag{4.3}$$

Where ρ is the mass density, c is the specific heat, k is the thermal conductivity, T is the temperature, q is the heat source, Q_p is the perfusion heat loss, and Q_m is the metabolic heat generation. Theoretical models have evolved significantly to include temperature dependence of the tissue properties, but development of a comprehensive model is difficult due to nonlinearities and property hysteresis [35]. As an example, it has been documented that above 40 °C, changes in electrical conductivity significantly affect the temperature distribution in tissue; specifically, the tissue conductivity increases and plateaus along with the temperature, but charring of tissue can result the creation of highly resistive, insulating zones [32]. Electrosurgical generators monitor and use changes in electrical properties (specifically impedance) [37] for feedback control of energy delivery, but the fact that tissue properties change over the course of a procedure makes numerical simulations difficult and cumbersome.

Resistive properties of tissue have been documented to change with applied pressure [29]. Larger forces applied to the tissue during cauterization have been

reported to cause larger and deeper coagulation zones up to a certain level, after which the force seems to have little effect [37]. Experiments on porcine spleen tissue have indicated that compression increases the resistivity up to four times when compressed 55%; a finite element simulation of bipolar cautery which included this dependence predicted higher temperatures outside of the electrode-electrode path due to a change in preferential current path around the compressed, resistive tissue [24]. Compression increases tissue resistance and hence, heat generation, in the target zone until the high resistivity diverts current; this phenomenon could explain why the size of the damage zone reached a maximum despite additional force application in [37].

Concerns about patient electrocution have been addressed by elevating the output frequency of electrocautery generators to levels above that which causes neuromuscular contraction. The effects of neuromuscular contraction and ventricular fibrillation associated with electrocution appear to end above frequencies of 100kHz. Modern electrosurgical generators operate between 300-600 kHz, therefore the effects of electrocautery can be limited to the production of heat, avoiding the possibility of unwanted muscle stimulation [26].

4.4 Electrosurgical Equipment

The main components of electrocautery surgical systems are the cautery tools (probes) and the electrosurgical generators used to provide the current. The purpose of electrocauterization ranges from cutting and ablating tissue to simple blood coagulation, therefore cautery systems are designed to provide a range of clinical results. The characteristics of the power delivered to the tissue and the geometries of the electrodes have drastic effects on the resulting thermal damage experienced by the tissue.

4.4.1 Electrosurgical Generators

Modern surgical generators are equipped with a range of power output settings (usually 0-50 Watts, standard 20 Watts) which allow the surgeon to dictate whether the device will be in *cut mode*, *coagulate mode*, or some intermediate mode [29, 23].

The power setting attains different levels of cauterization by modulating the magnitude of the applied voltage and the the waveform (continuous or interrupted) used to deliver the current. The applied voltage dictates the magnitude of the current supplied to the tissue, and the waveform dictates the time of current application. These two factors dictate the rate of heat production in the tissue, which directly relates to the level of tissue damage [29].

A continuous waveform applies a low voltage current continually and is used for cutting, whereas an interrupted waveform applies a high voltage current in short bursts, and is implemented to cause blood coagulation [23, 27]. In this way, similar amounts of energy are applied to the tissue by modulating the application time and waveform magnitude. Interrupted modes significantly decrease amount of time over which current is applied (6% of the application time for continuous waveforms), thereby decreasing the rate of heat generation in the tissue and limiting thermal damage to the tissue [26]. The differences between the continuous and interrupted waveforms are illustrated in Figure 4.2. Electrosurgical generators have become extremely complex and expensive ($20,000+ in many cases). Generators often control and modulate power delivery by tracking tissue damage through tissue impedance monitoring [29].

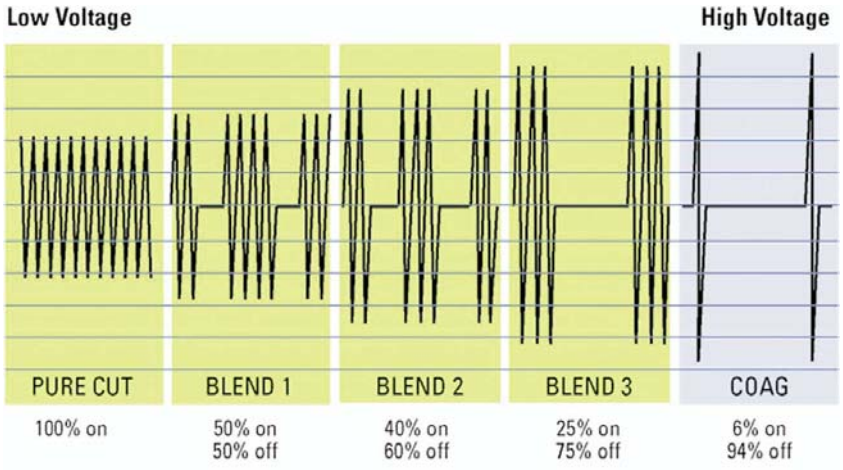

Figure 4.2. Common voltage waveform outputs for electrosurgical generators [23]. Cutting mode characterized by a low voltage continuous waveform, coagulation mode characterized by a high voltage interrupted waveform

4.4.2 Electrocautery Devices

Monopolar and bipolar cautery devices are usually embodied as grasping forceps or simple probes. A plethora of cautery devices are commercially available for laparoscopic and endoscopic surgery. Examples of these common devices are shown in Figure 4.3.

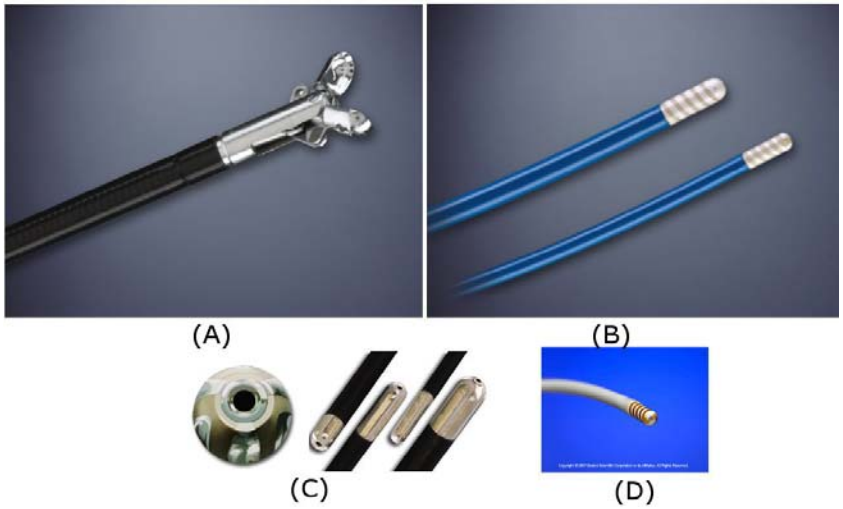

Figure 4.3. (A) Cook Medical monopolar forceps [38]; (B) Cook Medical Bipolar probe [39]; (C) ConMed bipolar probe[40]; (D) Boston Scientific bipolar probe [41].

The magnitude and rate of energy delivery to tissue has been shown to affect clinical results of electrosurgery. Clinical results also depend on the instrument-tissue interface and the method of energy delivery, *i.e.*, the electrode geometries have a significant effect on the resulting damage zone. Even subtle changes in the surface texture or geometry of an electrode have been shown to affect predicted temperature distributions in the tissue [35, 24, 37, 34].

The knowledge that clinical results depend on electrode geometry has resulted in the introduction of a limited number of novel cautery devices which aim to optimize thermal damage zones during cauterization. Because current cautery tools have been improved over years of use, the majority of recent research and development in this area includes implementing some form of multifunctionality, *i.e.*, an ability of one instrument to perform multiple functions. A 10.0mm bipolar scissors/coagulator was utilized in over 160 laparoscopic procedures with minimal complication and positive performance [19]. The device, pictured in Figure 4.4,

consists of scissors and a translating rod as conducting electrodes, enabling biopolar cauterization which was especially effective for hemostasis of vessels under 3.0mm.

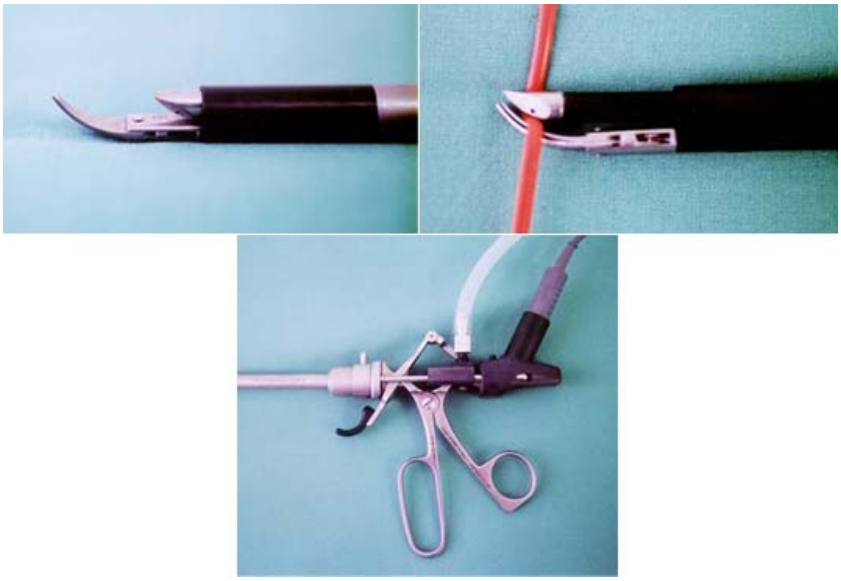

Figure 4.4. Multifunctional bipolar cautery tool and scissors for laparoscopy. Scissors and translating rod act as bipolar electrodes [19].

Laine et al. conducted experiments using standard bipolar probes and a prototype biplanar bipolar device to study how power setting, force application, and application duration related to energy delivery and cauterization [37]. The prototype device consisted of two flat electrodes applied superficially to tissue and rotated about an articulating joint (see Figure 4.5).

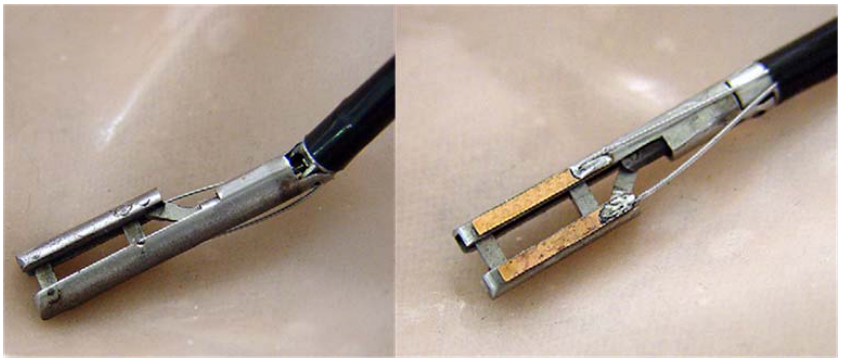

Figure 4.5. Bipolar cautery device consisting of two arms (left) and conducting electrodes mounted on each arm (right) [37].

As opposed to traditional and laparoscopic devices, many endoscopic devices sacrifice control, manipulation and force application ability because of the flexibility and size requirements constraining the design. Creative designs have been introduced to improve performance of endoscopic tools, *e.g.*, a monopolar cautery device which uses an inflatable balloon to maintain contact [30]. The device secures to the outside of an endoscope and consists of an overtube with a conducting mesh situated on the opposite side of the balloon, which inflates and contacts the inside of the esophagus, thereby pushing the mesh electrode onto the other side of the esophagus. The device is limited to esophageal use, and is pictured in Figure 4.6.

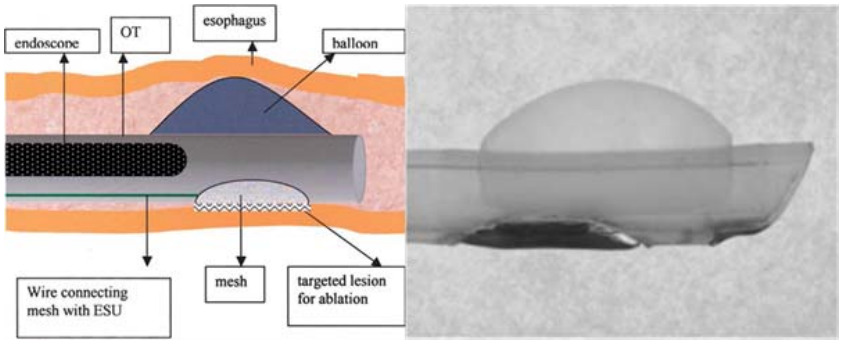

Figure 4.6. Monopolar device used for esophageal cautery consisting of an overtube (OT) with a mesh electrode and inflatable balloon to induce contact; modified from [30].

4.5 Testing of a Cautery Prototype

In order to test the feasibility of implementing a cautery adaptation for the multifunctional forceps design, a cautery prototype was assembled. Due to time constraints and high manufacturing costs, an earlier version of the tool mount was used for the assembly of the cautery tool tip prototype. The earlier tool mount design did not include the additional notches included to prevent wire interference, but the tool tip was able to operate sufficiently for cautery testing. The tool tip was spot welded to a stainless steel spring and retrofitted to a commercially available forceps handle (Olympus RadialJaw Hot Biopsy Forceps, 2.2 mm OD) to conduct the cautery tests. The actuating wires of the commercial handle were attached to the opening eyelets of the new tool tip and used for transmission of the

cauterizing current. The assembled cautery prototype is pictured in Figure 4.7.

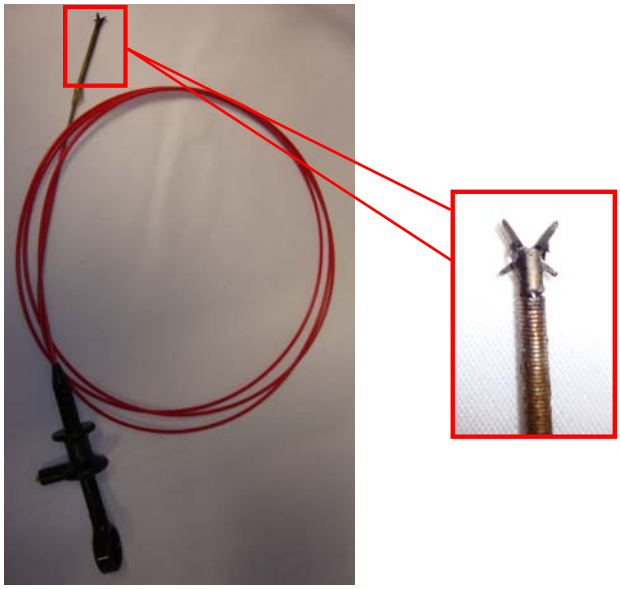

Figure 4.7. Cautery prototype consisting of an early tool tip prototype (patent pending) retrofitted to the handle of a commercial forceps.

4.5.1 Cautery Test Setup and Methodology

The goal of the cautery testing was to compare the cautery ability of the proposed tool design to that of a commercially available device (Olympus RadialJaw). These tests were designed to determine if the new design could effectively deliver energy to the target tissue and to quantify any significant differences in resulting tissue damage.

The characteristics of thermal damage have been investigated extensively and were discussed in Section 4.3. Quantification of thermal damage resulting from cautery is usually conducted by either tracking the resulting temperature distributions in the tissue [24] or visually investigating and/or measuring the size and severity of tissue damage [37, 34, 30]. The optical, electrical, and thermal properties of tissue have been shown to be strongly temperature-dependent above $50^o - 60^o$ [32], consequently the size and extent of the thermally affected zones can be visually differentiated in many cases. In this investigation, visual inspection and measurement of the damage zone was implemented in order to provide an initial comparison between the two tools.

A benchtop monopolar surgical setup was constructed to supply power to tissue samples. Raw pork chops were used as the target tissue; pork chops were selected because they enabled easy sample preparation and became highly discolored after cauterization, making damage zone differentiation more straightforward. The pork chop samples were cut into sections (approximately 15 mm wide x 100 mm long) and placed on an aluminum grounding plate which was used as the return electrode. The electrosurgical circuit was constructed similarly to the traditional bipolar circuit shown in Figure 4.1 (A); the equipment used to construct the circuit for the cautery tests is shown in Figure 4.8.

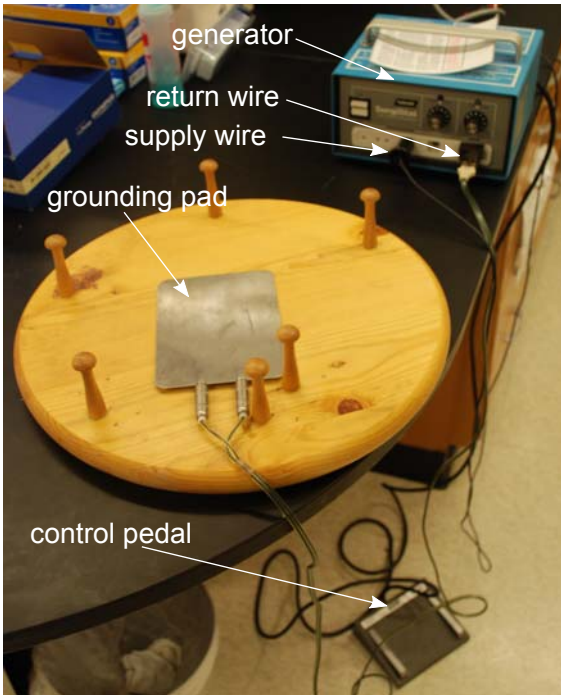

Figure 4.8. Equipment for cautery tests.

The power supply used was a Valleylab (Boulder, CO) SURGISTAT B-20 surgical generator with coagulation and cut mode capabilities. The generator could be operated in either cut or coagulation (coag) mode, at dial settings ranging from 0-10. The modes and dial settings control the power delivered to the tissue; relationships between the modes, dial settings, and resulting power delivery were provided by the manufacturer and are shown in Table 4.1 and Figure 4.9. These relationships were determined using a 500Ω load. For most surgical generators, the power output is strictly regulated in order to prevent injury, therefore these values

provide an approximate ceiling to the power supplied, regardless of the resistance supplied by the tissue.

Table 4.1. Power ratings for SURGISTAT B-20 surgical generator under 500Ω load.

Dial Setting	**Cut** (Watts)	**Coag** (Watts)
0	1.6	0
2	23.1	4.7
4	31.3	10.2
6	42.9	13.8
8	49.3	17.3
10	59.5	22

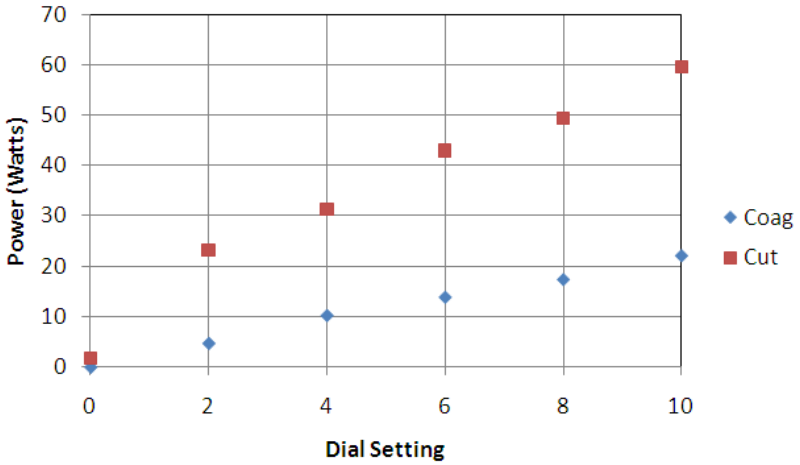

Figure 4.9. Plot of power rating data for SURGISTAT B-20 surgical generator under 500Ω load.

In order to perform initial cautery comparisons between the proposed design and the RadialJaw, tests were conducted using different techniques of application at varying power levels. Three different tests were carried out to test the superficial ablation ability of the tools. For the first test (Test A), the tip of each tool was applied to the tissue with minimal force ten times for five seconds on the coag 6 setting. After observing sufficient consistency in damage zones, fewer test iterations were used for subsequent tests. For the second test (Test B) a an identical procedure was carried out using the cut 5 setting and five test iterations. Lastly, for the third test (Test C), the tip of each tool was lightly applied to the tissue and moved in a circle to create a large damage zone; the coag 10 setting was used and

six tests were performed. Figure 4.10 shows of the tool in the process of cauterizing a piece of tissue and the resulting cautery zone.

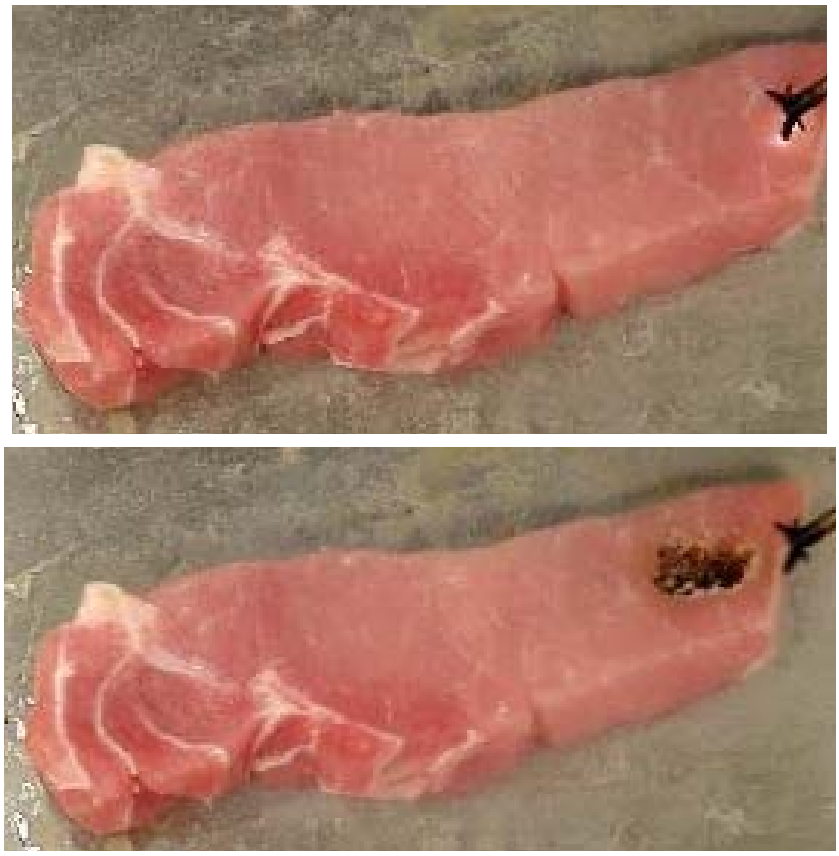

Figure 4.10. Photograph of the tool prototype cauterizing a piece of raw pork (top) along with the resulting cautery zone (bottom).

Following each test, every specimen was photographed next to a length scale using a digital camera (Nikon D80, 10.8 megapixels). Two main damage zones were tracked: (1) an area of high thermal damage characterized by charring or browning of the tissue and (2) a whitened zone of moderate thermal damage surrounding the high damage zone. Figure 4.11 (B) illustrates the differentiation between the two damage zones.

The images were imported into an image processing software (tpsDig v2.14, ©2009 F. James Rohlf). Using the image processing software, the outline of the damage zones were approximated using a series of manually placed points (approximately 30-60 points per outline); the location of the points was determined based on color changes in the tissue. Figure 4.11 shows the specimen photo from

Test A along with the outlines used to define the damage zones. Additionally, two points were marked on the length scale in each photo in order to scale pixels to length dimensions (mm).

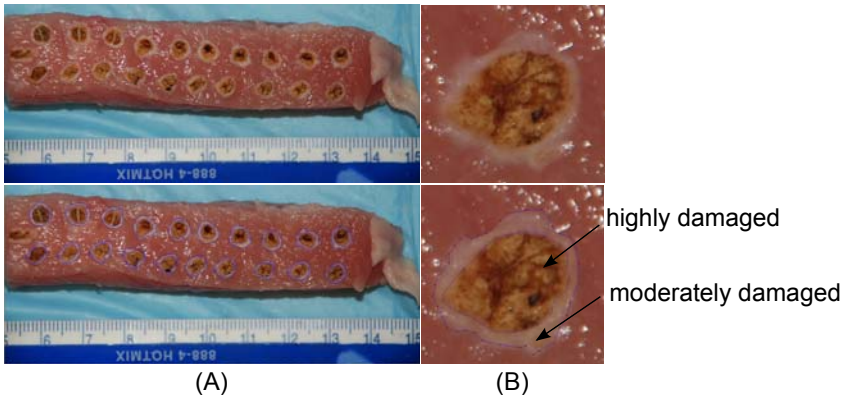

Figure 4.11. (A) Sample specimen photo (top-original, bottom-traced) from Test A. (B) Exploded view of one cauterized section showing the highly (inner) and moderately (outer) damaged zones indicated by arrows.

The pixel coordinates of the two scaling points and all outline points were exported to MATLAB for area determination. A boundary integral method utilizing Green's Theorem was implemented to calculate the area bounded by the polygon defined by the previously placed points. For each curve defined by a set of points (x,y), the area was determined by:

$$A = \frac{1}{2} \cdot \Sigma(y \cdot dx - x \cdot dy) \tag{4.4}$$

where a forward difference approximation is used: $dx = x_i - x_{i+1}, dy = y_i - y_{i+1}$. A MATLAB routine utilizing this method was developed for academic purposes by Dr. H. Joseph Sommer III at The Pennsylvania State University; this routine was used to calculate the areas of the cautery zones.

4.5.2 Cautery Test Results and Discussion

4.5.2.1 Quantitative Test Results and Discussion

The average size of the highly and moderately damaged zones along with the standard deviations are presented in Table 4.2. Additionally, the derived average areas

Table 4.2. Summary of area calculations for three cautery tests

		RadialJaw		Proposed Concept	
		High Damage	Moderate Damage	High Damage	Moderate Damage
Test A	mean area	12.3	22.7	11.5	18.9
	st. dev.	1.7	2.0	1.0	1.3
	mean r_{eff}	1.98	2.69	1.91	2.46
	$r^m_{eff} - r^h_{eff}$	0.71		0.54	
Test B	mean area	10.0	15.1	12.7	18.2
	st. dev.	1.0	1.4	1.9	2.3
	mean r_{eff}	1.79	2.19	2.01	2.41
	$r^m_{eff} - r^h_{eff}$	0.41		0.40	
Test C	mean area	34.7	46.2	35.8	44.4
	st. dev.	10.4	11.8	7.5	8.1
	mean r_{eff}	3.32	3.84	3.38	3.76
	$r^m_{eff} - r^h_{eff}$	0.51		0.38	

Note: Test A - Coag 6, Test B - Cut 5, Test C - Coag 10, circular motion

were used to determine effective circular radii r^m_{eff}, r^h_{eff} for the moderately and highly damaged zones, respectively. The average difference between the effective radii $r^m_{eff} - r^h_{eff}$ was used as a metric to determine how far the outer zone extended from the inner, highly damaged zone.

Since the tool tips were applied at only one location for Tests A and B, the data from these tests is indicative of the extent (size), severity, and shape of thermal damage zones. The data from Test A shows that both effective burn radii are smaller for the prototype than the RadialJaw, while Test B shows larger burn radii resulting from the prototype. The variation in burn zone size between the two tools is more extreme in Test B, reaching a maximum difference of 27% between the inner burn areas. Such a difference could be the result of a higher rate of energy delivery to the tissue, which would induce more rapid damage, thereby effecting the electrical and thermal properties of the tissue. More importantly, the difference between the effective burn zone radii indicate that only minimal changes are realized between the RadialJaw and the proposed design. Furthermore, the fact that this difference is similar but smaller for the proposed design indicates that a more controlled, localized cautery result could be possible when using the proposed design.

Because the tools were moved in a circular motion for Test C, the data can be used to determine the extent of thermal damage beyond the line of contact during a limited application time. The proposed design again exhibited a smaller difference in damage zones, indicating that a more localized burn could be possible.

The data presented in Table 4.2 shows that the proposed design produces similar cauterization results as those produced by the commercially available RadialJaw. Tests A and C were conducted on the coag 6 and coag 10 power settings, respectively. The fact that both of these tests produced results with smaller differences between damage zones indicates that, for lower power application settings, the proposed design produces more localized thermal damage zones. Such a characteristic can be useful if precise cautery treatments are desirable. It has been shown previously that differences in probe geometry induce changes in the characteristics of the damage zones. The differences in results from these tests can most likely be attributed to geometrical factors, which affect the magnitude of current density passing through different parts of the tissue.

4.5.2.2 Qualitative Evaluation and Summary

In addition to the quantitative measurements of damage zones, it is important to qualitatively evaluate the overall prototype performance during the tests. Despite the use only two actuation wires (instead of four), it was still possible to actuate the tool in both opening and closing quite effectively. The prototype proved to be robust and effective when spreading and grasping the target tissue; portions of the tissue could be excised by grasping with the tool and implementing cut cautery.

The charred tissue stuck to the surface of the electrodes acted as an electrical insulator and prevented cauterization at times. After a certain number of tests, charred tissue would have to be cleared from the tools to enable conduction and allow operation of the jaws. The RadialJaw necessitated more frequent cleaning than the prototype because of the hollow cavity on the interior of the jaws. Even when cauterizing with completely closed jaws, cauterized tissue would enter the cavity through the outer hole in the jaws and clog the opening mechanism. The prototype experienced fewer problems with mechanical clogging and sticking than the RadialJaw. Adhesion to the tissue during high-power cauterization occurred for both tools; such problems are often encountered during electrosurgery and

have lead to some select investigations on low-stick designs or specialized electrode coatings [42]. Once the efficacy of the prototype is proven, coatings or other methods to reduce sticking could be implemented.

In summary, the cautery performance of the prototype was comparable to a commercially available design currently used in surgery. The proposed tool design produced zones of high and moderate damage which were comparable in size to those of the RadialJaw. Additionally, the extension of the damage zone from the point of application was smaller for the proposed design, indicating that more localized cautery could be possible. Qualitatively, the proposed design prototype was able to sufficiently grasp and spread tissue while performing cautery activities, and encountered fewer problems with tissue clogging than the RadialJaw.

It has been shown that during cauterization, the characteristics of resulting thermal damage zones are dependent, in part, on the geometry of the electrode [35, 24, 37]. If a set of cautery objectives could be developed for a forceps tool of this size, an optimized outer geometry for the proposed design could be investigated. Depending on the nature of the objectives, the design could be tailored to produce ideal damage zones.

Chapter 5

Incorporation of Articulation Capability

5.1 Introduction

Over the past two decades, there has been considerable interest in the development of meso scale (1-5 mm diameter with micro scale features) mechanical appendages with the ability for dexterous articulation and manipulation. Emerging applications in several disciplines require appreciable forces to be generated by these mechanisms to enable manipulation of target objects. Specifically, the need for small scale, dexterous surgical tools with articulation and manipulation capabilities has driven much of the research in this area. This article evaluates dexterous mechanical systems developed in the past two decades in terms of scalability and force application.

The term articulation refers specifically to the two rotational degrees of freedom for a mechanism as shown in Figure 5.1. Articulation ability is fundamental in providing sufficient dexterity to a mechanical appendage. Articulation about the two axes shown allows access a wider field, thereby significantly increasing the mechanism's utility. The ability to exert force at the tip of a mechanism would further extend functionality, providing improved ability to manipulate objects.

Recent demands to miniaturize dexterous mechanisms have placed challenging constraints on articulators. A diverse set of design configurations originating from

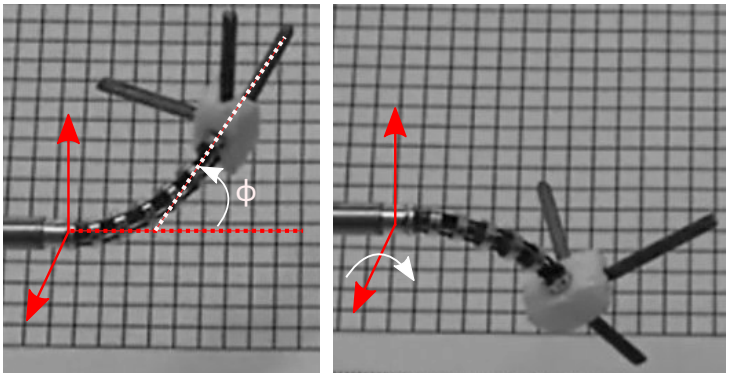

Figure 5.1. Two "wrist like" degrees of freedom shown by articulation to an off-axis angle ϕ [43].

several disciplines has been developed in response to these new constraints. Some designs have been inspired by nature and biology, such as the flexible robotic "trunk" developed by Hannan and Walker [44]. Shape memory alloys (SMAs) have been commonly used for medical applications [45, 46], including laparoscopic tools [47], optical scopes [48], or endoscopes [49, 50]. Systems have been introduced which implement servo-driven pulley systems [44, 51, 52, 53, 54, 55, 56] for applications when advanced control is required. The need for precisely controlled surgical tools in teleoperated surgical systems has driven the development of highly articulated wrist joints and other relevant technologies [57, 58, 59, 60, 61].

A vast majority of the demand for scaled down articulating manipulators has originated from the need for small, dexterous surgical instruments for minimally invasive surgery (MIS). The lack of large external incisions has made MIS a popular alternative to traditional open surgery, but surgical tools often fall short of necessary performance requirements. Medical devices such as endoscopes, which had previously been used exclusively for diagnosis, are now becoming more widely used for surgical procedures [62]. These surgeries require meso scale surgical tools which can articulate around complicated obstacles and effectively manipulate tissue.

The ability to implement these systems for surgical applications at the meso scale has not been sufficiently explored. Many modern meso scale articulating mechanisms have not been evaluated in terms of their ability to generate significant forces at the tip, and larger systems often possess certain design components which prevent scaling. Force requirements for meso scale tools in emerging minimally

invasive surgical procedures are on the order of several Newtons [58]. Categorizing the mechanical configuration and means of actuating these manipulators is useful for analyzing different designs in terms of force application or scaling potential. Mechanisms have been designed which can articulate sufficiently (90^o+), but now the focus must be shifted to optimizing these systems for force application. In order for further progress to be made, design configurations must be evaluated, designed, and optimized for scalability and force application. A summary of design and performance characteristics for tools discussed in this paper is provided in 5.1.

5.2 Review and Classification of Current Articulating Technologies

5.2.1 Manipulator Classification

Unique designs have been implemented to provide dexterous articulation capabilities to mechanical manipulators. In the most general sense, each of these differing systems is linked by two common enabling features: a configuration of mechanical elements (mechanical configuration) and a means to power or actuate that configuration (actuation). The characteristics of each system type enable further classification into subcategories. The mechanical configuration and actuation system of an articulating device are intrinsically interconnected, and therefore one is rarely designed without consideration of the other. Still, a separate discussion of these features is necessary to determine the extent to which the devices in each subcategory can be implemented.

Despite the diversity of these systems, nearly all articulating mechanisms can be classified by their mechanical configuration and actuation methodology through a very simple system (see Figure 2). The configuration of articulating mechanisms is characterized by either (1) continuous backbone(s) which run along the length of the manipulator or (2) discrete segments held together by some connecting force. The means of actuation which have been most commonly implemented are: (1) mechanical drive system, *e.g.*, pulleys or gears, (2) powering an active material, and (3) fluid. Each type of mechanical configuration and actuator classification possesses inherent strengths and weaknesses; these strengths and weaknesses dic-

Table 5.1. Summary of articulating mechanisms (Note: NP - information not provided).

Ref.#, Shown in Figure:	**Mechanical Configuration**	**Actuation**	**Size (OD,mm)**	**Articulation Range (deg.)**	**Tip Force(N)**
[43, 63, 64, 65, 66], 5.1, 5.3(B)	Continuous - SMA	Mechanical	4.2	70+	1+
[44]	Segmented	Mechanical	63-100	NP	NP
[47], 5.3(A)	Continuous	SMA	10	60	NP
[48]	Segmented	SMA-springs	4.0	90	NP
[49]	Continuous - spring	SMA-springs	2.0	60	NP
[50]	Continuous - tubes	SMA-springs	8.0	60	0.05
[52], 5.4(C)	Segmented	Mechanical	4.0	110	NP
[53], 5.4(A)	Segmented	Mechanical	6.0	90	4.9
[54], 5.6	Segmented - ball joint	Mechanical	2.4	90	NP
[55]	Segmented - links, hinges	Mechanical	3.0	60	NP
[56]	Segmented - compliant	Mechanical	5.0	90	NP
[58], 5.9	Segmented - links, hinges	Mechanical	13	NP	NP
[60], 5.10	Segmented - compliant hinge	Mechanical	4.75	NP	0.5
[67]	Segmented	SMA	8	90	1
[68]	Continuous	Fluid - Jets	2.7	NP	NP
[69], 5.8	Segmented	Fluid - Pneumatic	64-90	360+	80-250
[70, 71], 5.4(B)	Segmented - links, hinges	Mechanical	10	90	NP
[72, 73], 5.5	Segmented	Mechanical	12	NP	1-5
[74], 5.7	Segmented - ball joint	Mechanical	6	85	3-5

tate the scaling and force capabilities for each system. The devices listed in Table 5.1 have been categorized accordingly.

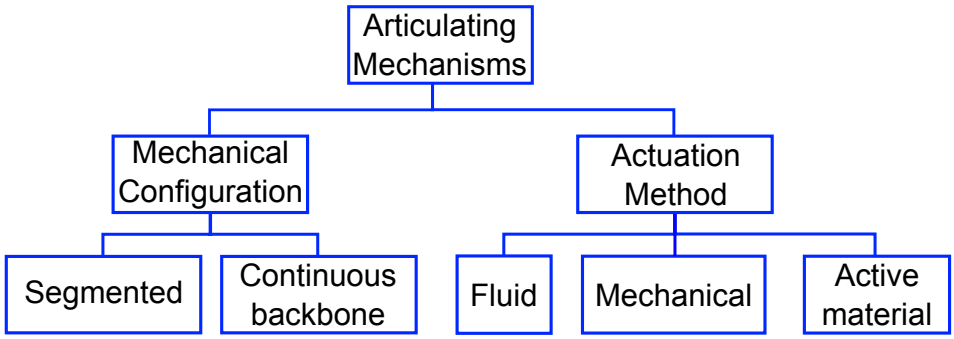

Figure 5.2. Classification of dexterous mechanical manipulators.

5.2.2 Mechanical Configuration

The configuration of an articulating mechanism must serve two functions: (1) it must enable dexterous articulation and (2) it must provide sufficient structural rigidity to the system. Current designs have implemented one of two generalized formats to attain these goals: a continuous backbone or a segmented configuration.

5.2.2.1 Continuous Backbone Mechanisms

Backbone configurations include one or several continuous components oriented perpendicular to the axes of rotation (see Figure 5.3). The backbones provide a high bending stiffness to the mechanism, making such a configuration very popular if stability is required. However, the articulation range of continuous configurations depends on the elastic strains which the backbones can endure. This places significant limitations on the articulation range of the mechanism and necessitates large actuating forces for articulation.

Four NiTi SMA tubes were used as backbones to support a 4.2 mm diameter "snake-like unit" for a surgical robot (see Figure 5.3(B)) [43, 63, 64, 65, 66]. The tubes were actuated mechanically for initial trials, enabling 70^o+ of articulation and about 1 Newton of force was produced at the tip. In a similar setup, NiTi SMAs were used as backbones to support and actuate a 10 mm diameter laparoscopic forceps by inducing the shape memory effect via resistive heating (see Figure

5.3(A)) [47]. The 10 mm tool was able to articulate 60^o off axis, but no data on force applied at the tip was provided.

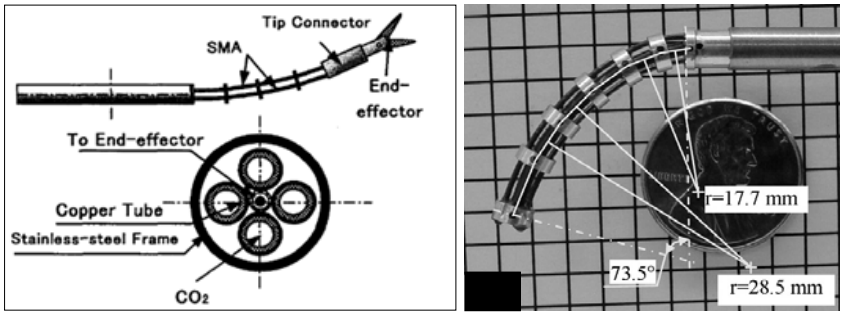

Figure 5.3. Continuous SMA backbone/actuating wire configurations with (A) 10 mm [47] and (B) 4.2 mm [43] outer diameters.

These and other continuous backbone configurations require large elastic deformations of their components in order to enable sufficient articulation. Miniaturizing the backbones allows increased compliance, making actuation easier. However, such miniaturization creates a tradeoff scenario between articulation ability and structural rigidity, thereby severely limiting the potential utility of these systems.

5.2.2.2 Segmented/Discrete Mechanisms

Segmented manipulators are made up of discrete components whose size, shape, orientation, and connectivity affect the overall function of the mechanism. The mechanical behavior of the system as a whole is dictated by how adjacent segments are connected and the number of segments in the mechanism. The performance of segmented configurations can be changed significantly through minor design changes in the discrete elements, or altering how those elements are connected. This characteristic provides broad performance versatility to any segmented design, which certainly contributes to their popularity. The mechanical performance is most sensitive to the following design aspects: the geometry of discrete segments, the connection method between adjacent segments, and the number of segments included. These three aspects of the design can be modulated to significantly change the resulting mechanical behavior of the system, though adjacent element connectivity is the most commonly changed.

Several methods of connecting adjacent segments have been employed for discrete structural designs, including traditional hinges, compliant flexure hinges, and "fitted" configurations. Segments which are directly connected via a traditional pinned hinge have very predictable and consistent motion (see Figure 5.4) [44, 52, 53, 70, 71]. Such hinges can also limit the available degrees of freedom (DoFs), increase the necessary actuation forces due to friction, and make scaling down difficult. These configurations possess an inherent barrier to downsizing, due to difficulties in assembling and machining the hinge components at reduced scales. Development of advanced fabrication techniques will be necessary to enable further miniaturization of segmented systems which utilize traditional hinges.

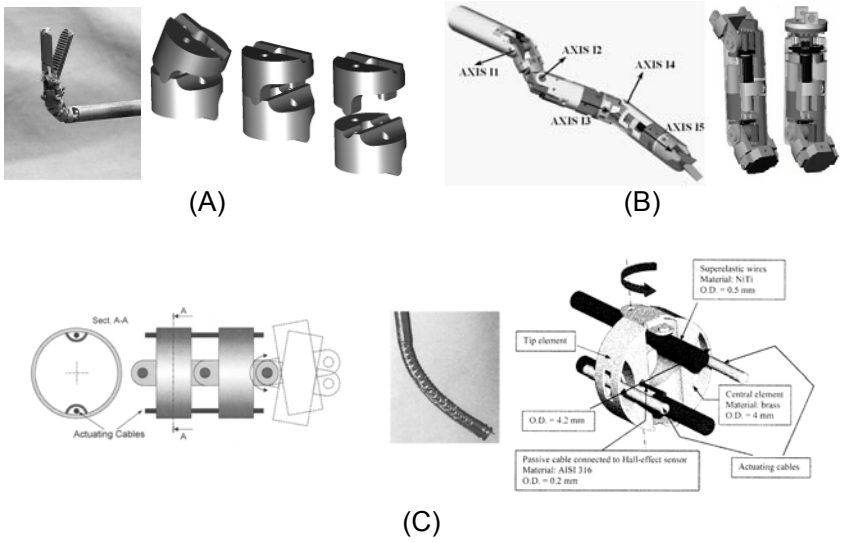

Figure 5.4. Segmented articulating configurations with direct hinge connections at different diameters: (A) 6.0 mm [53],(B) 10 mm [70, 71], and (C) 4.0 mm [52].

The use of compliant flexure hinges to join segments is less common, but flexure hinges can improve articulation precision, promote scalability, and are more straightforward to optimize. Designs using compliant flexure hinges have attained near meso scaling (5.0 mm diameter) and wide articulation ranges (90^o) [56]. Machining small design features can be difficult, but it is often times much more feasible than the machining of small parts for hinges. Segmented designs which incorporate flexure hinges possess great potential for scalability and optimization of force application because the elastic deformation in the hinges can be predicted much more accurately than interactions between assembly components.

In order to limit frictional losses between segments, several "fitted" configurations have been designed to be held together by connecting wires or the actuating wires which drive the articulation. If such configurations are properly designed, the frictional losses between segments can be minimized and minute components can be eliminated. A 12 mm diameter articulating mechanism was developed for MIS which operated by varying the stiffness of two (inner and outer) segmented tubes and advancing them independently (see Figure 5.5) [72, 73]. This design was reported to withstand 1-5 N of lateral force at the tip before significant deformation, but no articulation range is given. Other wire-connected designs have scaled down well, including a 2.4 mm diameter model (see Figure 5.6) [54] and an 8 mm diameter model [67]. Articulation up to 90^o was attained with these models, but force application remained low (1N) and was given little consideration.

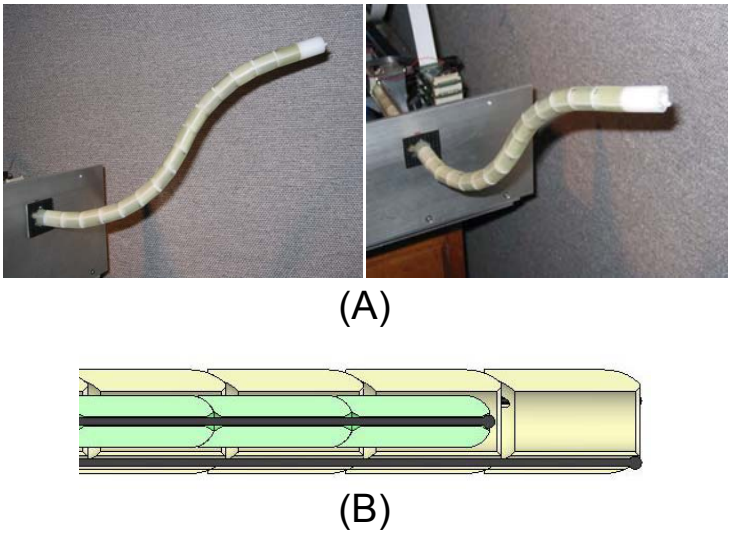

Figure 5.5. 12 mm diameter articulating mechanism consisting of inner and outer "snake-like" segmented tubes. Inner and outer tubes slide past each other to enable articulation [72, 73].

Another notable design for a 6 mm joint was presented by Van Meer et al [74] and attained significant lateral force application, though additional miniaturization is desired. The design incorporated a faceted sphere and a unique configuration of cylinders to limit motion (see Figure 5.7). The manipulator was able to articulate 85^o and able to apply loads between 3-5 Newtons. This design also utilized motor driven NiTi wires to allow additional articulation.

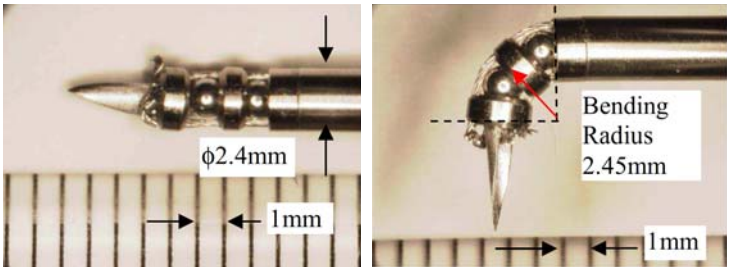

Figure 5.6. Segmented manipulator (2.4 mm diameter) using non-traditional joining technique [54].

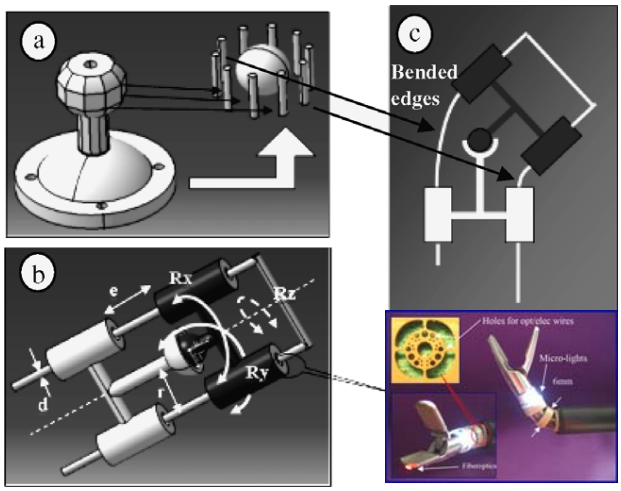

Figure 5.7. Schematic and images of a faceted sphere joint configuration for a 6 mm diameter forceps tool [74].

5.2.2.3 Summary of Mechanical Configurations

The configuration of an articulating mechanism dictates many of the system's performance characteristics. Continuous backbone configurations provide excellent bending stiffness, but are more difficult to actuate and control. Discrete or segmented configurations often suffer from insufficient rigidity but the designs are much more adaptable and sometimes more easily controlled. As can be seen from the performance data provided in Table 5.1, modern research has focused on the controllability and articulation range of these mechanisms, but insufficient consideration has been given to force application. Consequently, many miniature manipulators have been developed with wide ranges of articulation (90^o+ off-axis), but meso scale (<5 mm diameter) manipulators remain incapable of applying lateral forces of more than 1 Newton. Emerging applications for these manipulators

require lateral forces of several Newtons in order to be useful, therefore current meso scale mechanisms do not perform sufficiently. In order to develop mechanisms which meet developing needs, effort must be exerted to design, test, and optimize structural configurations which enable both articulation and significant force application.

In general, the structural configuration and components of a mechanism significantly affect force capabilities. In much of the current work, designs have been implemented without (or without mentioning) the reasoning behind selection of the configuration and geometrical details. If considerable time were given to exploring and analyzing novel mechanical configurations, superior systems could be developed. Furthermore, if sufficient resources were committed to optimizing the geometrical parameters of such configurations, improved rigidity and an increased potential for force application could result.

5.2.3 Actuation Methodology

Functional differences between actuation methodologies contribute significantly to both a system's performance and to how effectively that system scales. Consequently, it is useful to analyze the commonality and differences between actuation systems and categorize them by their function. The actuation methodologies for nearly all modern dexterous mechanisms can be described as at least one of the following: (1) purely mechanically driven, *e.g.*, servo driven, (2) active material driven, especially via SMAs, or (3) fluid driven, *e.g.*, pneumatic or hydraulic. There has been much system diversity within these classifications, but modern mechanism designs fit well into one of these categories with few exceptions.

5.2.3.1 Fluid-Actuation

Fluid actuation schemes make use of incompressibility or pressure differences to create mechanical motion. Traditional hydraulics are commonly used in industrial applications due to their robust performance and reliability, but these systems are often rigid and require large, bulky components and tight seals that can withstand high pressures. As a result, hydraulic systems become nearly impossible to implement at meso scales, but some hydraulic applications do exist. For an application

in neuroendoscopy, fluidic jets oriented perpendicular to the longitudinal axis of the 2.7 mm diameter catheter were used to propel the tip away from nearby sensitive spinal tissue [68]. Such a method has limited utility, as it requires a rigid structure to be in close proximity and cannot apply forces for manipulation, but this application is representative of creative fluidic actuation methods at the meso scale.

Depending on the required pressures, pneumatic systems can have similar problems with component size, along with inherent problems involving control and precision. At larger scales, pneumatic systems been implemented to provide complicated motion and advanced manipulation capabilities. Grissom et al. developed a soft robotic arm which was able to support several hundred Newtons of transverse force, articulate over 360^o, and perform complicated manipulation tasks [69] (see Figure 5.8). The assembly is actuated by flexible tubes which can be extended or contracted by modulating the internal pressure. This soft arm is very versatile, but significant miniaturization is impossible because the tube configuration is extremely intricate. In general, fluid-actuated systems can be quite effective at larger scales, but meso scale implementation for these systems is overwhelmingly difficult.

5.2.3.2 Mechanical Actuation

Mechanically driven systems articulate through a direct mechanical connection to a driving source. The connection commonly consists of a wire attached to one or more mechanical components, and the most widely implemented sources are manually or motor driven. The articulation of many mechanically driven manipulators is quite accurate and controllable, especially those which are actuated by servo motors. Most servo driven mechanisms include an integrated controller as well as a cable or pulley system. Motor driven mechanisms possess inherent drawbacks such as high complexity and a likelihood of backlash in the cable-pulley system. Most articulators with multiple DoFs implement several motors, thereby making these systems very complicated. Segmented configurations are usually implemented for mechanically driven mechanisms due to their potential for wide articulation ranges and mechanical versatility.

Motor driven "link and hinge" mechanisms (see Figure 5.9) are often used for

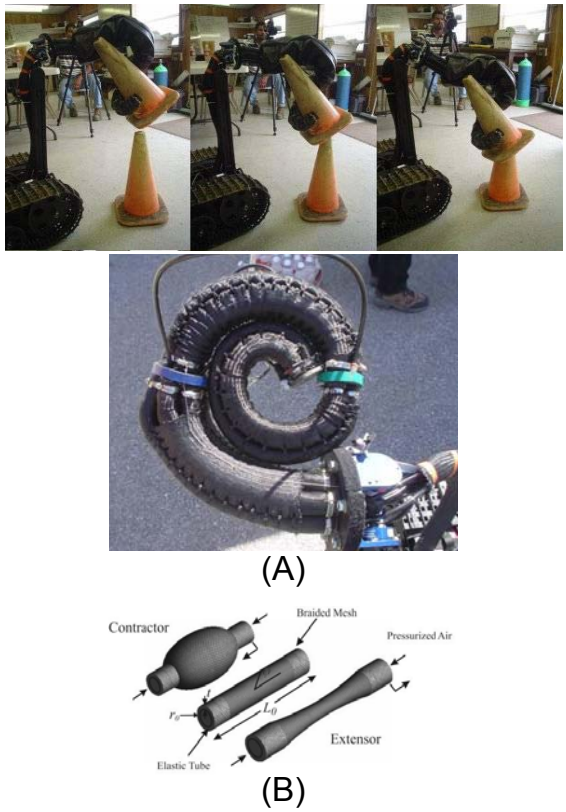

Figure 5.8. (A) Pneumatic robot arm performing complicated dexterous tasks and (B) tube actuators used to articulate the assembly. Diameter varies from 6.4 - 9 cm [69].

teleoperated [61] and laparoscopic [58] surgical applications which do not require extremely small scales (<10 mm diameter) or significant flexibility. These mechanisms can be very accurately controlled and monitored, so they are used when implementing haptic force feedback. Rigid link configurations are rarely used at smaller scales, though some micromanipulators have been developed which employ such configurations. Ikuta et al. presented a 3 mm diameter tip manipulator for remote microsurgery which included two hinges connecting rigid links [55]. The focus of the design was on implementation of a control methodology for remote surgery, therefore force application parameters were not discussed, but the maximum articulation range was about 60^o.

Several different types of mechanically driven articulators have been rather successfully scaled down to or near the meso level. A segmented instrument with a 2.4 mm diameter implemented a ball joint configuration (as shown previously in Figure 5.6) and was driven by two ultrasonic motors [54]. The manipulator could

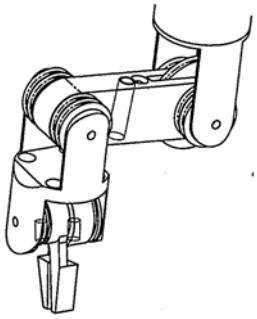

Figure 5.9. Rigid link mechanism for articulation [58].

bend up to 90^o, but no discussion on applicable tip force is presented. A motor driven 5.0 mm diameter tool tip for laparoscopic surgery attained a wide range of articulation (90^o) using flexure hinge connections, but again, no data on load bearing capacity was provided [56]. A 6 mm diameter joint coupled mechanism [53] attained bending angles in excess of 90^o and was reported to exert almost 5 Newtons in lateral force (as shown previously in Figure 5.4(A)). A telesurgical robot called the ViaCath System utilizes multiple servo motors to provide 6 DoFs to a 4.75 mm diameter articulating manipulator with interchangeable tool tips (Figure 5.10) [60]. Testing revealed a maximum lateral force application of 0.5 N, which limits the applicability of the tool tips. In many other cases, reviews have shown that the necessary technology exists to implement and control these advanced surgical systems [75, 76, 77], but mechanical insufficiencies in instrument performance are often limit their effectiveness.

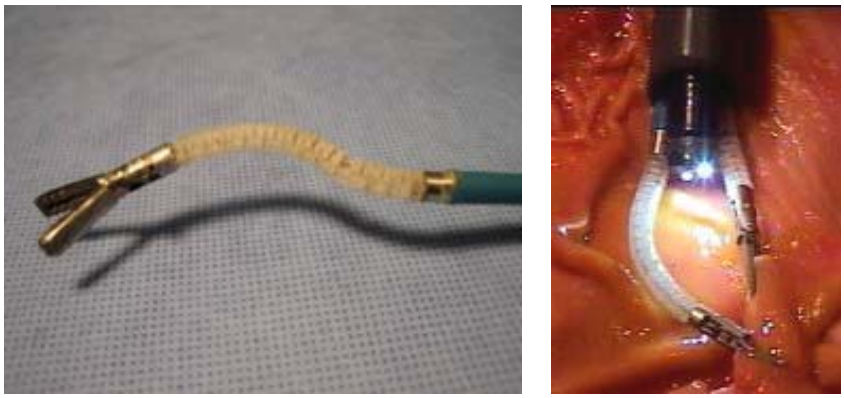

Figure 5.10. Surgical manipulator component (4.75 mm) of the ViaCath System for teleoperated surgery; increased lateral forces were desired [60].

Incorporation of servo motors and advanced control methodologies has improved performance characteristics for articulating segments. The need for complicated pulley systems and several motors to actuate these systems is problematic, causing difficulties in system integration and downsizing. To decrease the complexity of mechanically actuated systems, antagonistic springs are sometimes used in order to provide a "spring-back" effect, thereby eliminating the need for additional attachment points for the driving mechanism [44]. While incorporating antagonistic springs can reduce system complexity, it inherently reduces the controllability of mechanically driven assemblies.

It is obvious that modern work on meso scale articulating mechanisms focuses primarily on articulation range. The lack of data on stiffness and force application for scaled-down articulators makes scalability difficult to analyze in terms of maximum exerted force. Performance insufficiencies of meso scale manipulators have restricted technological advances in many fields, *e.g.*, surgical robotic system development. Performance evaluations of integrated telesurgical systems such as the ViaCath System and the daVinci®surgical system [78, 79] have reported insufficiencies in force application, thereby limiting the utility of such systems. The lack of focus on resulting force application has prevented significant improvements from being made for mechanisms at the meso scale. It is apparent that increasing the maximum lateral forces which these manipulators can apply is necessary to improve mechanism performance and expand utility to other applications.

5.2.3.3 Active Material Actuation

Especially within the last two decades, smart or active materials have gained popularity for use as actuators and sensors in a variety of systems. Piezoceramics, piezopolymers, magnetostrictive materials, and other active materials have all been utilized in modern design [46]. Shape memory alloys (SMAs) are by far the most popular active materials used in meso scale articulating mechanisms. Superelasticity and the shape memory effect provide two distinct uses for SMAs in articulating mechanisms. Using SMA components in place of traditional components can extend the articulation range of the mechanism due to superelasticity, or an SMA component can be activated to induce articulation.

Referring to a mechanism as "SMA actuated" indicates that the motion of the

mechanism is driven by energizing the SMA, *i.e.*, invoking the shape memory effect. The shape memory effect enables deformation through temperature modulation, which is often accomplished via resistive heating of the SMA components. Actuating SMAs are usually incorporated as wires or coils (springs); the subsequent discussion focuses on SMA actuated mechanisms.

Directly actuated standard SMA wires have been used to actuate many articulating manipulators. An 8.0 mm diameter segmented articulating tip for arthroscopic applications which was driven directly by SMA connecting wires could articulate 90^o and apply 1 N at the tip [67]. SMA wires are also used quite often in robot actuation, including a 15 mm diameter worm robot [80], two link leg manipulators for a robotic insect [46], and larger scale applications for land mine extraction [81]. If additional stiffness is desirable, the SMA actuators can be sized or configured to contribute to the structure of the manipulator. One group used three large SMA wires as backbones which were electrically heated to induce articulation up to 60^o (as shown previously in Figure 5.3(A)) [47]. The backbones could be selectively heated and cooled to actuate the mechanism, and these backbones provided additional bending stiffness to the manipulator. SMA backbone or wire mechanisms often have a limited articulation range but can produce tip forces more consistently. SMA coils or springs have often been implemented to increase articulation range.

Using SMA coils in place of traditional wires can give mechanisms a flexible neutral shape when not being actuated, and such coils have been fabricated down to the micro scale (76μm outer coil diameter, 25 μm wire diameter, [48]). An earlier application for an 8.0 mm diameter endoscope utilized a 3 NiTi spring setup, but was incapable of generating tip forces beyond 0.05 N [50]. Other scaled down designs which incorporated energized SMA coils for actuation have been developed with success. A 4.0 mm diameter articulating section developed for a fiberscope tip application was capable of articulating 90^o off axis, but lateral force evaluations were not reported (see Figure 5.11(A)) [48]. For a significantly different setup, SMA coils powered a 2.0 mm diameter endoscope tip, which could articulate up to 60^o off axis and was structurally supported by a steel spring (as shown in Figure 5.11(B)) [49].

SMA powered articulation is developing, but problems including response time,

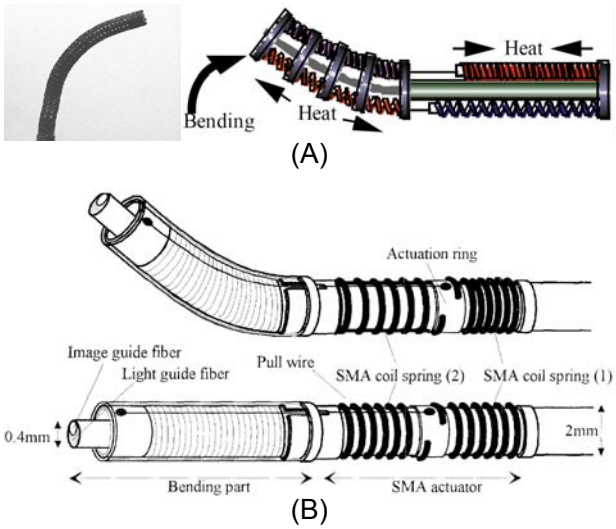

Figure 5.11. Meso scale mechanisms (A) 4.0 mm outer diameter [48] and (B) 2.0mm outer diameter [49] actuated by SMA coils (springs).

tip force generation, and control system complexity are severely limiting potential applications. Response time, *i.e.*, the time required to heat and/or cool the SMA component, is a critically limiting factor because it dictates the speed at which the manipulator can articulate. For these systems, the SMA components are activated by resistive heating, but in most cases, no cooling method has been implemented. The benefits of improved cooling are often times outweighed by the overwhelming difficulty of implementing a more effective means of heat transfer at such a reduced scale. Because of these size constraints, alternative cooling methods are often not included, thereby limiting the minimum response time to several seconds in many cases. Application of lateral forces remains insufficient for many applications, attaining maximums below 1 N in the few cases where it was reported.

SMA actuated mechanisms have not attained sufficient force application capabilities because the need for force application has only recently being considered. Early applications for SMA powered articulation, *e.g.*, optical scopes, required extensive articulation range, but minimal force application. Consequently, research for meso scale articulation has focused mainly on providing sufficient articulation range and precise control. The SMAs can be very precisely controlled, but complicated control algorithms and experimental testing necessary to quantify the shape memory effect are both needed. Because of this need, a vast majority of research

efforts are placed on the design and implementation of a control system, thereby limiting the work done to optimize the force capabilities of the mechanism.

5.2.4 Discussion of Meso Scale Feasibility

Advances in robotics and mechanism design have produced a variety of complex macro scale mechanical manipulators with many capabilities and much versatility. The lack of strict size constraints provides an opportunity for very unique design which incorporate traditional hinge connections and a variety of actuation methods, making design implementation convenient. Design requirements for miniature mechanical designs often limited to articulation ranges, *i.e.*, only articulation range is considered while force application is ignored. Many applications for meso scale mechanisms straddle the requirements for macro and micro devices, requiring precise articulation control and appreciable force generation of several Newtons [58].

5.2.4.1 Mechanical Configurations

The mechanical configuration and assembly characteristics of an articulating system can prevent scalability to the meso level. Traditional joining methods such as pin joints or hinges include micro scale components which are very difficult to manufacture and assemble. Additionally, significant frictional losses can occur in very small hinged assemblies due to lubrication difficulties, making force transmissions increasingly inefficient. At the meso scale, both continuous backbone and segmented mechanisms often employ either a compliant joint or "wire-connected" configuration to reduce frictional losses. At small scales, compliant hinges and minute features needed for wire-connected mechanisms can be difficult to machine, but these methods are conducive to design optimization. If a sufficient machining method is available, both compliant hinges and wire connections could be effectively implemented at the meso scale.

Segmented configurations provide more versatility than continuous backbone configurations, and are often times more straightforward to implement due to a lack of complex mechanical connections. Continuous backbone mechanisms can lose the benefit of high structural rigidity at smaller scales, and extreme articulation can induce large stresses in the backbone components, necessitating significant

performance trade-offs. Further investigation and optimization of structural configurations, especially those which are segmented, could yield versatile mechanism designs with highly improved capabilities.

5.2.4.2 Actuation Methodologies

Characteristics of the actuation scheme for certain articulating designs provide barriers to downsizing. Most fluid-actuated systems are nearly impossible to scale down past the meso level because design elements needed to maintain pressurization cannot be assembled and force generation drops significantly at reduced scales. Mechanical or active material methods are much more plausible as means to actuate meso scale mechanisms.

Mechanically actuated manipulators have shown promise for miniaturization, attaining large articulation ranges and even applying some appreciable tip forces [53]. Using actuating wires as structural components has reduced the complexity of some designs, thereby promoting miniaturization [43, 63, 64, 65, 66]. Given time to investigate additional configurations and optimize structural components, mechanically actuated manipulators could perform adequately at reduced scales.

SMA actuated mechanisms have been proven to scale down to the meso level and perform satisfactorily under pure articulation requirements, but their force application capabilities must be improved. To date, such mechanisms have been unable to generate the forces required in many applications. It is difficult to develop structural configurations which enable large forces to be applied via SMA actuation, but the success and versatility of these materials is encouraging. As new SMA configurations are developed and their implementation at reduced scales is understood, significant performance improvements are likely to occur over time.

5.2.5 Summary and Conclusions on Current Technologies

Mechanisms and robotic assemblies with multiple DoFs and advanced dexterous capabilities have been successfully implemented at large scales (>10 cm) by utilizing diverse methods and configurations. Scaling these mechanisms down to the meso level (1-5 mm) is often impossible, thereby necessitating the development of new designs and actuation schemes. Modern concepts and configurations possess

their own unique drawbacks and limitations, which severely limit their effectiveness and applicability.

Discretely segmented mechanisms provide a good deal of versatility to mechanisms in terms of articulation and manipulation capabilities, but a force application design focus is needed. Many researchers have implemented smart materials, specifically SMAs, to actuate mechanical manipulators at the meso scale. Despite the high power/mass ratios of SMAs and the accurate control of these devices, the maximum applicable force from these mechanisms remains low. Manipulators which are purely mechanically driven have shown good articulation range and can be controlled very well when directly servo driven, but few designs have been reported to exert appreciable force from articulation.

Recent research focus has been placed on designing mechanisms that can be adequately controlled throughout a given range of articulation. At small scales, several diverse system designs have performed sufficiently for these objectives, but little consideration has been given to force production. The majority of current studies have defined the motion of the mechanism as the objective and either disregarded force production or mentioned it as an afterthought. Consequently, consistent production of forces of more than 1 Newton at the tip of meso scale manipulators has yet to be attained, thereby limiting the utility of these designs. Now that meso scale articulation has been implemented, the objective of maximizing force production can be realized. If designs are developed and optimized for an additional force objective, a set of more useful mechanisms with improved force capabilities will emerge.

5.3 Preliminary Investigation of a Meso Scale Articulating Segment

5.3.1 Introduction

Additional tool dexterity and maneuverability at the surgical site is desirable for endoscopic surgery. Such dexterity can enable the completion of more complicated, intricate surgical maneuvers. Endoscopes possess the ability to articulate off the longitudinal axis for viewing, but most endoscopic tools which are used to perform

the surgical tasks remain incapable of dextrous articulation. Much work has been done to advance the capabilities of meso scale manipulators, but very few have attained the sufficient combination of dexterity and strength which would provide utility for endoscopic surgery. The previous portion of this chapter discussed both performance successes and insufficiencies of many such tools, and the following investigations are intended as an introduction to a potential approach for improving articulation performance.

The performance of many previous designs has been hindered by the minuteness of the assembly components. Many of the proposed designs have consisted of multiple individual elements connected in a complicated assembly; the small size of these parts (mm sized, with micro-sized features) leads to manufacturing and assembly complications. Contact between adjacent elements necessitates the use of computationally intensive nonlinear kinematic models to predict position, and causes significant frictional losses. In an attempt to limit several such complications, a single piece, compliant concept is proposed which utilizes elastic deformation to dictate articulation. A means of evaluating the concept's ability to both articulate and apply lateral forces at the tip is presented, along with a quantitative evaluation of the concept's feasibility for implementation.

5.3.2 Proposed Articulation Concept and Objectives

The articulation of compliant mechanisms is based on mechanical deformation, therefore these mechanisms have the ability provide large deflections and consistent, repeatable motion. A single-piece compliant mechanism with repeating segments is proposed as an initial design concept. As discussed previously, a useful means of evaluating the utility of a meso scale manipulator is to quantify both the maximum articulation range and the maximum lateral force (*i.e.*, force perpendicular to the longitudinal axis) which the design can generate. The concept is intended to be included proximally to the tool tip on an endoscopic tool, thus providing articulation ability to tool. The objectives of this investigation are:

1. To present a method of evaluating the maximum articulation range and lateral force application ability of any compliant design concept.

2. To explore the effects which the design parameters have on the performance metrics.

3. To evaluate the potential of such a concept for endoscopic implementation.

To evaluate the potential efficacy of a compliant design, a simple configuration is proposed which incorporates a slightly modified corner filleted flexural hinge. Since the desired application is for an endoscopic surgical tool, the same diametric constraints for the tool tip design (OD$\leq$3.0 mm) are applicable for the articulating section design. Consequently, the outer diameter of the concept was set as 3.0 mm. The articulating section must house the actuating wires for the tool tip, therefore sufficient clearance must be provided for these wires. Furthermore, the design must be able to be actuated by pull wires for implementation with endoscopic tools.

The proposed design configuration consisted of a flexure hinge connecting two larger links. The concept is to actuate the design via pull wires attached to the thick links, thereby causing bending of the overall structure. A generalized model of the proposed concept with geometrical parameter labels is shown in Figure 5.12. Geometrical parameters defined for the design were similar to those used for traditional corner flexure hinges [82]. The design parameters for the concept consisted of hinge length L, hinge width w, hinge thickness t, fillet radius r; these parameters were varied to determine their respective effects on articulation performance.

5.3.3 Simulation of Multiple Designs

In order to evaluate the articulation and lateral force application abilities of the design concept, a single segment of the repeated design was analyzed. By determining the limits of one segment, the performance of the overall structure made up of repeated segments can be estimated. Because this design relies entirely on elastic deformation to attain articulation, 316 stainless steel was proposed as the modeling material (material properties: E=193 GPA, ν=0.3, σ_{Yield}=240 MPa).

Because compliant structures rely on elastic deformation, these structures should be designed to operate only within the elastic zone, *i.e.*, stresses in the structure should remain below the yield stress (σ_Y). ANSYS finite element software was used to analyze the stresses induced in the segment during deformation. Two separate studies were conducted to quantify the articulation ability and lateral force

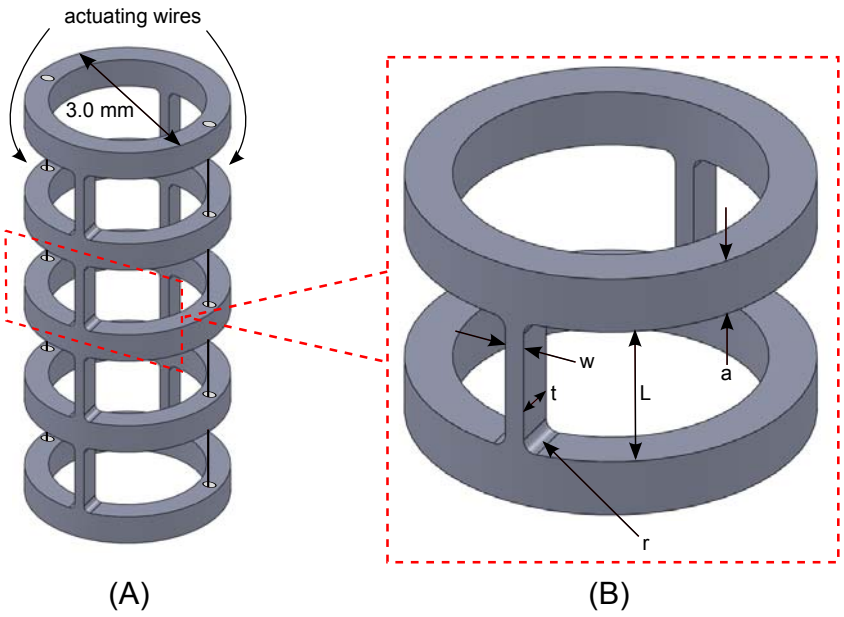

Figure 5.12. (A) Articulating section concept with repeating segments and actuating wires shown; (B) magnified diagram of repeating segment with four labeled design parameters. Note: link thickness indicated by a

application ability of a single segment. For each design analysis, the model was meshed with SOLID186 3D elements having twenty nodes per element, quadratic displacement behavior, and three degrees of freedom at each node. Mesh sizes were defined based on geometrical parameters, but each design mesh consisted of approximately 13,000 elements. One example of a meshed model is shown in Figure 5.13.

The free displacement study was designed to determine the maximum off-axis angle to which each design could be rotated before the yield stress was reached. Half model symmetry was implemented for this analysis and boundary conditions were applied to mimic actuation by pull wires (see Figure 5.13). The displacement of the bottom area was fixed in all directions (U_x, U_y ,U_z) to simulate mounting to the tool shaft, symmetry boundary conditions (U_y=0) were applied to the faces generated by the section cut, and the vertical displacement of one corner was set to a nonzero value to simulate actuation by a pull wire. For each design, the displacement at this corner was iteratively increased until the yield stress was reached.

The second study aimed to quantify the maximum lateral force which the seg-

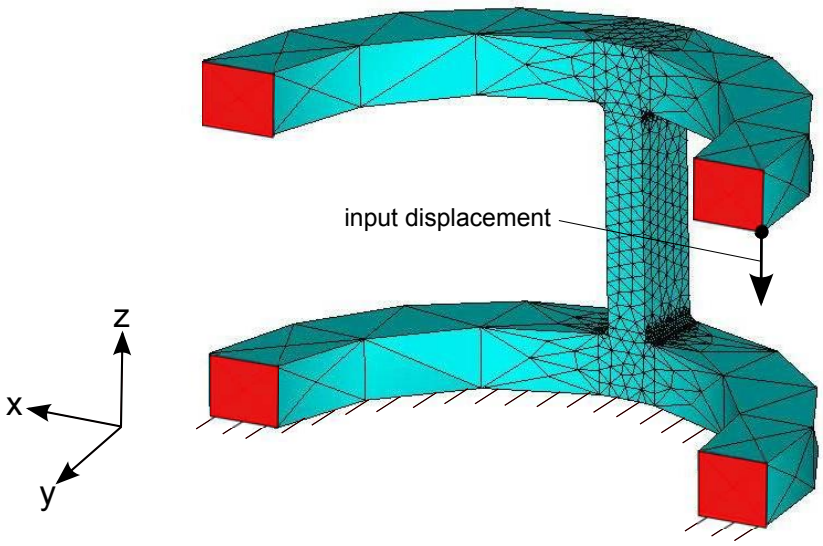

Figure 5.13. Boundary conditions applied to a single segment meshed model. Note that geometrical symmetry allows analysis of a half model. Bottom area fixed in all directions, symmetry BC's (U_y=0) applied to sectioned areas (red), and lower corner of top link displaced in the negative z direction.

ment could apply. The lateral force analysis was designed to simulate a completely blocked tip condition. This analysis implemented boundary conditions which were identical to the free displacement study, along with an additional condition constraining the x displacement of the upper corner of the top link. Referring to Figure 5.13, all boundary conditions would be the same for the blocked force case, and the corner directly above the displaced corner would be fixed in the x direction. These boundary conditions simulated contact with a rigid object which would occur while actuating the segment in a normal fashion, thereby exerting a lateral reaction force on that object in the x direction. For each design, the displacement applied to the lower corner of the upper link was iteratively increased until the yield stress was reached. The resulting reaction force in the x direction represents the maximum force that the segment can apply without yielding.

For each of the two studies, the design parameters were varied over manually selected ranges to evaluate the performance of a wide range of potential designs. The ranges of the designs were based on physical intuition, geometrical feasibility, and analysis of initial models. The ranges of the geometrical parameters are given in Table 5.2.

Table 5.2. Ranges of parametric variation for the articulation and lateral force studies.

Parameter	Articulation Study Range	Lateral Force Study Range
length L (mm)	0.8-1.6	1.0-2.5
width w (mm)	0.075-0.25	0.04-0.2
radius r (mm)	0.01-0.06	0.035-0.05
thickness t (mm)	0.25-0.35	0.33-0.38

The maximum lateral force which the design segments could apply was determined by summing the reaction force in the x direction at the corner constrained in the x direction. The thickness of the links was much larger than the width of the flexure hinge, therefore the bending deflection of the links was insignificant in comparison to that of the flexure hinge. Consequently, the resulting off-axis articulation of the segment could be approximated by determining the orientation of a vector normal to the top face. The articulation angle ϕ was approximated geometrically using the deformed locations of the two top corner points as shown in Figure 5.14. The articulation angle ϕ was determined from the x,z locations of the two top corner points as shown in Equation 5.3.

$$\phi = \arctan\left[\frac{Z_1 - Z_2}{X_1 - X_2}\right] \tag{5.1}$$

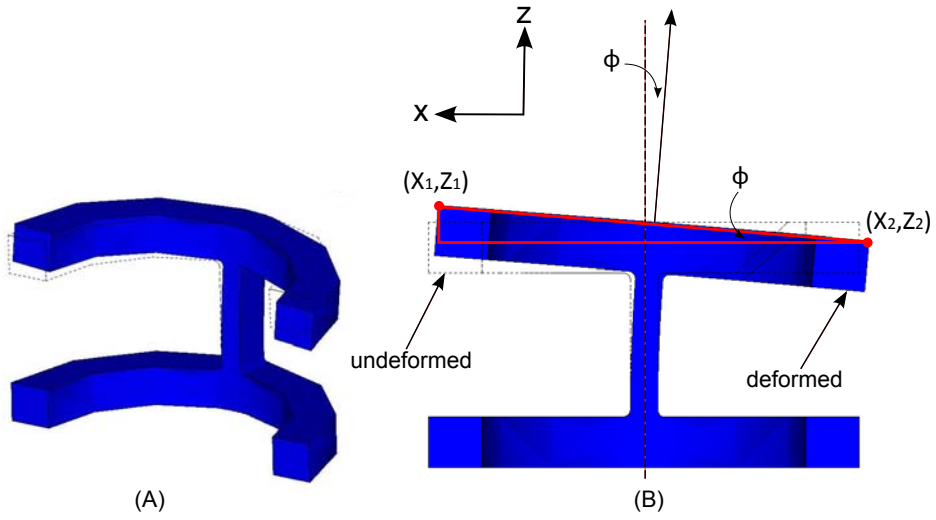

Figure 5.14. (A) Diagram of an deformed shape shown with the undeformed dashed outline and (B) deformed shape shown in x-z plane with deformed coordinates (X_1, Z_1) and (X_2, Z_2) used to calculate articulation angle ϕ.

5.3.4 Results and Discussion

The results for all design iterations were imported into MATLAB for data processing. Plots relating the geometrical design parameters to the maximum articulation range and lateral force application ability were fabricated.

For the free displacement designs, 3D plots of the maximum ϕ relative to each of the design parameters is presented in Figures 5.15 and 5.16. By observing the data presented in Figure 5.15 it is apparent that the articulation range can be be maximized by increasing the length, decreasing the width, and increasing the radius. This performance trend follows closely with that of traditional corner-filleted hinges [82], which is expected from the inherent similarity between a corner-filleted hinge and the proposed design.

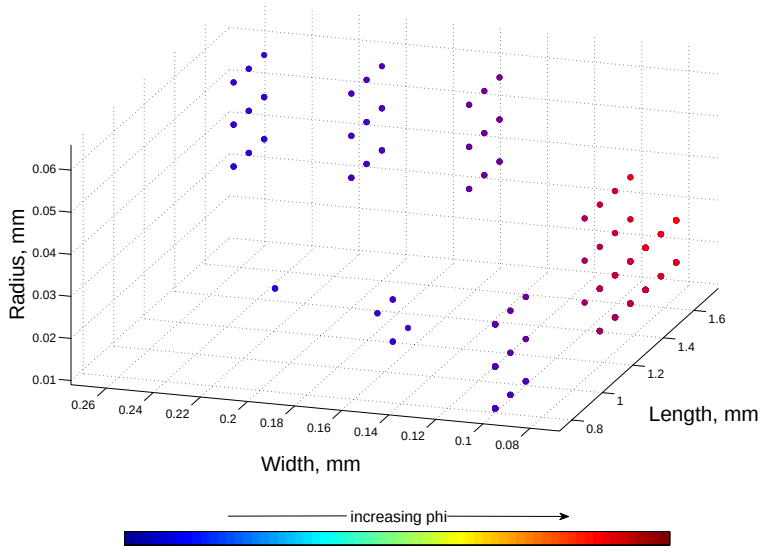

Figure 5.15. Plot of maximum articulation angle ϕ (represented in color) relative to design parameters length L, width w, and radius r.

Additionally, evaluation of the data presented in Figure 5.16 indicates that for a given set of configurations characterized by constant length, constant width, and varying thickness, little variation in the maximum articulation range results. Again, this conclusion follows logically and can be verified by modeling the hinge

as a beam in bending; the stress in the hinge can be simply represented by:

$$\sigma_{bend} = \frac{M \cdot c}{I_{zz}} \tag{5.2}$$

$$I_{zz} = \frac{1}{12} \cdot t \cdot w^3 \tag{5.3}$$

where σ_{bend} is the bending stress, I_{zz} is the polar area moment of inertia about the axis of revolution, c is the distance from the neutral axis, and M is the moment resulting from the revolution/displacement. It follows that the induced stress is proportional to both the inverse of the thickness t and the inverse of the w to the third power, thereby indicating that the effect of the thickness on the stress and maximum articulation range will have a small effect. This analysis coincided with the results presented in Figure 5.16.

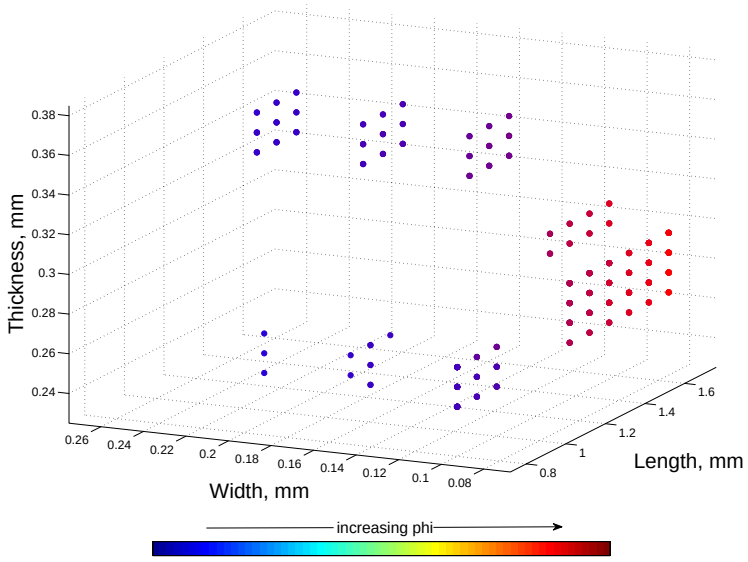

Figure 5.16. Plot of maximum articulation angle ϕ (represented in color) relative to design parameters length L, width w, and thickness t.

Of all the designs analyzed under the free displacement constraints, a maximum articulation angle of 2.6^o was obtained; the geometrical parameters of this design are shown in Table 5.3. If many of these segments are constructed in parallel to form an articulating section, the articulation of the entire section will be the aggregate articulation sum of each individual segment. For this segment design, more than twenty two repeated segments would be necessary to achieve a total

maximum off-axis articulation of 60^o, and the resulting section would be over 50 mm long. Such a design is not practical, but a more comprehensive exploration of the design space guided by a formal optimization routine could yield a far superior design. This investigation has shown that performance varies appreciably with geometry and the proposed configuration is capable of attaining relatively significant articulation by means of elastic deformation.

For the blocked force analysis, 3D plots of the applied lateral force relative to each of the design parameters is presented in Figures 5.17 and 5.18. The trends in these figures can be qualitatively evaluated in terms of how the lateral force application ability is affected by varying the design parameters. Similar to the trend in the free deflection case, Figure 5.18 shows that minimal changes in lateral force occur when the thickness of the hinge is varied. In contrast to other trends observed for the free displacement case, the resulting lateral force increases with decreasing length and increasing width. This trend agrees with physical insight because decreasing length and increasing width both result in increases in lateral bending stiffness. Since the boundary conditions induce bending in the hinge, two different hinges with a high and low bending stiffness will necessitate a high and low force, respectively, to produce the same displacement.

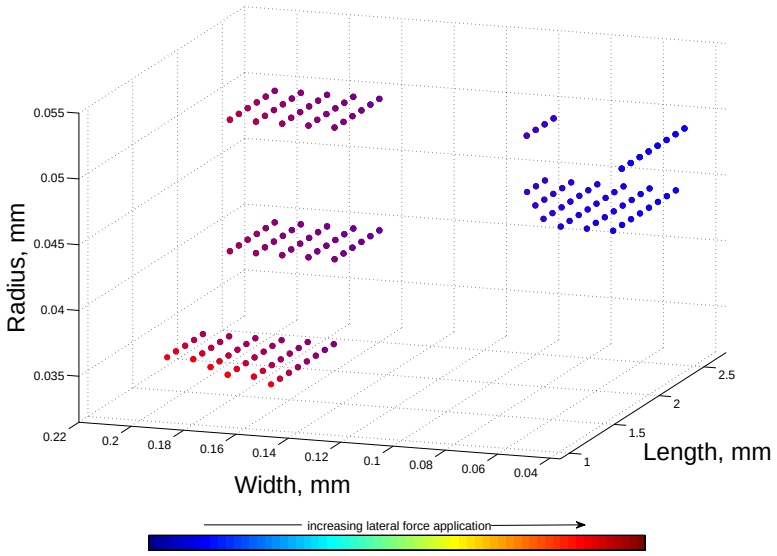

Figure 5.17. Plot of maximum lateral force (represented in color) relative to design parameters length L, width w, and radius r.

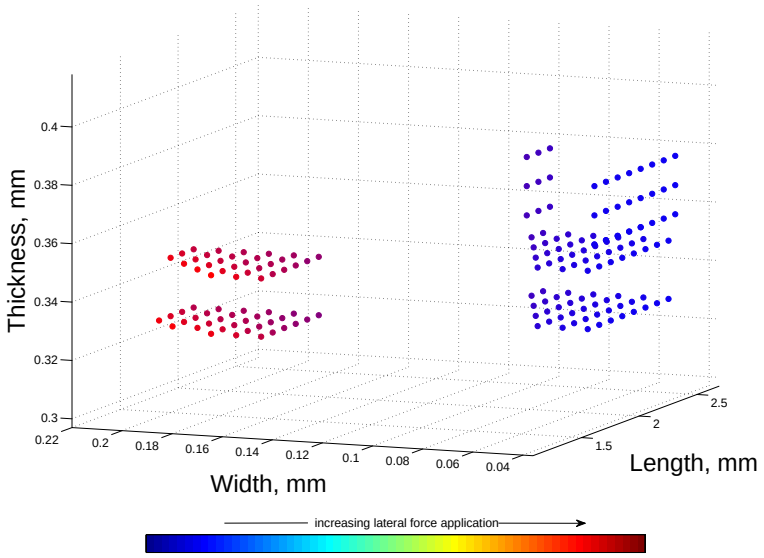

Figure 5.18. Plot of maximum lateral force (represented in color) relative to design parameters length L, width w, and thickness t.

Of the set of designs which were analyzed, the maximum lateral force application was found to be less than one Newton (0.37N), the corresponding design parameters for that design are listed in Table 5.3. These results are on the same order of magnitude as those forces reported in the literature for similar meso-sized mechanisms. As for the free displacement analysis, lateral force results have only been attained for a very small subset of the entire potential design space, therefore this value does not indicate the maximum optimized value for this design configuration. The exploration of various designs which was conducted for the lateral force application case does, however, provide valuable qualitative design guidance.

Table 5.3. Geometrical parameters corresponding to the best performing designs in the free displacement and lateral force cases.

Parameter	**Articulation Results**	**Lateral Force Results**
length L (mm)	1.6	1.1
width w (mm)	0.075	0.17
radius r (mm)	0.03	0.035
thickness t (mm)	0.28	0.35
Maximum ϕ (deg.)	2.6	-
Lateral force (N)	-	0.37

5.3.5 Summary and Conclusions

An approach has been developed and implemented to evaluate the articulation and force application capabilities of compliant segments for articulating applications. A simplified geometry was evaluated based on the effect which parametric variation of the design variables had on the articulation and force application abilities. Results of these initial investigations agreed with results obtained for traditional flexural hinges, and the trends observed above can be used to guide future design iterations or concept development.

Currently, the most effective designs attained do not perform sufficiently for implementation as an articulating mechanism. However, strong dependence of the articulation and force application abilities on the geometrical parameters has been shown, and this characteristic can be exploited to produce a design with superior performance. Also, since only one design concept was studied, exploration of other concepts could yield improved results. Coupling this method of analysis with a formal optimization routine could produce one or several designs which perform well enough for potential application. Material selection can also have a significant effect on the performance of the design, especially the maximum angle of articulation. If a nonlinear material such as superelastic Nitinol or Delrin is used, the articulation ability of a given design can be improved.

Chapter 6

Conclusions, Recommendations, and Future Work

6.1 Summary

This thesis presents details regarding the design, analysis, and experimental testing of a multifunctional forceps for use in endoscopic surgery. After proposing a design concept, methods of evaluating the mechanical advantage (MA) and load bearing capacity of the tool were developed. Using these methods, an *ad hoc* optimization strategy was implemented to develop and prototype a tool tip design which met both geometrical and performance constraints. Using the manufactured prototype, several benchtop tests were conducted to validate the accuracy of the analytical MA model. A cautery prototype was assembled by retrofitting the tool tip prototype with the handle of a commercially available forceps (Olympus RadialJaw hot biopsy forceps). Using an electrosurgical generator, testing was carried out to compare tissue damage zones caused by the prototype to those caused by the commercially available tool. Cautery testing revealed that the resulting damage zones were comparable for the prototype and commercial tool, indicating that the proposed design could posses the potential for clinical implementation as an effective cauterizing tool. A comprehensive review of small-scale dexterous technologies was conducted, and the resulting conclusions guided initial investigations into the design of an articulating segment. Preliminary analyses of design concepts

for a compliant articulating segment indicate that such a concept has the potential for significant articulation range and force output. Research contributions, recommendations for future work, and summaries of the conclusions drawn from each investigation are presented and discussed in the following sections.

6.2 Conclusions

A method of incisionless surgery called Natural Orifice Transluminal Endoscopic Surgery (NOTES) has proven to be a practical and desirable alternative to both traditional open surgery and minimally invasive laparoscopic surgery. The obvious benefits resulting from the elimination of necessary external incisions during NOTES procedures have driven significant clinical research efforts for implementing such procedures. Currently, development of these experimental procedures is hindered by insufficient performance of traditional endoscopic tools. A set of design objectives and constraints was developed for a multifunctional forceps to be used during a novel surgical procedure for transgastric access.

An analytical means of evaluating the force application efficiency of proposed designs was developed by determining the relationship between input and output forces (MA). The model was used to predict the performance of the tool tip in terms of the design objectives stated above. Relative to several commercially available tool designs, the MA model predicts appreciable increases in force transmission from the actuating wires to the tool tip for the proposed design.

Benchtop testing of a prototype showed good agreement between the MA model and actual tool performance when the tool was closing. Discrepancies between the MA model and experimental data during tool opening can be attributed to increased frictional losses caused by manufacturing inconsistencies. Despite such discrepancies in the opening load cases, qualitative behavior of the the experimental data agreed well with model predictions, indicating that the derived model is a valid means of predicting tool performance in the absence of significant frictional losses. Experimental testing of a prototype and a commercial tool were carried out for comparison of cautery performance. Varying levels of power delivery and methods of application were implemented to quantify differences in the thermal damage of soft tissue. Using an optical measurement technique, the size of damage zones

were digitized and compared. Results show that the size of the resulting damage zones were similar for both tools under a variety of power levels and delivery methods, and the size variation of such zones was also similar for the two tools. The consistency of the cautery tests indicate that the proposed design has the potential to perform adequately as a cautery instrument in clinical applications.

Based on a comprehensive review of previous literature, means of categorizing articulating mechanisms based on structure and actuation method was developed. The reported performance parameters of the reviewed mechanisms and assemblies were collected and evaluated based on the developed categorization methodology. By aggregately evaluating these performance parameters, the effects of certain design characteristics on articulation range, force application, and scaling could be identified. Based on this evaluation, it was determined that a mechanically-actuated, single-piece, segmented assembly is likely to provide the best potential for a design which can attain high ranges of articulation and force application at the meso scale. Consequently, a compliant design which implements corner-filleted flexure hinges was introduced, analyzed, and evaluated in terms of articulation and force application ability. Initial analysis indicates that using a "stacked" embodiment of this design could provide additional dexterous capabilities to the endoscopic forceps if additional investigations and design optimizations are performed.

6.3 Research Contributions

This work has contributed to the field of design of endoscopic surgical tools and could lead to advances in endoscopic surgery as a minimally invasive therapeutic technique. Efforts described herein have yielded a multifunctional endoscopic forceps design which is predicted to both provide improved grasping and spreading capabilities and possess clinically feasible cautery ability. The iterative design methodology which was developed and implemented for this work can be applied throughout the field of surgical device design. This method involves iterating between performance (MA model) and constraint (FEA) evaluations to determine a design which satisfies the constraints and performance goals. When a formal optimization routine would be overly cumbersome to implement, this method serves as a effective alternative and produces practical results.

This work provides several reviews of recent progress made in a variety of technical research areas. The development and progression of minimally invasive surgery as a therapeutic technique is presented in Chapter 1, along with a detailed review of one specific experimental NOTES technique. Such a review is useful to consider when developing tools for these procedures. Performance insufficiencies of current endoscopic tools and the need to implement multifunctional tools for endoscopic and NOTES procedures are discussed to highlight specific tool improvements which need to be made in order to allow developing surgical procedures to advance. The summary of modern electrosurgery techniques and equipment presented in Chapter 4 provides a useful overview of clinical ablative techniques. The review presented in this work could serve as a basis for developing energy delivery devices which optimize thermal damage zones.

Chapter 5 presents a review of state of the art meso scale articulating mechanisms. This summary of design characteristics and how they relate to mechanism performance is useful when developing design configurations for articulating mechanisms. Given a known set of design constraints and objectives, the trends observed by this technology summary can be used to select design and actuating configurations which promote certain performance metrics. The trends observed in this review guided initial investigations into the design of a compliant meso scale articulator. Though a design with superior performance characteristics (articulation and force application) was not fully developed, the method of evaluating the articulation range and lateral force application as a function of multiple design parameters is a robust and effective design approach. This design approach provides a very comprehensive investigation of how small modifications of each design parameter affects the performance of the design.

The results of this research have aided the advancement of tool development for minimally invasive surgery and NOTES, in particular. The continued improvement of endoscopic tools contributes to clinical efforts to improve the efficacy of experimental minimally invasive techniques. The investigations presented in this work have led to an endoscopic forceps design which is predicted to possess high clinical practicality. The initial configuration presented here for an articulating segment could serve as a design basis for providing additional utility and dexterity to this tool. In Summary, this work has yielded a practical endoscopic forceps tool

which can be coupled with a proposed articulating segment as well as effective design methodologies for both the tool tip and articulating mechanism.

6.4 Recommendations and Future Work

There are several ways to expand or further develop the work presented in this thesis. Major subsequent steps which could be taken include: an objective investigation into the validity of the design objectives and constraints, experimental determination of the forces necessary to manipulate soft tissues during NOTES procedures, investigations into geometry and material selections for optimized cautery effects, further development, implementation, and testing of an articulating segment for improved dexterity, as well as the design and implementation of a functioning handle to operate the tool tip and clinical testing of the entire tool.

The forceps design presented here was based on a set of constraints and objectives which were developed in consultation with practicing surgeons. These constraints were developed based on intuition and experience as opposed to experimental testing and quantification. These constraints and objectives are logical and most likely qualitatively accurate, but quantifying the importance and true effective ranges of these constraints and objectives would be useful for developing a truly optimized design. For example, one of the requirements for this design was a minimum opening angle of θ=45^o. This value is based on intuition alone, and consequently may not be the ideal maximum opening angle; other constraints can be considered in a similar manner. It is recommended that if further optimization of a forceps design is to be completed, some form of quantitative evaluation/testing of design constraints and objectives should be carried out.

A major point of uncertainty is the range of forces necessary to manipulate soft tissues during surgery. Quantification of such forces is extremely difficult as a multitude of tissues are encountered during surgery. Benchtop investigations regarding the forces necessary to spread or tear tissue (as described in the experimental surgical technique STAT, Chapter 1, Section 1.3) during surgery could provide a better range for the maximum force which the tool must be able to withstand. Gaining a better quantitative understanding of the forces incurred on instruments during surgery would provide a more realistic load bearing constraint.

There have been several investigations regarding the effects of geometry and power delivery methods on thermal damage zones. The proposed tool configuration has been shown to perform similarly to a commercial cautery device, but more in-depth studies could be conducted to determine how the damage zones could be optimized by varying geometrical parameters. Furthermore, a more advanced manufacturing and assembly method could be used to selectively insulate the tool, thereby enabling bipolar cautery instead of monopolar cautery. Bipolar cautery devices produce smaller residual damage zones than monopolar devices and are quickly becoming the standard in modern surgery. In order to compete with current and developing endoscopic tools, bipolar cautery should be provided for this tool.

Further development of the compliant articulating segment described in Chapter 5, Section 5.3 is necessary to obtain a feasible, effective design with the potential for actual implementation. The method of parametric variation has shown that the concept possesses promise in attaining the articulation and force application goals previously stated, but further exploration of the design space is needed. Furthermore, other flexure hinge or topological configurations could be explored in attempts to improve articulation performance in addition to the introduction of superelastic or other nonlinear elastic materials.

Due to minimal frictional losses and the simplification of component assembly procedures, compliant mechanisms possess potential for articulation capability at the meso scale. Advances in superelastic materials have provided higher strain capabilities to these materials, and the performance of compliant mechanisms can be improved if these materials are implemented. Studying the resulting improvements in articulation ability will provide an indication of whether compliant designs could be practical for application to surgical devices.

The design and implementation of a handle for assembly into a full-scale working prototype could also be completed. A mechanism should be designed to control the translation of both sets of actuating wires separately. Implementing a mechanism such as this is a non-trivial task due to the small tolerance on the resulting translation. Because the required translations are so small, ensuring that each set of wires translates equally is a challenging but feasible task. Once a full-scale prototype is assembled, benchtop and clinical testing should be conducted to evaluate the surgical efficacy of the tool.

Bibliography

[1] Reardon, P. R., J. I. Kamelgard, B. Applebaum, L. Rossman, and F. C. Brunicardi (1999) "Feasibility of laparoscopic cholecystectomy with miniaturized instrumentation in 50 consecutive cases," *World Journal of Surgery*, **23**(2), pp. 128–132.

[2] Kalloo, A. N., V. K. Singh, S. B. Jagannath, H. Niiyama, S. L. Hill, C. A. Vaughn, C. A. Magee, and S. V. Kantsevoy (2004) "Flexible transgastric peritoneoscopy: a novel approach to diagnostic and therapeutic interventions in the peritoneal cavity," *Gastrointestinal Endoscopy*, **60**(1), pp. 114–117.

[3] Beger, H. G., A. Schwarz, and U. Bergmann (2003) "Progress in gastrointestinal tract surgery: the impact of gastrointestinal endoscopy," *Surgical Endoscopy and Other Interventional Techniques*, **17**(2), pp. 342–350.

[4] Rattner, D. W. and S. J. C. on NOTES (2008) "NOTES: Where have we been and where are we going?" *Surgical Endoscopy*, **22**(5), pp. 1143–1145.

[5] Moyer, M. T., E. M. Pauli, R. S. Haluck, and A. Mathew (2007) "A self-approximating transluminal access technique for potential use in NOTES: an ex vivo porcine model (with video)," *Gastrointestinal Endoscopy*, **66**(6), pp. 974–978.

[6] Hawes, R. H., D. W. Rattner, D. Fleischer, C. J. Gostout, A. Kalloo, M. Kochman, M. Marohn, J. Ponsky, R. Rothstein, S. Schwaitzberg, C. D. Smith, L. Swanstrom, M. Talamini, C. C. Thompson, and N. J. C. on NOTES (2008) "NOTES^{TM}: where have we been and where are we going?" *Gastrointestinal Endoscopy*, **67**(6), pp. 779–780.

[7] Rattner, D., A. Kalloo, and S. A. W. Group (2006) "ASGE/SAGES Working Group on Natural Orifice Translumenal Endoscopic Surgery," *Surgical Endoscopy and Other Interventional Techniques*, **20**(2), pp. 329–333.

[8] "Laparoscopic Surgery," (Accessed January 27, 2010).
URL http://www.sangwannursinghome.com/laparoscopy.html

[9] "Upper GI Endoscopy," (Accessed January 28, 2010).
URL http://ccf.eznetpublish.ihealthspot.com/Home/tabid/6851

[10] Swain, P. (2007) "A justification for NOTES-natural orifice translumenal endosurgery," *Gastrointestinal Endoscopy*, **65**(3), pp. 514–516.

[11] Pauli, E. M., M. T. Moyer, R. S. Haluck, and A. Mathew (2008) "Self-approximating transluminal access technique for natural orifice transluminal endoscopic surgery: a porcine survival study (with video)," *Gastrointestinal Endoscopy*, **67**(4), pp. 690–679.

[12] Kantsevoy, S. V., S. B. Jagannath, H. Niiyama, S. S. C. Chung, P. B. Cotton, C. J. Gostout, R. H. Hawes, P. J. Pasricha, C. A. Magee, C. A. Vaughn, D. Barlow, H. Shimonaka, and A. N. Kalloo (2005) "Endoscopic gastrojejunostomy with survival in a porcine model," *Gastrointestinal Endoscopy*, **62**(2), pp. 287–292.

[13] "Disposable biopsy forceps," (Accessed January 29, 2010).
URL http://www.yziawa.com/product_list.asp?id=382

[14] "EndoChoice disposable COL forceps w/ needle," **2010**(Accessed 1/29/2010).
URL http://www.endochoice.com/Devices/Biopsy-Forceps

[15] "Single plug bipolar hemostasis probe," **2010**(Accessed 1/29/2010).
URL http://www.endochoice.com/Devices/Bipolar-Probes

[16] Mehta, N. Y., R. S. Haluck, M. I. Frecker, and A. J. Snyder (2002) "Sequence and task analysis of instrument use in common laparoscopic procedures," *Surgical Endoscopy and Other Interventional Techniques*, **16**(2), pp. 280–285.

[17] Frecker, M. I., J. Shadler, R. S. Haluck, K. Culkar, and R. Dziedzic (2005) "Laparoscopic Multifunctional Instruments: Design and Testing of Initial Prototypes," *Journal of the Society of Laparoendoscopic Surgeons*, **9**, pp. 105–112.

[18] Frecker, M. L., K. M. Powell, and R. Haluck (2005) "Design of a multifunctional compliant instrument for minimally invasive surgery," *Journal of Biomechanical Engineering-Transactions of the Asme*, **127**(6), pp. 990–993.

[19] Eitenmueller, J. P. and E. Volckmann (2008) "Clinical experience with bipolar multifunctional coagulation scissors in laparoscopic surgery," *Surgical Endoscopy and Other Interventional Techniques*, **22**(2), pp. 421–425.

[20] Ayodeji, I. D., W. C. J. Hop, G. W. M. Tetteroo, H. J. Bonjer, and E. J. R. de Graaf (2004) "Ultracision Harmonic Scalpel and multifunctional tem400 instrument complement in transanal endoscopic microsurgery - A prospective study," *Surgical Endoscopy and Other Interventional Techniques*, **18**(12), pp. 1730–1737.

[21] Lazeroms, M., A. LaHaye, W. Sjoerdsma, W. Schreurs, W. Jongkind, G. Honderd, and C. Grimbergen (1996) "A hydraulic forceps with force-feedback for use in minimally invasive surgery," *Mechatronics*, **6**(4), pp. 437–446.

[22] Aguirre, M. E. and M. Frecker (2008) "Design Innovation Size and Shape Optimization of a 1.0 mm Multifunctional Forceps-Scissors Surgical Instrument," *Journal of Medical Devices*, **2**(1), pp. 015001–1–7.

[23] Massarweh, N. N., N. Cosgriff, and D. Slakey (2006) "Electrosurgery: History, principles, and current and future uses," *Journal of the American College of Surgeons*, **202**(3), pp. 520–530.

[24] Dodde, R. E., S. Miller, J. Geiger, and A. Shih (2008) "Thermal-electric finite element analysis and experimental validation of bipolar electrosurgical cautery," *Journal of Manufacturing Science and Engineering-Transactions of the Asme*, **130**(2), pp. –.

[25] Dumot, J. A. and B. D. Greenwald (2008) "Argon plasma coagulation, bipolar cautery, and cryotherapy: ABC's of ablative techniques," *Endoscopy*, **40**(12), pp. 1026–1032.

[26] Harrell, A. G., K. W. Kercher, and B. T. Heniford (2004) "Energy Sources in Laparoscopy," *Surgical Innovation*, **11**, pp. 201–209.

[27] Nduka, C. C., P. A. Super, J. R. T. Monson, and A. W. Darzi (1994) "Cause and Prevention of Electrosurgical Injuries in Laparoscopy," *Journal of the American College of Surgeons*, **179**(2), pp. 161–170.

[28] Ramsay, J. W. A., N. A. Shepherd, M. Butler, P. T. Gosling, R. A. Miller, D. M. A. Wallace, and H. N. Whitfield (1985) "A Comparison of Bipolar and Monopolar Diathermy Probes in Experimental-Animals," *Urological Research*, **13**(2), pp. 99–102.

[29] Rodriguez, S. A., D. G. Adler, B. Chand, J. D. Conway, D. L. Diehl, S. V. Kantsevoy, R. S. Kwon, P. Mamula, R. J. Shah, L. M. W. K. Song, and W. M. Tierney (2008) "Technology Status Evaluation Report: Mucosal ablation devices," *Gastrointestinal Endoscopy*, **68**(6), pp. 1031–1042.

[30] Salameh, F., T. Kudo, H. Seidler, T. Kawano, and T. Iwai (2004) "An animal model study to clarify and investigate endoscopic tissue coagulation by using a new monopolar device," *Gastrointestinal Endoscopy*, **59**(1), pp. 107–112.

[31] Rey, J. M., D. Schramm, D. Hahnloser, D. Marinov, and M. W. Sigrist (2008) "Spectroscopic investigation of volatile compounds produced during thermal and radiofrequency bipolar cautery on porcine liver," *Measurement Science and Technology*, **19**(7), pp. –.

[32] Ryan, T. P., S. J. Patel, R. Morris, P. J. Hoopes, J. Bergeron, and R. Mahajan (2005) "Three-dimensional finite element simulations of vertebral body thermal treatment," *Thermal Treatment of Tissue: Energy Delivery and Assessment III*, **5698**, pp. 137–155 282.

[33] Palanker, D., A. Vankov, and P. Jayaraman (2008) "On mechanisms of interaction in electrosurgery," *New Journal of Physics*, **10**, pp. –.

[34] Palanker, D. V., A. Vankov, and P. Huie (2008) "Electrosurgery with cellular precision," *IEEE Transactions on Biomedical Engineering*, **55**(2), pp. 838–841.

[35] Berjano, E. J. (2006) "Theoretical modeling for radiofrequency ablation: state-of-the-art and challenges for the future," *Biomedical Engineering Online*, **5**, pp. –.

[36] Pennes, H. H. (1948) "Analysis of Tissue and Arterial Blood Temperatures in the Resting Human Forearm," *Journal of Applied Physiology*, **1**(2), pp. 93–122.

[37] Laine, L., G. L. Long, G. J. Bakos, O. J. Vakharia, and C. Cunningham (2008) "Optimizing bipolar electrocoagulation for endoscopic hemostasis: assessment of factors influencing energy delivery and coagulation," *Gastrointestinal Endoscopy*, **67**(3), pp. 502–508.

[38] "Hot Maxx®Reusable Hot Biopsy Forceps," (Accessed 1/15/2010).
URL `http://www.cookmedical.com/esc/dataSheet.do?id=4839`

[39] "Quicksilver®Bipolar Probes," (Accessed 1/15/2010).
URL `http://www.cookmedical.com/esc/dataSheet.do?id=698`

[40] "Quicksilver Bipolar Probes," (Accessed 1/15/2010).
URL `http://www.conmed.com/EndoTech_SuperConductor.php`

[41] "BiCap SuperConductor Bipolar Probe," (Accessed 1/15/2010).
URL `http://www.bostonscientific.com/Device.bsci?page=HCP`

[42] Sha, D., R. Connolly, S. Schwaitzberg, and A. Levine (2001) "The development of non-sticking, passively cooled electrosurgical instruments," *Proceedings of the Ieee 27Th Annual Northeast Bioengineering Conference*, pp. 11–12 108.

[43] Simaan, N., R. Taylor, and P. Flint (2004) "High Dexterity Snake-Like Robotic Slaves for Minimally Invasive Telesurgery of the Upper Airway," in *Lecture Notes in Computer Science*, Springer-Verlag Berlin Heidelberg, Saint-Malo, France, pp. 17–24.

[44] Hannan, M. and I. Walker (2001) "Analysis and experiments with an elephant's trunk robot," *Advanced Robotics (VSP and Robotics Society of Japan)*, **15**(8), pp. 847–858.

[45] Sreekumar, M., T. Nagarajan, M. Singaperumal, M. Zoppi, and R. Molfino (2007) "Critical review of current trends in shape memory alloy actuators for intelligent robots," *Industrial Robot: An International Journal*, **34**(4), pp. 285–294.

[46] Stevens, J. M. and G. D. Buckner (2005) "Actuation and Control Strategies for Miniature Robotic Surgical Systems," *Journal of Dynamic Systems, Measurement, and Control*, **127**, pp. 537–549.

[47] Hashimoto, M., T. Tabata, and T. Yuki (1999) "Development of Electrically Heated SMA Active Forceps for Laparoscopic Surgery," in *Proceedings of the SPIE - International Conference on Robotics & Automation*, IEEE, Detroit, MI, pp. 2372–2377.

[48] Tohyama, O., S. Maeda, K. Abe, and M. Murayama (2001) "Shape memory alloy actuators and their reliability," in *Proceedings of the SPIE - Device and Process Technologies for Microelectronics II* (H. B. H. Lorenzo Faraone and A. M. S. J.-C. Chiao, eds.), SPIE, pp. 111–118.

[49] Maeda, S., K. Abe, K. Yamamoto, O. Tohyama, and H. Ito (1996) "Active Endoscope with SMA (Shape Memory Alloy) Coil Springs," in *Proceedings of the IEEE*, pp. 290–295.

[50] Montesi, M., B. Martini, A. Pellegrinetti, P. Dario, L. Lencioni, and A. Montano (1995) "An SMA-based flexible active endoscope for minimal invasive surgery," *Journal of Micromech. Microeng.*, **5**, pp. 180–182.

[51] Ikuta, T. H., Koji and S. Daifu (2003) "Hyper Redundant Miniature Manipulator "Hyper Finger" for Remote Minimally Invasive Surgery in Deep Area," in *International Conference on Robotics and Automation*, vol. 1, IEEE, Taipei, Taiwan, pp. 1098–1102.

[52] Dario, P., M. C. Carrozza, M. Marcacci, S. D'Attanasio, B. Magnami, O. Tonet, and G. Megali (2000) "A Novel Mechatronic Tool for Computer-Assisted Arthroscopy," in *IEEE Transactions on Information Technology in Biomedicine*, vol. 4, pp. 15–29.

[53] Nakamura, R., E. Kobayashi, K. Masamune, I. Sakuma, T. Dohi, N. Yahagi, T. Tsuji, D. Hashimoto, M. Shimada, and M. Hashizume (2000) "Multi-DOF Forceps Manipulator System for Laparoscopic Surgery," in *Medical Image Computing and Computer-Assissted Intervention*, vol. 1935, Springer Berlin/Heidelberg, pp. 653–660.

[54] Harada, K., K. Tsubouchi, and M. G. Fujie (2005) "Micro Manipulators for Intrauterine Fetal Surgery in an Open MRI," in *Proc. of IEEE - International Conference on Robotics and Automation*, Barcelona, Spain, pp. 502–507.

[55] Ikuta, K., K. Yamamoto, and K. Sasaki (2003) "Development of Remote Microsurgery Robot and New Surgical Procedure for Deep and Narrow Space," in *International Conference on Robotics and Automation*, IEEE, Taipei, Taiwan, pp. 1103–1108.

[56] Peirs, J., D. Reynaerts, H. V. Brussel, G. D. Gersem, and H.-W. Tang (2003) "Design of an advanced tool guiding system for robotic surgery," in *International Conference on Robotics & Automation*, Taipei, Taiwan, pp. 2651–2656.

[57] Rosen, J. and B. Hannaford (1999) "Force Controlled and Teleoperated Endoscopic Grasper for Minimally Invasive Surgery - Experimental Performance Evaluation," in *IEEE Transactions on Biomedical Engineering*, vol. 46, pp. 1212–1221.

[58] Madhani, A. J., G. Niemeyer, and J. K. Salisbury (1998) "The Black Falcon: A Teleoperated Surgical Instrument for Minimally Invasive Surgery," in *IEEE International Conference on Intelligent Robots and Systems*, vol. 2, Victoria, B.C., Canada.

[59] Song, Y., G. An, J. Zhang, , and Y. Chen (2008) "Medical robotic system for minimally invasive spine surgery," in *2nd International Conference on Bioinformatics and Biomedical Engineering*, Shanghai, China, pp. 1703–1706.

[60] Abbott, D. J., C. Becke, R. I. Rothstein, and W. J. Peine (2007) "Design of an Endoluminal NOTES Robotic System," in *IEEE International Conference on Intelligent Robots and Systems*, San Diego, CA, pp. 410–416.

[61] Tendick, F., S. S. Sastry, R. S. Fearing, and M. Cohn (1998) "Applications of Micromechatronics in Minimally Invasive Surgery," *IEEE/ASME Transactions on Mechatronics*, **3**(1), pp. 34–42.

[62] Ponsky, J. L. (2006) "Endoluminal surgery: past, present and future," *Surgical Endoscopy*, **20**, pp. S500–S502.

[63] Simaan, N. and R. Taylor (2004) "A Dextrous System for Laryngeal Surgery," in *Proceedings of the SPIE - International Conference on Robotics and Automation*, IEEE, New Orleans, LA, pp. 351–357.

[64] ——— (2005) "Snake-Like Units Using Flexible Backbones and Actuation Redundancy for Enhanced Miniaturization," in *Proceedings of the IEEE - International Conference on Robotics and Automation*, IEEE, Barcelona, Spain, pp. 3012–3017.

[65] Kapoor, A., N. Simaan, and R. H. Taylor (2005) "Suturing in confined spaces: Constrained motion control of a hybrid 8-DoF robot," in *Proceedings of the IEEE: International Conference on Advanced Robotics*, IEEE, Seattle, WA, pp. 452–459.

[66] Xu, K. and N. Simaan (2006) "Actuation Compensation for Flexible Surgical Snake-like Robots with Redundant Remote Actuation," in *Proceedings of the IEEE - International Conference on Robotics and Automation*, IEEE, Orlando, FL, pp. 4148–4154.

[67] Dario, P., C. Paggetti, N. Troisfontaine, E. Papa, T. Ciucci, M. Carrozza, and M. Marcacci (1997) "A miniature steerable end-effector for application in an integrated system for computer-assisted arthroscopy," in *International Conference on Robotics and Automation*, Albuquerque, NM, pp. 1573–1579.

[68] Ascari, L., C. Stefanini, A. Menciassi, S. Sahoo, P. Rabischong, and P. Dario (2003) "A New Active Microendoscope for Exploring the Subarachnoid Space in the Spinal Cord," in *Proceedings of the IEEE: International Conference on Robotics and Automation*, vol. 2, IEEE, Taipei, Taiwan, pp. 2657–2662.

[69] Grissom, M. D., V. Chitrakaran, D. Dienno, M. Csencits, M. Pritts, B. Jones, W. McMahan, D. Dawson, C. Rahn, and I. Walker (2006) "Design and experimental testing of the OctArm soft robot manipulator," *Proceedings of the SPIE*, pp. F1–F10.

[70] Salle, D., P. Bidaud, and G. Morel (2004) "Optimal Design of High Dexterity Modular MIS Instrument for Coronary Artery Bypass Grafting,"

in *International Conference on Robotics and Automation*, New Orleans, LA, USA, pp. 1276–1281.

[71] Dombre, E., M. Michelin, F. Pierrot, P. Poignet, P. Bidaud, G. Morel, T. Ortmaier, D. Salle, N. Zemiti, P. Gravez, M. Karouia, and N. Bonnet (2004) "MARGE Project: Design, Modeling, and Control of Assistive Devices for Minimally Invasive Surgery," *Lecture Notes in Computer Science*, **3217**(1 Part 2), pp. 1–8.

[72] Degani, A., H. Choset, A. Wolf, and M. A. Zenati (2006) "Highly Articulated Robotic Probe for Minimally Invasive Surgery," in *IEEE International Conference on Robotics and Automation*, Orlando, FLA, pp. 4167–4172.

[73] Degani, A., H. Choset, A. Wolf, T. Ota, and M. A. Zenati (2006) "Percutaneous Intrapericardial Interventions Using a Highly Articulated Robotic Probe," *IEEE International Conference on Biomedical Robotics and Biomechatronics*, pp. 7–12.

[74] Van Meer, F., J. Philippi, D. Esteve, and E. Dombre (2007) "Compact generic multi-channel plastic joint for surgical instrumentation," *Mechatronics*, **17**, pp. 562–569.

[75] Cleary, K. and C. Nguyen (2001) "State of the Art in Surgical Robotics: Clinical Applications and Technology Challenges," *Computer Aided Surgery*, **6**, pp. 312–328.

[76] Taylor, R. H. (2006) "A Perspective on Medical Robotics," *Proceedings of the IEEE*, **94**(9), pp. 1652–1664.

[77] Kazanzides, P., G. Fichtinger, G. D. Hager, A. M. Okamura, L. L. Whitcomb, and R. H. Taylor (2008) "Surgical and interventional robotics - Core concepts, technology, and design," *IEEE Robotics and Automation Magazine*, **15**(2), pp. 122–130.

[78] Leven, J., D. Burschka, R. Kumar, G. Zhang, S. Blumenkranz, X. Dai, M. Awad, G. D. Hager, M. Marohn, M. Choti, C. Hasser, and R. H. Taylor (2005) "DaVinci Canvas: A telerobotic surgical system with integrated, robot-assisted, laparoscopic ultrasound capability," in *Medical Image Computing and Computer-Assisted Intervention*, Palm Springs, CA.

[79] Guthart, G. S. and J. K. Salisbury (2000) "The Intuitive Telesurgery System: Overview and Application," in *International Conference on Robotics and Automation*, San Francisco, CA, pp. 618–621.

[80] Reynaerts, D., J. Peirs, and H. V. Brussel (1999) "Shape memory micro-actuation for a gastro-intestinal intervention system," *Sensor and Actuators*, **77**, pp. 157–166.

[81] Dilibal, S., R. M. Tabanli, and A. Dikicioglu (2004) "Development of shape memory actuated ITU Robot Hand and its mine clearance compatibility," *Journal of Materials Processing Technologies*, **155-156**, pp. 1390–1394.

[82] Lobontiu, N. (2003) *Compliant mechanisms: Design of Flexure Hinges*, CRC Press.